PLANT SPECIES BIOMETRIC USING FEATURE HIERARCHIES

A plant identification system using both global and local features of plant leaves.

K.K. Pahalawatta

A thesis submitted
in partial fulfilment of the requirement
for the Degree of Master of Science in Computer Science.

Department of Computer Science and Software Engineering
University of Canterbury
CHRISTCHURCH 2008.

Saram ca sarato natva
asaram ca asarato
te saram adhigaccanthi
samma samkappa gocara

What is real they deem as real, what is unreal they deem as unreal, - they who abide in the pasture ground of right thoughts, arrive at the real
(Lord Buddha).

With love
to Patalee and Janindu

ACKNOWLEDGEMENTS

I express my deepest gratitude for the advice, guidance and suggestions given to me by my supervisor, Dr. Richard Green, Senior Lecturer, Department of Computer Science and Software Engineering, University of Canterbury, in the task of carrying out of this research. I gratefully appreciate the knowledge and training received from him, and the benefits I had from his deep involvements in the computer vision field.

My special thanks are due to Dr. R. Mukundan, my associate supervisor and Prof. Tim Bell for their helpful advice. I also like to thank all the other staff in the department of Computer Science and Software Engineering for their enormous support.

Finally, to my wife Patalee who was of enormous help and support in the culmination of this work which was probably not fully appreciated at the time, thank you indeed.

CONTENTS

LIST OF TABLES

LIST OF FIGURES

ABSTRACT

Biometric identification is a pattern recognition based classification system that recognizes an individual by determining its authenticity using a specific physiological or behavioural characteristic (biometric). In contrast to number of commercially available biometric systems for human recognition in the market today, there is no such a biometric system for plant recognition, even though they have many characteristics that are uniquely identifiable at a species level. The goal of the study was to develop a plant species biometric using both global and local features of leaf images.

In recent years, various approaches have been proposed for characterizing leaf images. Most of them were based on a global representation of leaf peripheral with Fourier descriptors, polygonal approximations and centroid-contour distance curve. Global representation of leaf shapes does not provide enough information to characterise species uniquely since different species of plants have similar leaf shapes. Others were based on leaf vein extraction using intensity histograms and trained artificial neural network classifiers. Leaf venation extraction is not always possible since it is not always visible in photographic images.

This study proposed a novel approach of leaf identification based on feature hierarchies. First, leaves were sorted by their overall shape using shape signatures. Then this sorted list was pruned based on global and local shape descriptors. The consequent biometric was tested using a corpus of 200 leaves from 40 common New Zealand broadleaf plant species which encompass all categories of local information of leaf peripherals.

Two novel shape signatures (full-width to length ratio distribution and half-width to length ratio distribution) were proposed and biometric vectors were constructed using

both novel shape signatures, complex-coordinates and centroid-distance for comparison. Retrievals were compared and the biometric vector based on full-width to length ratio distribution was found to be the best classifier. Three types of local information of the leaf peripheral (leaf margin coarseness, stem length to blade length ratio and leaf tip curvature) and the global shape descriptor, leaf compactness, were used to prune the list further.

The proposed biometric was able to successfully identify the correct species for 37 test images (out of 40). The *proposed biometric identified all the test images (100%) correctly if two species were returned compared to the low recall rates of Wang et al. (2003) (30%, if 10 images were returned) and Ye et al. (2004) (71.4%, if top 5 images were returned). The biometric can be strengthened by adding reference images of new species to the database, or by adding more reference images of existing species when the reference images are not enough to cover the leaf shapes.*

Chapter 1

Introduction

Biometric identification is a pattern recognition based classification system that recognizes an individual by determining its authenticity using a specific physiological or behavioural characteristic (biometric). In human recognition, fingerprints, face, iris, speech, gait and hand geometry are the most commonly used biometrics (Maltoni *et al.*, 2003) and a number of commercially available biometric systems for human recognition can be seen in the market today. In contrast, for plants, even though they have many characteristics that are uniquely identifiable at a species level, there is no such a biometric system for plant identification.

Living plant recognition is a promising but challenging task in the field of pattern recognition and computer vision. In recent years, various approaches have been proposed for characterizing leaf images. Most of them were based on a global representation of leaf peripheral with Fourier descriptors, polygonal approximations and centroid-contour distance curve. Global representation of leaf shapes does not provide enough information to characterise species uniquely since different species of plants have similar leaf shapes. Others were based on leaf vein extraction using

intensity histograms and trained artificial neural network classifiers. Leaf venation extraction is not always possible since it is not always visible in photographic images. To overcome such impoverished global representation of overall leaf shape in prior research, this study proposes the extraction of local information of the leaf contour, which is shape of the leaf margin, shape of the leaf base and shape of the leaf apex. Contour detection and contour representation techniques extract biometric information. The proposed biometric system was tested on common 40 New Zealand broadleaf plant species that covers all the categories of local information of leaf peripheral. A reference database containing 200 leaf images (five leaf images from each species) was used for image matching.

The biometric system that has been developed to extract the uniquely identifiable global and local features of leaves efficiently is described in this thesis. The introductory chapter contains a high-level overview of the remainder of the thesis. Biometric systems are introduced in section 1.1. Section 1.2 and 1.3 describe the plant species biometric and the proposed solution respectively. Objectives of the study are shown in section 1.4. Section 1.5 outlines the reminder of the thesis.

1.1 Biometrics and Biometric Systems

Biometric authentication systems generally use a pattern recognition approach that verifies or identifies an individual's authenticity of its uniquely identifiable physiological or behavioural characteristic, which is called a biometric. Verification systems either reject or accept the submitted claim of identity by comparing it with the pre-stored biometrics of the same individual while identification systems

recognize an individual by searching the matching queried biometric in the entire database. In human context, a variety of biometrics (Figure 1.1) is in use in various applications.

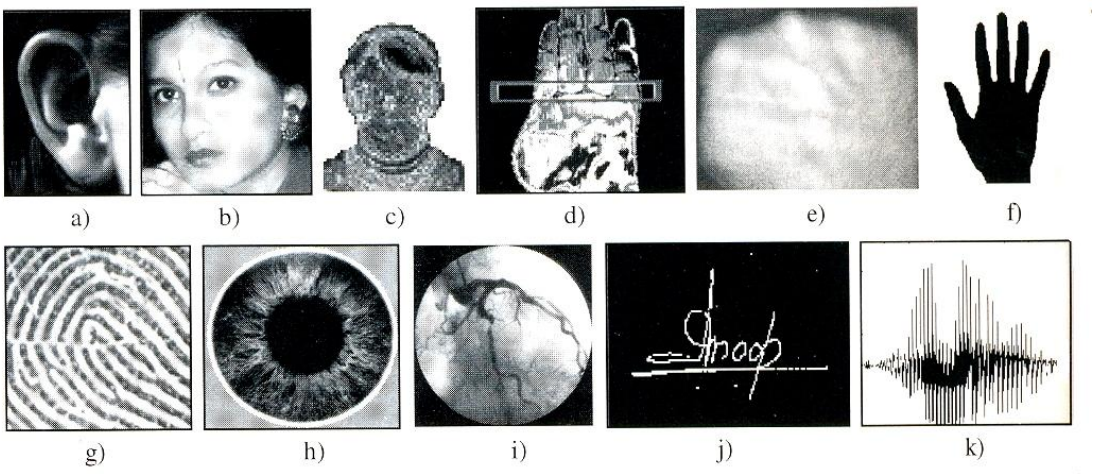

Figure 1.1. Human biometrics: a) ear, b) face, c) facial thermogram, d) hand thermogram, e) hand vein, f) hand geometry, g) fingerprint, h) iris, i) retina, j) Signature, and k) voice (adopted from Maltoni *et al*., 2003).

However, whatever the biometric is, it should be universal (each individual should have that biometric), distinctive (biometric should be unique to each individual), permanent (unchangeability over period of time) and collectable (it can be measured quantitatively) (Maltoni *et al.*, 2003). Out of the biometrics in figure 1.1, fingerprints have been used as a personal identification tool for over 100 years due to their uniqueness and unchangeability, and a number of commercial applications for fingerprint recognition are available on the market today (Maltoni *et al*., 2003; Chang & Fan, 2002; Fitz & Green, 1996; Kawagoe & Tojo, 1984). Successful recognition of images of faces of various people in various poses has also been achieved using neural networks learning methods (Cottrell, 1990).

1.2 The Problem: Plant Species Recognition

Plants are basically identified according to their morphological features such as number of ovaries in the fruit or number of stamens in the flower. A number of manual and computer-aided keys for plant identification using morphological features (Philips 2002; Ashton *et al.* 1997) are available in the literature. Identifying plants using such keys is a very time consuming task and has been carried out only by trained botanists. However, in addition to this time intensive task, there are several other drawbacks in identifying plants using these features such as the unavailability of required morphological information and use of botanical terms that only experts can understand. Fortunately, in addition to the shapes and structures of reproductive organs, shape, size, texture and colour of the leaves also play an important role in plant identification. Although almost all the broadleaf species have unique features in their leaves, there is no identification method that completely relies on the leaves itself in the existing literature and no botanist will agree on such a system. This may be perhaps due to the difficulty in explaining the "exact" features (shape, texture, colour, size etc.) in the leaves of each species literally or lack of clear definitions to the available technical terms that describe these features.

In plant identification, taxonomists classify overall leaf shape (Figure 1.2), shape of the leaf edge (Figure 1.3), shape of the leaf apex (Figure 1.4) and base (Figure 1.5) into broader categories[1].

[1] http://dallas.tamu.edu/weeds/anat.html (Texas Agricultural Experiment Station, Texas A&M University - Commerce)

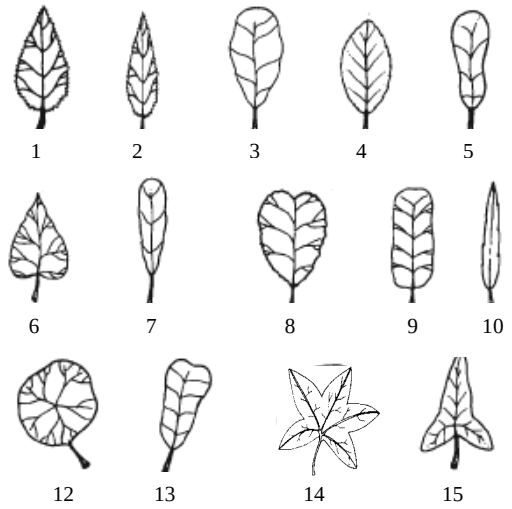

Figure 1.2. Common leaf shapes

1. Oval 2. Lanceolate 3. Obovate
4. Elliptical 5. Spatulate 6. Cordate
7. Oblanceolate 8. Obcordate 9. Oblong
10. Linear 11. Peltate 12. Cuneate
13. Reniform 14. Hastate

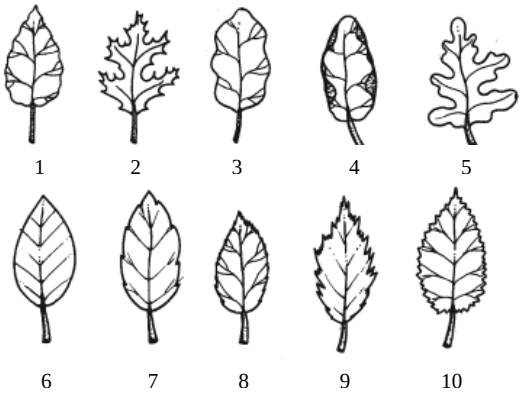

Figure 1.3. Common leaf margins

1. Crenate 2. Incised 3. Sinuate
4. Undulate 5. Lobed 6. Entire
7. Serrate 8. Serrulate 9.Doubly Serrate
10. Dentate

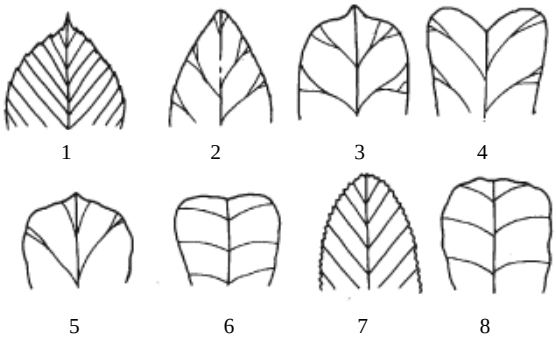

Figure 1.4. Common leaf apexes

1. Acuminate 2. Acute 3. Cuspidate
4. Emarginate 5. Mucronate 6. Obocordate
7. Obtuse 8. Truncate

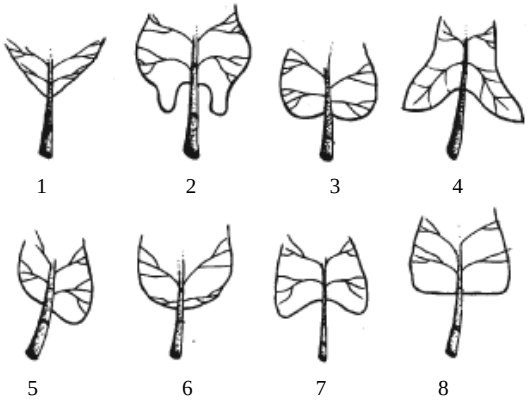

Figure 1.5. Common leaf bases

1. Acute 2. Acuminate 3. Cordate
4. Hastate 5. Oblique 6. Rounded
7. Sagitate 8. Truncate

These categories are described basically by visual shapes and the definitions of these shapes have no clear demarcations. Therefore, in some situations it is very difficult to classify leaves into these categories.

1.3 A Solution: Plant Species Biometric

The goal of the study is to develop a plant species biometric which will be developed using both global and local features that are specific to leaf images of different species. The study will mainly focus on the extraction of local information of the leaf contour characters, which is shape of the leaf margin, shape of the leaf base and shape of the leaf apex. In leaf contours, these characters satisfy all the biometric requirements: universality, distinctiveness, permanence and collectability, mentioned above.

Development of a biometric algorithm for visual plant identification will help professionals as well as non-professionals to identify plants efficiently and accurately. Compared to the complex structures of flowers and fruits, leaves are simpler and easily available. On the other hand, leaves of plants are planar and input of their shapes is easy and so the motivation for this research is a system to recognize the unique features of leaves that will be a solution to problem of identifying plants using morphological features. Such a system will promote an interest in studying plant taxonomy and dendrology, and will lift the school biology education standards at various levels. Furthermore, the findings of the study will contribute to enhance the knowledge in the area of computer-aided pattern recognition.

1.4 Objectives of the study:

As mentioned above, the goal of this research is to develop a biometric algorithm to identify plants using leaf patterns beyond overall leaf shape alone, which prior research has shown to be insufficient for classification.

There are three main objectives.

1. Analysis of existing pattern recognition techniques to identify the techniques and algorithms that can be used to detect leaf contours accurately, to represent the leaf margins preserving both global and local features and to match the leaf shapes efficiently.
2. Propose and develop a method to separate and to quantify the singularities on the leaf contour. Singularities of a leaf contour are the shape of the entire leaf, shape of leaf apex, shape of leaf margin and shape of leaf base as described in the figures 1.2 to 1.5.
3. Identify and extract the other parameters from the leaf image that can be used to differentiate leaves. These parameters will be based on leaf size, texture and colour.

1.5 A guide to the thesis

Chapter 2 provides the overall image of the process of shape based image retrieval. It describes different edge detection techniques, shape representation techniques with global and local features and various image classification techniques that are

available in the literature. Chapter 3 is mainly concentrated on plant biometrics. An extensive literature survey on plant biometrics was carried out and the prior attempts are deeply analysed in this chapter. The methodology of the proposed biometric is explained in Chapter 4. The results which are obtained from variety of techniques are analysed and discussed in detail in Chapter 5. Finally, Chapter 6 presents the conclusions and discusses future directions of this research.

Chapter 2

Shape Based Image Retrieval

Shape is one of the most important image features of recognizing objects by human perception. Humans generally describe objects either by giving examples or by sketching the shape. In computer vision, shape is the most commonly used feature for characterising objects and in image retrieval. For example, for face recognition, fingerprint recognition and iris recognition, well-established techniques have been developed and number of biometric systems are commercially available based on shape-based image retrieval.

Shape-based image retrieval can either be region-based or contour-based. In region-based retrieval all the pixels within the shape are taken into account to represent the image while in contour-based retrieval only the pixels in region boundary are considered. Commonly, moment invariants are used to represent regions in region-based methods (Mukundan, 2005; Cho-Huak & Roland, 1998) and the representation schemes such as global shape descriptors, polyline representations, shape signatures (Zhang & Lu, 2001), and spectral descriptors are used in contour based systems.

Shape-based image retrieval mainly consists of three steps:

i. edge detection

ii. shape representation

iii. shape matching and similarity measure

The remainder of the chapter describes these steps in more detail. Section 2.1 describes various edge detection techniques. Shape representation with global shape descriptors, curve fittings, shape signatures and spectral descriptors are explained in section 2.2. The last step: similarity measurement and matching is in section 2.3.

2.1 Edge detection

The first step of the shape-based image retrieval is the edge detection and it is one of the most commonly used operations in image analysis. Marr-Hildreth edge detector, Canny's edge detector, and Shan-Castan (ISEF) edge detector are examples of the more popular edge detectors (Parker, 1997; Heath *et al*. 1997). Parker (1997) has compared two of the above edge detectors (Canny's and ISEF) and found that the performance of both of the edge detectors depend on the use of a better choice of parameters. Canny's edge detector is the most commonly used edge detector. (Nam & Hwang, 2005; Nam *et al*., 2005a; Nam *et al*., 2005b). Some researchers prefer their own edge detection technologies due to inappropriateness of available edge detectors for their studies (Fu & Chi, 2003).

2.1.1 Contour detection with thresholding and boundary following algorithms

One of the difficulties with applying these edge detectors to several images is that for each image, several parameters need to be set manually depending on the noise of the image. On the other hand, these edge detectors will not give continuous series of contour points for a object. For example, different edge images obtained using Canny's edge detector (Parker, 1997) are in figure 2.1. Figure 2.1(a) is the original image. Figure 2.1(b) to 2.1(d) are the obtained edge images with different values for the high hysteresis threshold (h), low hysteresis threshold (l) and the sigma (σ). Figure 2.2 describes the noise variation of the obtained images using same parameter values for different images.

Because of these drawbacks, a simple thresholding and denoising technique followed by a contour following algorithm has been commonly applied to get the boundary of the object. Figure 2.3 shows the various images in different steps of this technique.

Thresholding

Thresholding is used to separate subimages that represent objects from the image background. There are many techniques that have been developed to select the optimum threshold value (Mokhtarian & Abbasi, 2004; Zhang *et al*., 2004; Mündermann *et al*., 2003; Saitoh & Kaneko, 2000;) and among them, the techniques based on intensity histogram of the image are commonly used (Wang *et al.,* 2003; Jain *et al.,* 1995).

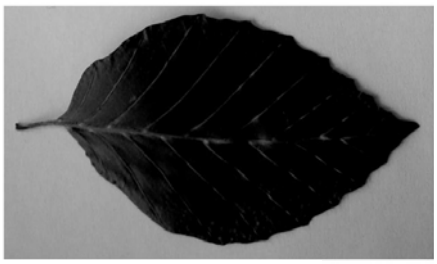

(a) Original Image

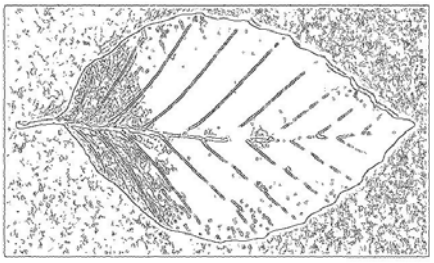

(b) h = 5, l = 30, σ = 1.0

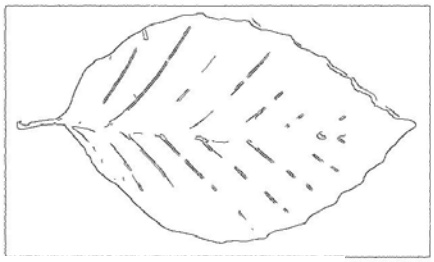

(c) h = 15, l = 1, σ = 1.0

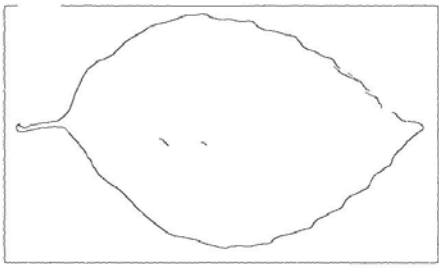

(d) h = 20, l = 1, σ = 1.6

Figure 2.1. Edge detection by Canny's edge detector with different parameters: high hysteresis threshold (h), low hysteresis threshold (l) and sigma (σ).

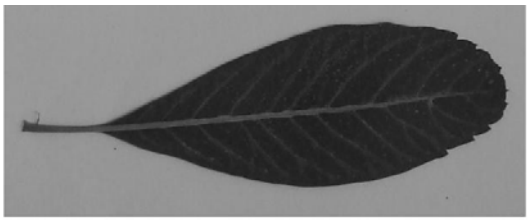

(a) Original image

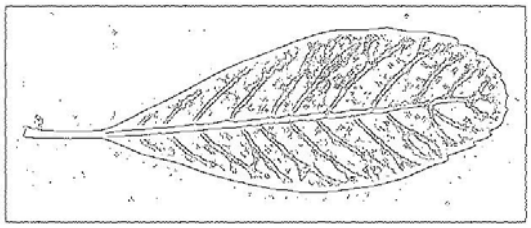

(b) h = 20.1, l = 1, σ = 1.6

(c) Original image

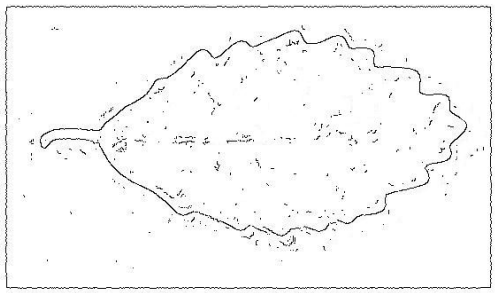

(d) h = 20.1, l = 1, σ = 1.6

Figure 2.2. Edge detection by Canny's edge detector with same parameters but different images. (a) & (c) are original images. (b) & (d) are the detected edges with the parameters: high hysteresis threshold (h) = 20, low hysteresis threshold (l) = 1 and sigma (σ) = 1.6 of the original images (a) & (c) respectively.

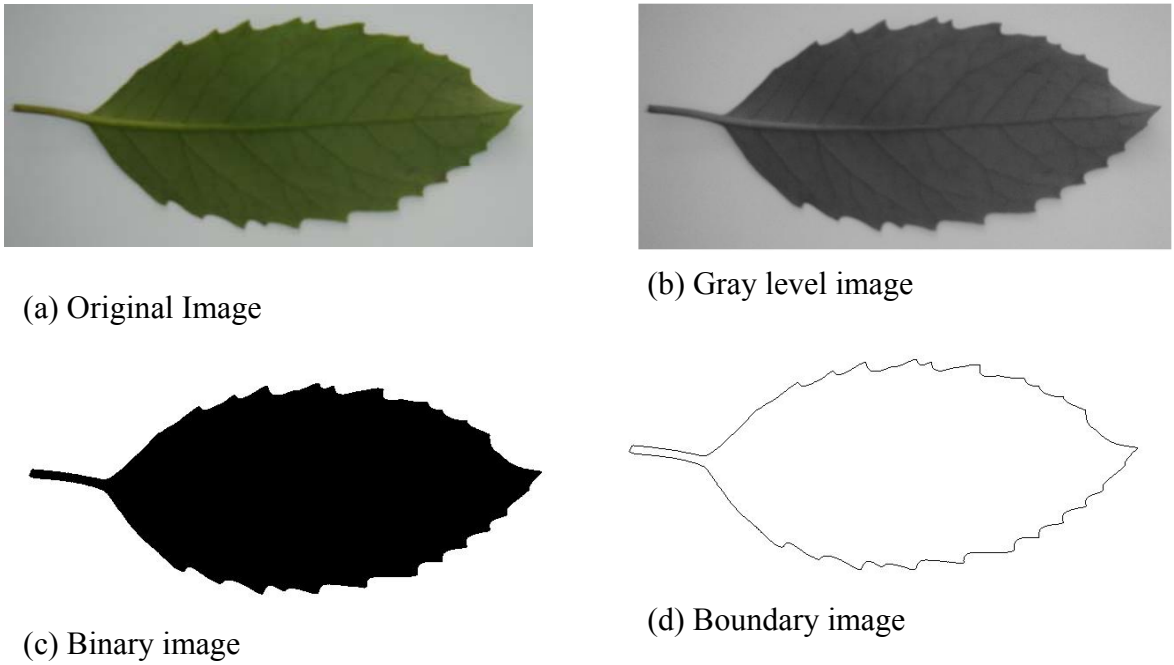

(a) Original Image

(b) Gray level image

(c) Binary image

(d) Boundary image

Figure 2.3. Images in different steps of the boundary detection technique: (a) Original leaf image, (b) gray level image (c) Binary image after thresholding (d) leaf boundary.

Denoising with size filtering

After thresholding, it is very common to have some small regions which do not belong to the object of interest due to noise. Size filters are used to filter out those small regions which have the area (number of pixels) less than a predefined threshold minimum value.

Boundary following algorithm

The boundary of a connected component S is the set of pixels of S that are adjacent to S. The following Boundary Following Algorithm (Jain *et al*., 1995) was applied to get the image boundary in this study.

1. *Find the starting pixel $s \in S$ for the region using a systematic scan, say from left to right and from top to bottom of the image.*
2. *Let the current pixel in boundary tracking be denoted by c. Set c = s and let the 4-neighbour to the west of s be* $b \in \overline{S}$.
3. *Let the eight 8-neighbours of c starting with b in clockwise order be* $n_1, n_2, \ldots, n_8$. *Find* n_i, *for the first i that is in S.*
4. *Set* $c = n_i$ *and* $b = n_{i-1}$.
5. *Repeat steps 3 and 4 until c = s.*

2.2 Shape representation

Many investigations on shape representation such as chain codes, centroid-contour distance curve, medial axis transform, Fourier descriptors, moment invariants and wavelet descriptors have been carried out (Wang *et al*., 2003; Loncaric, 1998). It is required that these shape representation schemes should be invariant to translation, scale and rotation because these three transformations do not change the shape of the object. Of the various shape representation methods, contour based shape representation methods can be classified into the four groups: Polygonal approximations (Im *et al*., 1998), global shape descriptors (Mokhtarian & Abbasi, 2004; Saitoh & Kaneko, 2000), shape signatures (Mokhtarian & Abbasi, 2004; Zhang & Lu, 2001) and spectral descriptors (Sajjanhar *et al*., 2007; Zhang & Lu, 2002; Zhang & Lu, 2001;).

2.2.1 Global Shape Descriptors

Global shape descriptors are used to discriminate shapes with large dissimilarities. They are simple to compute and robust in representation and increase the efficiency of the system. Area, circularity, eccentricity and axis orientation are common examples for global shape descriptors.

Area

Area is the number of pixels in an object and for a binary image $B[i,j]$, area A is given by

$$A = \sum_{i=1}^{n} \sum_{j=1}^{m} B[i, j].$$

Area is invariant to translation and rotation but not to scale.

Circularity (or Compactness)

Circularity or compactness is the ratio of perimeter (P) squared to the area (A).

$$\text{Circularity} = P^2/A \geq 4\pi$$

There are many definitions for the perimeter of a region (Jain *et al*., 1995). The number of steps taken by the boundary following algorithm was taken as the perimeter in this study.

Eccentricity

Eccentricity explains how the regions points are scattered around the centre of the region, centroid, which is explained in section 2.2.2.1.

Eccentricity of a region is given by the formula:

$$eccentricity = \sqrt{\frac{\lambda_{\max}}{\lambda_{\min}}}$$

where λ_{max} and λ_{min} are the eigenvalues of the matrix

$$\begin{bmatrix} \mu_{2,0} & \mu_{1,1} \\ \mu_{1,1} & \mu_{0,2} \end{bmatrix}$$

$$\text{where } \mu_{p,q} = \sum_x \sum_y (x - \bar{x})^p (y - \bar{y})^q$$

Here, x and y are coordinates of the region and $(\bar{x}, \bar{y})$ is the centroid.

2.2.2 Shape Signatures

Shape signature is any 1-D function representing 2-D areas or boundaries. Although they are sensitive to noise and not robust, they are local representations of shape features. Commonly used shape signatures are centroid contour distance, complex coordinates, curvatures and cumulative angular function (Wang *et al*. 2003; Zhang & Lu, 2001; Wang *et al*. 2000; Kauppinen *et al*., 1995).

2.2.2.1 Centroid Contour Distance Curve (CCD)

Centroid of any 2-D object is defined as follows.

$$m_{pq} = \iint_R x^p y^q dxdy, \qquad x_C = \frac{m_{10}}{m_{00}}, \qquad y_C = \frac{m_{01}}{m_{00}}$$

For a discrete pixel boundary image, this is simply the average of boundary coordinates.

$$x_c = \frac{1}{N}\sum_{t=0}^{N-1} x(t), \qquad y_c = \frac{1}{N}\sum_{t=0}^{N-1} y(t)$$

Tracing an object contour can be considered as circling around its centroid. As shown in figure 2.4, a point *P* on the contour is determined by the centroid *C*, the distance *R* between the points *P* and the centroid *C* (termed as the centroid-contour distance), and the angle α.

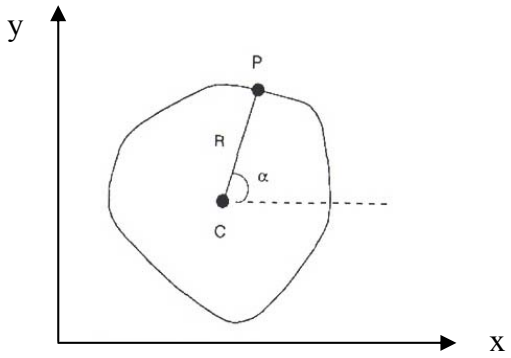

Figure 2.4. Illustration of the centroid-contour distance curve (CCD).

Centroid-distance function $r(t)$ is the distance of the boundary point $(x(t), y(t))$ from the centroid (x_c, y_c) of the shape and can be calculated using the formula:

$$r(t) = ([x(t) - x_c]^2 + [y(t) - y_c]^2)^{\frac{1}{2}} \ , \ t = 1, 2 \ldots .N,$$

assuming that the boundary of the object has *N* pixels numbered from 1 to *N*. Due to the subtraction of centroid, which represents the position of the shape, it can be proved that the centroid distance is also invariant to translation.

From a fixed starting point on the contour, plotting the centroid contour distance against t one can obtain the CCD, where this CCD represents a two-dimensional object by a one-dimensional curve (Wang *et al*. 2003; Wang *et al*. 2002; Wang *et al*. 2000).

2.2.2.2 Complex Coordinates (Position Function)

If the boundary of a particular shape has N pixels numbered from 1 to N and the t^{th} pixel along the contour has position (x_t,y_t) then the contour can be described as two parametric equations:

$$x(t) = x_t$$

$$y(t) = y_t, \quad t=1, 2, 3, \ldots\ldots N$$

The complex coordinates function can be defined as

$$z(t) = x(t) + i\, y(t) \text{ where } \quad i = \sqrt{-1}$$

In order to make this shape representation invariant to translation, the following shifted coordinates function can be used.

$$z(t) = [x(t) - x_c] + i[y(t) - y_c] \ , t=1, 2, 3,\ldots\ldots N$$

Here, (x_c,y_c) is the centroid of the shape.

2.2.2.3 Curvature

Curvature of a curve at a particular point is the first derivative of the boundary tangent at that point. Based on this definition, a curvature function is expressed as the differentiation of successive tangent values calculated in window *w* at each point on the curve (Figure 2.5).

$$c_i = \tan^{-1}\frac{y_i - y_{i-w}}{x_i - x_{i-w}} - \tan^{-1}\frac{y_{i-1} - y_{i-1-w}}{x_{i-1} - x_{i-1-w}}, \quad i = 1, \quad 2,.....N$$

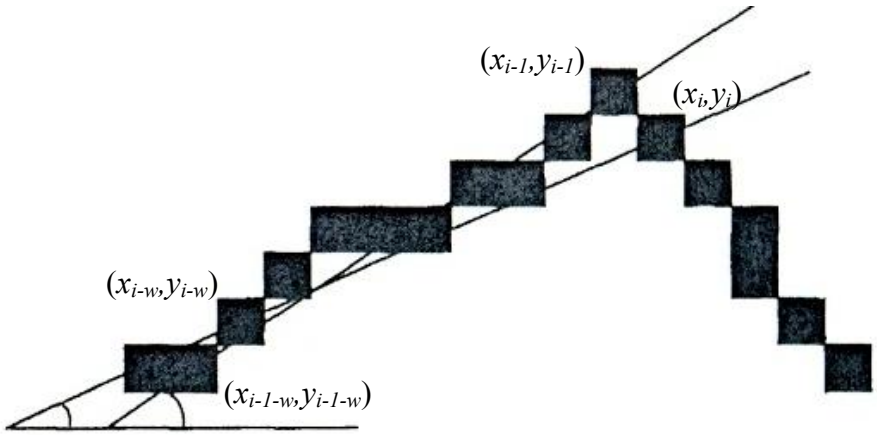

Figure 2.5. Two successive tangent values t_i and t_{i-1} of a boundary segment. The window size w=9. The curvature is $c_i=t_i-t_{i-1}$. (Adopted from Kauppinen *et al*., 1995).

2.2.3 Spectral Descriptors

Wavelet descriptors (Yang *et al*., 1998; Tieng & Boles, 1997) and the Fourier descriptors (Zhang & Lu, 2001) are the most commonly used spectral descriptors for shape representation. Wavelet descriptors are not rotationally invariant and therefore consume lot of time in the matching process. It is easier to achieve rotational invariance using Fourier Descriptors.

2.2.3.1 Fourier Descriptors

Fourier series can be used to approximate closed contours. If the contour is expressed as a sequence of coordinates $\mathbf{u}(n) = [x(n),y(n)]$ for $n = 0,1,2,\ldots, N\text{-}1$, then each coordinate pair can represent as a complex number so that

$$u(n) = x(n) + jy(n) \text{ for } n = 0,1,2,...., N\text{-}1.$$

The discrete Fourier transform representation of a one-dimensional sequence $u(n)$ is defined as

$$u(n) = \sum_{k=0}^{N-1} a(k) e^{\frac{j2\pi kn}{N}}, \quad 0 \le n \le N\text{-}1$$

$$a(k) = \frac{1}{N} \sum_{n=0}^{N-1} u(n) e^{\frac{-j2\pi kn}{N}}, \quad 0 \le n \le N\text{-}1.$$

The complex coefficients $a(k)$ are called the Fourier descriptors of the contour. With these Fourier descriptors, global shape features are captured by the first few low frequency terms and the finer features of the shape are captured by the higher frequency terms. Major advantages of this method are that it is easy to implement and is based on well-developed theory on Fourier analysis. The disadvantage is that Fourier transformations do not provide local shape information since such local shape information is distributed to all coefficients after the Fourier transformation (Loncaric 1998).

2.2.4. Polyline representation

There are many curve models such as line segments, circular arcs, conic sections, cubic splines and snakes that are used to fit contours (Jain *et al*., 1995). A polyline is a sequence of line segments joined end to end. When a contour is closed, polygonal approximations are used to approximate the shape boundary using a polyline. The polyline representation for a contour fits the edge list with a sequence of line segments. There are number of polygonal approximation algorithms available in the literature (Rosin, 2003; Im, 1998; Fu *et al.,* 1997). According to Rosin (2003) who has tested 21 algorithms including five optimal algorithms to assess the behaviour of them, most of the algorithms exhibit large variations over the applied dataset and some non-optimal algorithms behave better than the optimal ones. To represent the leaf contours, Im (1998) used a polygonal approximation, and Nam & Hwang (2005) used another kind of polygonal approximation, a revised Minimum Perimeter Polygon.

2.2.4.1 Hop-Along Algorithm for polygonal approximation of the boundary

The hop-along algorithm (Jain *et al*., 1995) that approximates a contour by a sequence of line segments is as follows.

1. *Start with the first k edges from the list.*
2. *Fit a line segment between the first and last edges in the sublist.*
3. *If the normalized maximum error is too large, shorten the sublist to the point of maximum error. Return to step 2.*

4. *If the line fit succeeds, compare the orientation of the current line segment with that of the previous line segment. If the lines have similar orientations, replace the two line segments with a single line segment.*
5. *Make the current line segment the previous line segment and advance the window of edges so that there are k edges in the sublist. Return to step 2.*

2.3 Classification and Similarity Measure

The final step of image retrieval is image matching and browsing. Generally, similarity between two objects is measured by simply evaluating the Euclidean distance (Veltkamp, 2001) between each object's points (Nam *et al*. 2005; Wang *et al*. 2003; Wang *et al*. 2000). After extracting points of interests from the image shape, matching can be performed using the Euclidean distances.

For example, when a centroid–contour distance curve is used, dissimilarity between two images can be measured using the following distance function, *D*.

$$D = \sqrt{\frac{\sum_{i=1}^{n} \left| f_1(i) - f_2(i) \right|}{n}}$$

where $f_1(i)$ and $f_2(i)$ are the centroid-contour distances of the i^{th} point of two object contours, and n is the number of sample points on the centroid contour distance curve.

Nearest Neighbourhood Classifier

A commonly used classification technique, Nearest Neighbour Classifier recognizes objects based on feature vectors. For a two dimensional space, if a prototype object (model object that has the ideal feature values to represent all the reference images of a particular species) is used, the situation is illustrated in figure 2.6

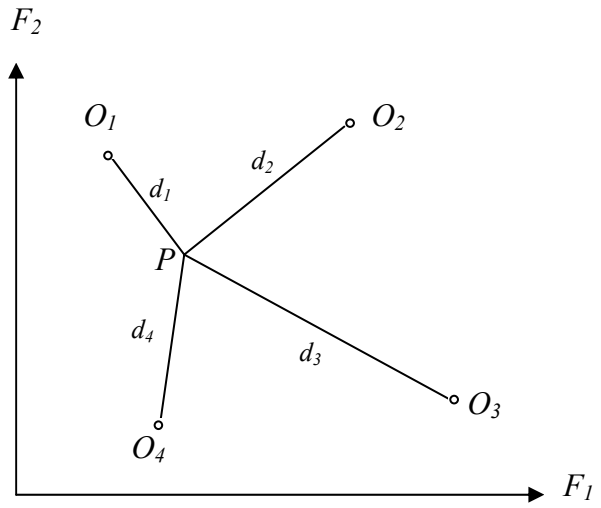

Figure 2.6. Nearest Neighbourhood Classifier. Point *P* represents the test image. Points O_1, O_2, O_3 and O_4 are the Prototypes of reference images. d_1, d_2, d_3 *and* d_4 are the Euclidean distances between the feature vectors of point *P* and the points O_1, O_2, O_3 and O_4 respectively (adopted from Jain *et al.*, 1995).

The Euclidean distance *d* between the feature vectors of the test image and a reference image can be calculated using the following formula.

$$d = \left(\sum_{i=0}^{Nc} \left| f_p^i - f_o^i \right|^2\right)^{1/2}$$

Where f_p is the feature vector for test image and f_o is the feature vector for a reference image. *Nc* is the number of harmonics needed to index the shape. If d_i is the distance between the test image and the i^{th} reference image then the test image can be assigned to the reference image R where

$$d_R = \min_{i=1}^{M}[d_i].$$

M is the number of reference images

Figure 2.7 illustrates the situation where no prototype object is found.

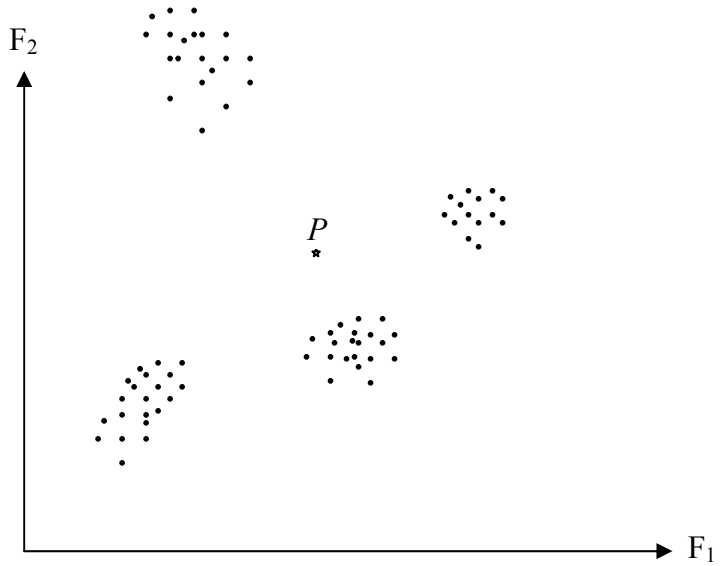

Figure 2.7. Feature space where no prototype species can be found. All reference images of a particular species are represented as a cluster of points in the feature space. Point *P* represents the test image (adopted from Jain *et al.*, 1995).

In figure 2.7, each species represents a cluster of points in the feature space. Therefore, either the distance to the closest point or the distance to the centroid of the cluster of points of each species from the test image can be considered.

Chapter 3

Plant biometrics

Identification of plants is currently a very demanding and time-consuming task and mainly carried out by botanists using morphological features such as number of ovaries in the fruit and number of stamens in the flower. Generally, these features are subjectively extracted by manual inspection. To make this task more efficient and accurate, various studies have been carried out to automate plant identification process with the aid of image processing techniques.

Automatic recognition of wild flowers using shape features of leaves and flowers (Saitoh & Kaneko, 2000), leaf image retrieval with combination of different shape based features of leaves (Wang *et al*., 2000), feature extraction of leaves using image processing techniques (Cunha, 2003), and recognizing plant species of Acer family by leaf shapes (Im *et al*., 1998) are examples of studies pursuing computer based plant biometrics. Most of the studies were based on global shape descriptors (area, perimeter, width and length, compactness, eccentricity) (Cunha, 2003; Saitoh & Kaneko, 2000; Wang *et al*., 2002), global representations of leaf peripheral such as polygonal approximations (Im *et al*., 1998; Nam *et al*., 2005a; Nam *et al*., 2005b),

shape signatures (centroid-contour distance) (Wang *et al*., 2000; Wang *et al*., 2002; Wang *et al*., 2003; Saitoh & Kaneko, 2000), and the local feature extraction techniques (angle code histogram) (Wang *et al*., 2002). Others were based on leaf vein extraction using intensity histograms and trained artificial neural network classifiers (Fu & Chi, 2003). Some of them (Wang *et al*., 2003) achieved relatively low accuracy due to the fact that the techniques they applied only extracted global information.

A two-step approach for leaf image retrieval based on the eccentricity (ECC) and centroid-contour distance curve (CCD) was presented by Wang *et al.* (2000). Furthermore, they have proposed a thinning-based starting-point locating algorithm (closest point on the contour for each end-point on the skeleton) for CCD, which is effective in identifying starting-point(s) and reducing the rotation-and-matching time. In the first step, the ECC was used to rank leaf images, and the top scored images are further ranked using CCD together with ECC in the second step. Two data sets, 135 leaf images from one plant and 233 images from ten plants have been used. Results showed that the proposed starting-point locating algorithm is more efficient than the Fourier transformation and the correlation methods.

A further modification to the above method has been done by Wang *et al.* (2003). In this study they have added another feature, angle code histogram (ACH), for the above two-step leaf image retrieval approach. In the second step, in addition to CCD and ECC, ACH was also used to rank the top scored images resulted from the first step described in Wang *et al*. (2000). For locating the starting points, a further improved algorithm (by removing the very short skeleton branches) was also proposed. A database containing 1400 colour leaf images from 140 species have been

used and the results show that this method is computationally more efficient compared to the existing two methods (curvature scale space method and modified Fourier descriptor method) in feature extraction and feature matching time. However, they obtained relatively low recall rates (defined as a percentage of number of returned images which has the same class to the number of database images which have the same class) and it reflects that overall leaf shape only is not sufficient to distinguish different plant species because different species of plants may have very similar leaf shapes. Leaf-features such as leaf margin, shape of the leaf apex and the base, venation, colour and the texture of the leaf surface, leaf arrangement are also very important in plant identification (Wang, *et al.*, 2003).

Using 1032 leaf images, Nam & Hwang (2005) implemented a prototype shape-based leaf image retrieval system. They have used a hybrid-search scheme that uses the leaf shape and the leaf arrangement on the stem. Results showed that their system is more efficient than the methods involving centroid-contour distance curve, Fourier descriptors, curvature scale space descriptor, moment invariant and minimum perimeter polygon. Using the same findings of the study Nam & Hwang (2005) with a new hybrid-search scheme that uses leaf shape, leaf arrangement and venation, Nam *et al*. (2005b) presented a leaf image retrieval system (CLOVER) for mobile devices.

Most of these studies have been carried out to apply image retrieval techniques for a range of leaves without any prior categorization (Nam & Hwang, 2005; Nam *et al*., 2005a; Nam *et al*. 2005b; Saitoh & Kaneko, 2000; Wang *et al*., 2003). However, leaves are very different in shape. Studies show that different shape signatures have different effects on shape retrieval. For example, with character recognition, the shape

signature cumulative angular function has been used most successfully, whereas in discriminating general shapes, centroid distance is more robust (Zhang & Lu, 2001). On the other hand, very limited techniques have been applied to a small range of shapes to ensure successful results. In this case, polygonal approximation is very appropriate for discriminating the images of maple leaves (Im *et al*., 1998).

The remainder of the chapter is organized as follows. The following section, Section 3.1, explains the different biometrics and features, which were used in plant recognition in prior research. Section 3.2 lists out various local and global feature extraction and representation methods related to plant identification.

3.1 Plant Biometrics

3.1.1 Overall leaf shape

Of all the different types of biometrics that have been tested for plant species recognition, overall leaf shape was the most commonly used biometric in previous studies due to its simpler structure, planar shape and the availability of 2D images. However, due to the variations in overall leaf shape of any particular species and the similarities of overall leaf shapes across different species, the recognition task is challenging.

Im *et al*. (1998) tried to recognise species in the maple-family (Acer) and were able to identify nine Maple species (figure 3.1) successfully. According to the overall leaf shape of these species, first he classified them into the two groups: species which

have three apices (figure 3.1(g) to figure 3.1(i)) and species which have more than five apices (figure 3.1(a) to figure 3.1(f)). In the next step, within these two groups, he further classified them into individual species using leaf shape features.

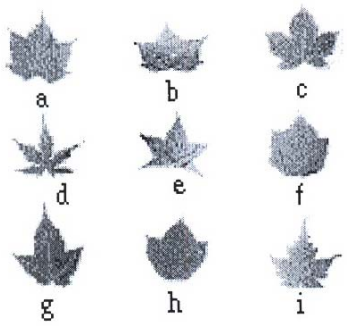

Figure 3.1. Nine maple leaf shapes of the study by Im *et al.* (1998).

With 400 images from 40 different Chrysanthemum varieties, Abbasi *et al*. (1997) introduced a semi-automatic method for leaf classification based on leaf shape. Their method finds the most similar class to an input image and the final decision was done by the user manually. Four classes of images each with 5 sample images are shown in figure 3.2. They had 40 different classes and each class contained 10 sample images.

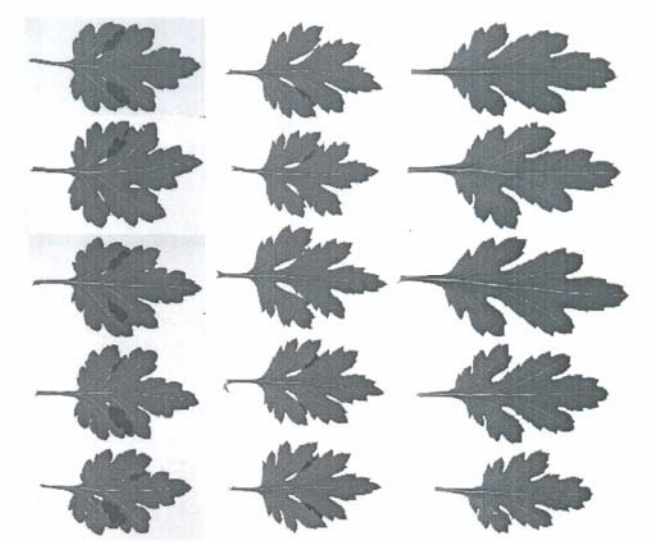

Figure 3.2. Four classes of Chrysanthemum leaf images (adopted from Mokhtarian & Abbasi (2004)).

Considering the images in figure 3.2, one can easily appreciate that the problem of automatic classification of leaf images is a difficult task (figure 3.2 is adopted from Mokhtarian & Abbasi (2004) since they have randomly selected a subset of images from the same database (National Institute of Agricultural Botany leaf images) for both studies: Mokhtarian & Abbasi (2004) & Abbasi *et al.* (1997)).

For a set of simple type leaves, Ye *et al*. (2004) achieved a 71.4% recall rate when the top five returned images were considered. Leaves of a simple type are defined using the following criteria.

1) The leaf should be a single leaf
2) The leaf has no lobes
3) Leaf should be oblong or elliptic or orbiculate shape

They used both text and shape based retrieval system.

Mündermann *et al*. (2003) worked with lobed leaves (such as oak) and proposed a method to model those type of leaves using 2D leaf silhouettes as inputs to their system.

Using shape as the main biometric, Wu *et al*. (2006), Zhang *et al*. (2004), Wang *et al*. (2003), Wang *et al*. (2002) and Wang *et al*. (2000) are the other authors who have tried to develop leaf retrieval systems for a whole range of leaves (without any prior categorization).

One of the difficulties of getting leaf shape as a biometric is the presence of self intersection leaf parts. Mokhtarian & Abbasi (2004) addressed this issue which is a

common problem in 2 dimensional shape representation analysis. The following figure 3.3 illustrates how this can be affected in shape base leaf image retrievals.

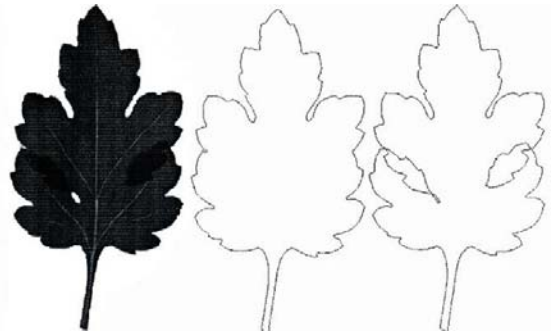

(a) (b) (c)

Figure 3.3. An example of self interaction. (a) Gray level image. (b) The boundary of object without considering self-interaction. (c) The defined new boundary of the object (adopted from Mokhtarian & Abbasi (2004)).

3.1.2 Type of Leaf arrangement

Type of leaf arrangement (figure 3.4) is a very significant feature in manual plant identification. Some authors have tried to include leaf arrangement around the stem of the plant into the biometric system. For example, Nam & Hwang (2005) implemented a prototype shape-based leaf image retrieval system for domestic aquatic plants in Korea. In addition to leaf shape, they also considered the different leaf arrangement around the stem of the plant. Again, the studies of Nam *et al*. (2005a) for recognition of domestic native plants in Korea and Nam *et al*. (2005b), a mobile content-based leaf image retrieval system, show the importance of having the type of leaf arrangement in plant species biometrics.

For all the studies of Nam & Hwang (2005), Nam *et al*. (2005a) and Nam *et al*. (2005b), all the images have been collected from the book "*The Korean Plant Picture Book*". In most cases, it is very difficult to capture the type of the leaf arrangement from normal photographs.

Figure 3.4. Three types of leaf arrangements (adopted from Nam *et al*. (2005a)).

3.1.3 Leaf venation

Leaf vein structure (venation pattern) is another unique feature that differentiates plant species and in manual key-based species identification processes it plays an important role. Though the leaf venation is distinctive and permanent over a period of time it cannot be considered as a reliable biometric since it is not universal (some species do not show a clear venation pattern) and also extraction of venation pattern from an image of a leaf is a challenging task. However, in recent years, a few studies can be seen on venation and vein-like object extraction.

In the study, CLOVER: A Mobile Content-Based Leaf Image Retrieval System, Nam *et al*. (2005b) tried to include vein representation of leaves into their biometric system (again the images were taken from the book "The Korea Plant Picture Book"). Following figure (figure 3.5) shows the different venation patterns they have tried to recognise from leaf images.

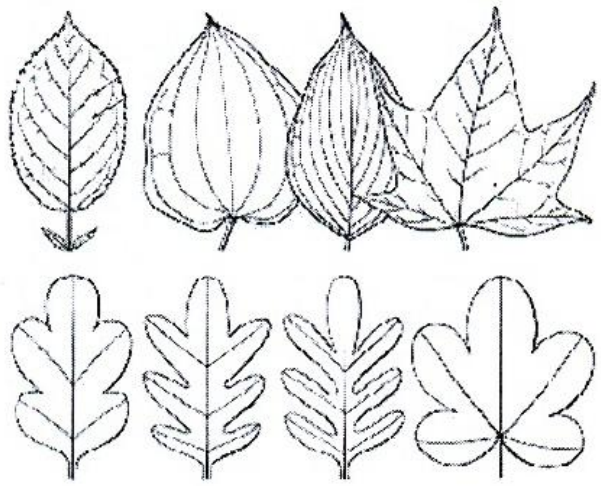

Figure 3.5: Different venation patterns (Adopted from Nam *et al*. (2005b)).

Again, A venation based leaf classification system was introduced by Park *et al*. (2006) using the images from the book “Illustrated flora of Korea”.

Fu & Chi (2003) proposed a two stage approach (a preliminary segmentation based on the intensity histogram of the leaf image and a fine checking using a trained artificial neural network classifier) to extract the venation pattern of twenty one different leaf images and obtained better results than the use of conventional edge detectors. For an example, their method can produce a solid line to represent a vein, while others can only produce two edge lines which are approximately parallel (figure 3.6).

A leaf extraction method based on Snakes technique was introduced by Li *et al*. (2005) and extracted satisfactory venation patterns over some existing edge extraction techniques: Laplacian and adaptive threshold. Their results are shown in Figure 3.7.

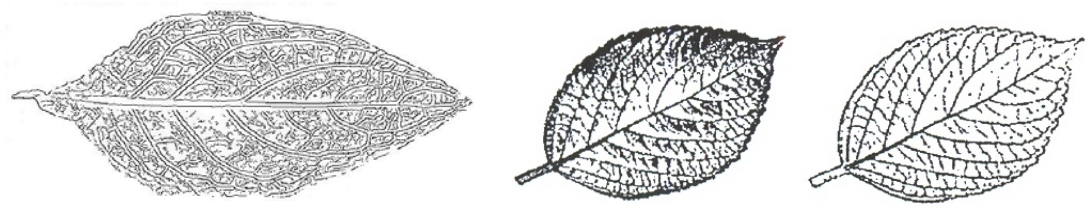

(a) (b)

Figure 3.6. Leaf Venation extracted by two different techniques: (a) Edges detected by the Canny's edge detector, (b) Edges detected by Fu & Chi (2003) (adopted from Fu & Chi (2003)).

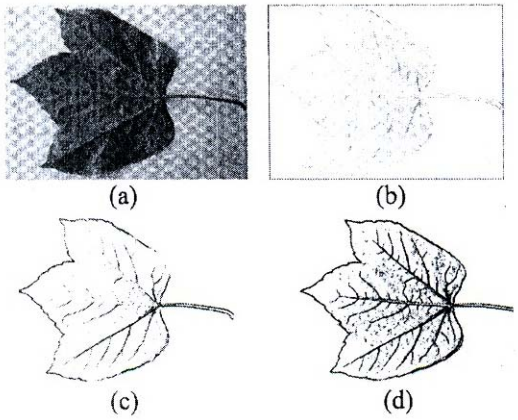

Figure 3.7. The results of leaf vein extraction by Li *et al*. (2005). (a) Original Image, (b) Edge extraction using Laplacian (c) Edge extraction based on adaptive threshold and (d) Edges from the proposed method (adopted from Li *et al*. (2005)).

3.1.4. Shape of the flower parts

Even though, these are the most important and distinct morphological features in manual plant identification process, due to the following factors it is reasonably difficult to use them in computer vision based biometric systems.

a. Unlike leaves, flower parts are more into 3D shape. So, image matching is comparatively complicated.
b. Compared to leaves flower parts are not easily available.

c. Specimen preparation time: It is very difficult to photograph the flower parts directly since most of them are hidden by the other parts of the flower. Therefore, prior preparation is essential before photograph them.

Using the flower features together with the leaf pattern, a system was developed by Saitoh & Kaneko (2000) for wild flower recognition. They used four shape features (the average petal width over the average petal length, number of petals, moment around the average point of the flower region, roundness) and four colour features (based on HSV values) of flowers.

3.1.5 Bark patterns

Plant barks also show distinguishable patterns, which allow humans to recognise them satisfactorily. Chi *et al*. (2003) proposed an effective technique to recognize plants using their bark texture features, which was extracted from the bark images of eight plant species.

3.2 Feature extraction and representation

3.2.1 Polygonal approximation

A boundary can be approximated by a polygon with arbitrary accuracy. The approximation is exact when the number of segments in the polygon is equal to the number of points in the boundary for a closed curve. There are many different approaches to approximate the boundary of a shape by a polygon with the fewest number of vertices while preserving the “essence” of the boundary shape (Gonzalez *et al*., 2004; Rosin, 2003).

Im *et al*. (1998) represented contours of leaves by polygons whose vertices are critical points of curvature of contours (figure 3.8).

Polygonal approximation

Polygonal approximation of a mid-most piece of a leaf

Figure 3.8. Polygonal approximation of the selected maple species (adopted from Im *et al*. 1998).

After smoothing the contour of the leaf using the Gaussian filter (Jain *et al*. (1995), curvature was calculated and the points that have positive high curvatures were selected as the critical points of the contour. The polygonal approximation composed of n line-segments was represented by the tuple (l_1,....., l_n, θ_1, ..., θ_{n-1}), where l_i ($I = 1, \ldots\ldots, n-1$) is the relative arc length between two adjacent nodes, and θ_i ($I = 1, \ldots\ldots, n-1$) is the angle formed by two adjacent segments.

Another attractive approach to polygonal approximation is to find the minimum-perimeter polygon (MPP) of a region or boundary (Gonzalez *et al*., 2004). Figure 3.9 describes the concept of MPP. Figure 3.9(a) is the set of concatenated cells in which the boundary is enclosed. If the boundary is thought of as a rubber band and allowed to shrink within the inner and outer walls of the set of concatenated boundary cells, the result is the minimum-perimeter polygon as in figure 3.9(b).

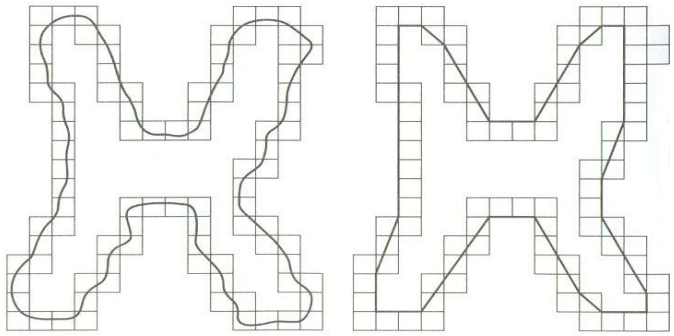

Figure 3.9. Minimum-perimeter polygon. (a) boundary of the shape. (b) Minimum-perimeter polygon (adopted from Gonzalez *et al*. (2004)).

An improved minimum perimeter polygon algorithm was used by Nam *et al*. (2005a), Nam *et al*. (2005b) and Nam & Hwang (2005) to represent leaf contours. Figure 3.10 shows their polygonal approximations for two sample leaves with different cell sizes.

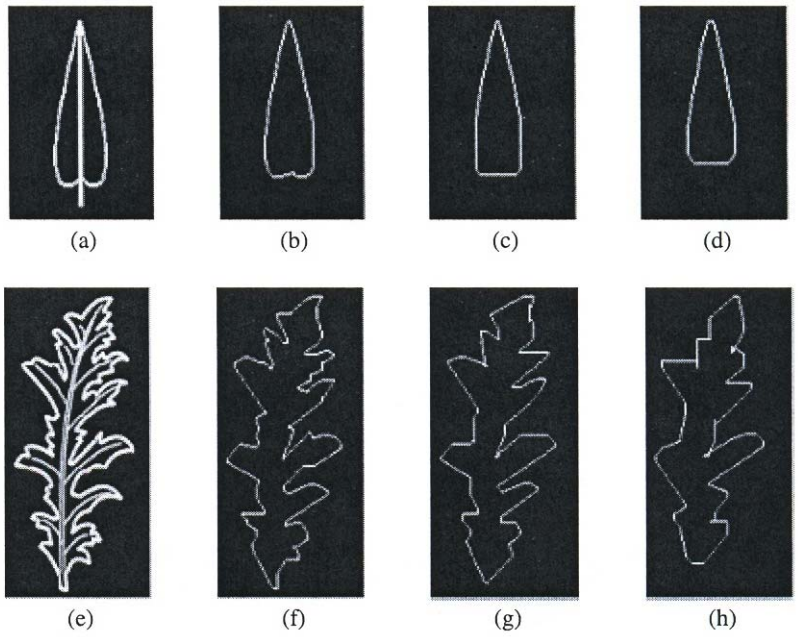

Figure 3.10. Minimum-perimeter polygons of two sample images. (a) & (e) are the original images, (b) & (f), (c) & (g) and (d) & (h) are the minimum-perimeter polygons with the cell size 2, 3 and 5 respectively (adopted from Nam *et al*. (2005a)).

3.2.2. Centroid Distance Curve

Centroid-distance curve is the other commonly used boundary representation method. Here again, as in the polygonal approximation approach, selection of the minimum number of points along the boundary (down-sampling) without loosing the shape information is a challenging task. The larger the number of sampling points, the more details of the shape can be represented and so more accurate results can be obtained with a smaller the number of sampling points to improve computational efficiency but with a reduction in accuracy. Previous studies show different approaches in down-sampling (Ye *et al*., 2004; Wang *et al*., 2003; Wang *et al*., 2002; Zhang & Lu, 2001; Saitoh & Kaneko, 2000; Wang *et al*., 2000) and the most common approaches are

(a) Equal angle sampling: Boundary points are selected so that the central angles between two contour points are equal

(b) Equal arc-length sampling: select boundary points spaced at equal arc length along the boundary

(c) Equal point sampling: selects boundary points spaced at equal number of points along the boundary

(d) High curvature points sampling: The *n* top high curvature points will be selected

3.2.3. Angle code histogram

Since the centroid-distance curve cannot represent local features such as ripples or serrated margins of leaves effectively, some authors prefer to include angle code histogram (Peng & Chen, 1997) in their plant identification process. In this approach, each closed contour is represented by a sequence of line segments with two

successive line segments forming an angle. The angles at contour points on each closed contour are computed and the resulting sequence of successive angles is used to characterise the contour (Wang *et al*., 2003; Wang *et al*., 2002).

3.2.4. Curvature scale space representation

Mokhtarian & Abbasi (2004) and Abbasi *et al*. (1997) represent contours using curvature scale space images. Figure 3.11 shows two curvature scale space images for two leaf contours: one with self-intersection leaf parts and the other without the self-intersection.

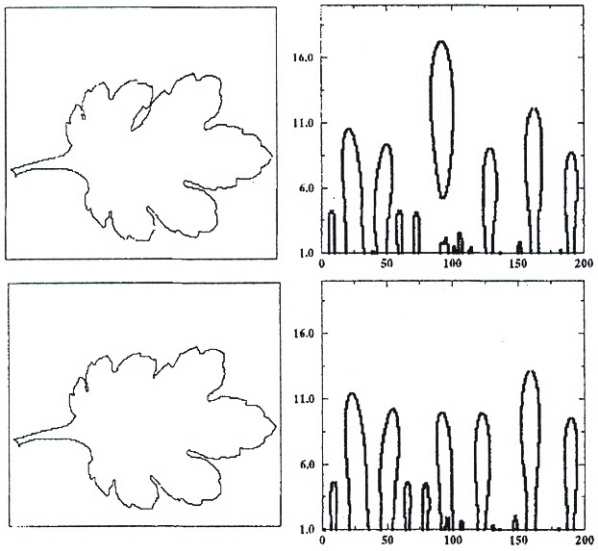

Figure 3.11. Curvature scale space images of two leaf contours (adopted from Abbasi *et al*., 1997).

3.2.5. Global shape descriptors

Global shape descriptors have been used extensively in plant classification. Some of them are listed below with the references.

- Eccentricity: This is a region-based parameter and illustrates how the region points are scattered around the centroid of the region. Eccentricity is a translation, scale and rotation invariant property. Some authors used this feature for the first-stage image retrieval (to select top candidates first) (Mokhtarian & Abbasi, 2004; Wang *et al*., 2003; Wang *et al*., 2000; Wang *et al*., 2002; Abbasi *et al*., 1997).

- Stem length: The ratio of stem length to leaf length is a significant feature in leaf classification. Ye *et al*. (2004) has used this feature to minimize the error of apex or base angle calculation (see below).

- Apex angle (or base angle): Apex angle is defined as the angle from the apex (or base) to the pair of points using a line perpendicular to the mid-vein at a predefined position (Ye *et al*., 2004; Saitoh & Kaneko, 2000)

- Width-length ratio of the leaf: This is the ratio of the maximum width to the maximum length of the leaf. The length of the leaf should be predefined since some authors prefer it without the stem length and others include the stem length (Ye *et al*., 2004; Saitoh & Kaneko, 2000).

- Width-length ratio of the petal: This can be obtained from the centroid-contour distance curve (Saitoh & Kaneko, 2000).

- Aspect ratio of the CSS image: This reflects the size of the major concavity of the image boundary (Mokhtarian & Abbasi, 2004; Abbasi *et al*., 1997).

- Circularity: This measures the roundness or the compactness of a shape (Mokhtarian & Abbasi, 2004; Saitoh & Kaneko, 2000; Abbasi *et al*., 1997)

- Number of petals: This is obtained from the centroid-contour distance curve. In some flowers number of petals are only countable by manual inspection but not by image processing (Saitoh & Kaneko, 2000)

- Moments: A set of moments which are invariant to translation, rotation and scale are usually used in region-based shape representation (Wu *et al*., 2006; Saitoh & Kaneko, 2000).

- Solidity: Solidity expresses the degree of splitting depth in a leaf.

$$Shape\_solidity = \frac{S_1}{S_2},$$

where S_1 is the internal area connecting the valley points of leaf dents and S_2 is the external area connecting the top points (Wu *et al*., 2006; Saitoh & Kaneko, 2000)

- Margin Coarseness: This feature expresses the coarseness of the leaf margin.

$$M\arg in\_coarseness = \frac{P}{P'},$$

where P is the perimeter of leaf contour, and P' is the length of internal boarder (Wu *et al*., 2006)

Chapter 4

Biometric Development

The proposed plant biometric system integrated a number of processes: specimen collection and image preparation, binarisation, leaf boundary detection, normalisation, shape representation, information extraction and finally shape retrieval.

4.1 Specimen collection

A corpus of two hundred (200) leaf images was collected from forty (40) different plant species. For each species, five leaves were collected from different trees. The species were named with the alphabetical letters in the sequence of a, b, c, …..z, aa, ab, ac…..etc. The numbers from 1 to 5 followed by the species name was used to differentiate various images of the same species. For example, a1, a2, a3, a4 and a5 are the five different leaves collected from the species "a". From each species one image was considered as the query image and the other four images were kept as reference images.

4.2 Image preparation

Coloured Photographs of all the 200 leaves were taken using a five Mega pixel digital camera with a contrasting background under normal light conditions. All the images were stored as .pgm (portable gray map) files.

4.3 Thresholding with auto adaptive thresholding algorithm

Because leaf colour and background lighting at the time the photograph was taken differ from image to image, a single threshold cannot be applied to binarize all the images. Therefore, an auto adaptive thresholding technique based on the intensity histogram of the image was constructed. This technique uses the following three steps.

1. An intensity histogram is constructed using the grayscale indices of the pixels.
2. Identify the two major peaks (ranges that give the maximum number of pixels) which corresponds to the object and the background.
3. Obtain the range that gives the minimum number of pixels between the two major peaks identified in step 2. Median of this range is calculated as the threshold.

Figure 4.1 shows the grayscale image (a) and the binarized image (b) of a sample leaf image with the intensity histogram (c). Table 4.1 is the corresponding frequency table.

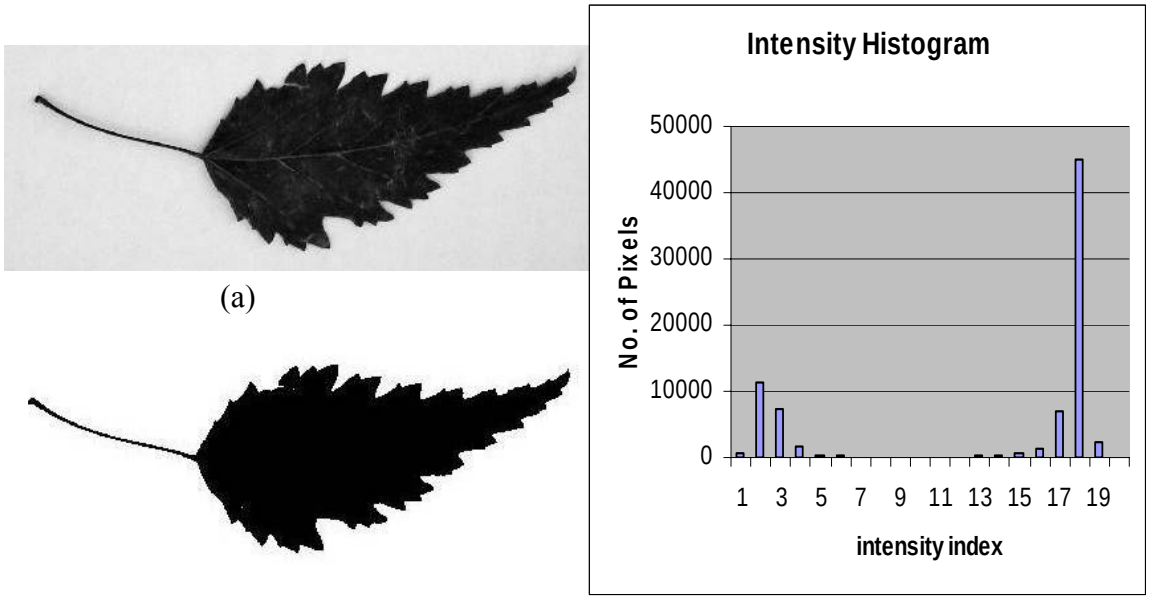

(a)

(b)

(c)

Figure 4.1. (a) Grayscale image, (b) Binarized image, (c) Intensity histogram.

Index	Range	Frequency
1	0 - 12	509
2	13 - 25	11224
3	26 - 38	7420
4	39 - 51	1586
5	52 - 64	461
6	65 - 77	215
7	78 - 90	137
8	91 - 103	103
9	104 - 116	89
10	117 - 129	103
11	130 - 142	118
12	143 - 155	136
13	156 - 168	197
14	169 - 181	274
15	182 - 194	564
16	195 - 207	1342
17	208 - 220	6962
18	221 - 233	45113
19	234 - 246	2449
20	247 - 255	0

Peak frequency that corresponds to the object

Selected frequency to calculate the threshold

Peak frequency that corresponds to the background

Table 4.1. Frequency table that corresponds to the leaf image in figure 4.1 (a)

4.4 Boundary detection

The uppermost left pixel of the object was considered as the starting point of the list of boundary points (edgelist[0]). The boundary following algorithm (section 2.1.1), was applied to the images. Resulted ordered list of boundary points (x and y coordinates of the image boundary in a clockwise sequence) was stored in a structure array (edgelist[]).

For example, The list of boundary points and the boundary image of the image in figure 4.1(b) are in table 4.2 and figure 4.2 respectively.

Edgelist index(i)	Boundary Coordinates	
	x	y
0	85	154
1	86	153
2	87	152
3	88	152
-	-	-
-	-	-
546	485	150
547	484	151
548	483	151
549	482	152
550	481	152
551	480	152
-	-	-
-	-	-
1109	89	156
1110	88	156
1111	87	156
1112	86	156
1113	85	156
1114	85	155

Table 4.2. Edgelist of the image in figure 4.1(b). Some parts of the list have been omitted.

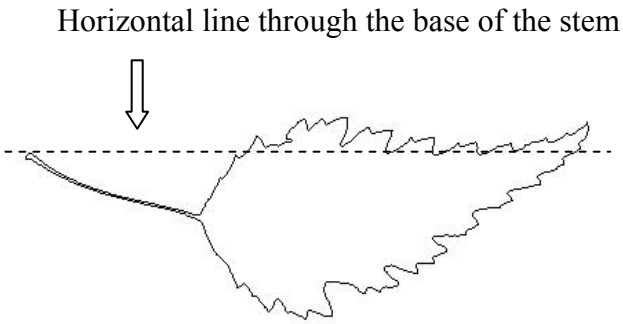

Figure 4.2. Boundary image of the image in figure 4.1(b).

The complete source code for boundary following algorithm is given in Appendix II (a).

4.5 Contour rotation

All the pictures were taken so that the stem of the leaf resides the left side of the image (i.e. the leftmost point always to be a pixel at the tip of the stem) as in figure 4.1(a).To maintain the rotational invariant property, all the contours were rotated until the line connecting the leftmost point and the furthermost point from the leftmost point becomes horizontal. The technique of achieving rotational invariant property by contour rotation is explained in figure 4.3.

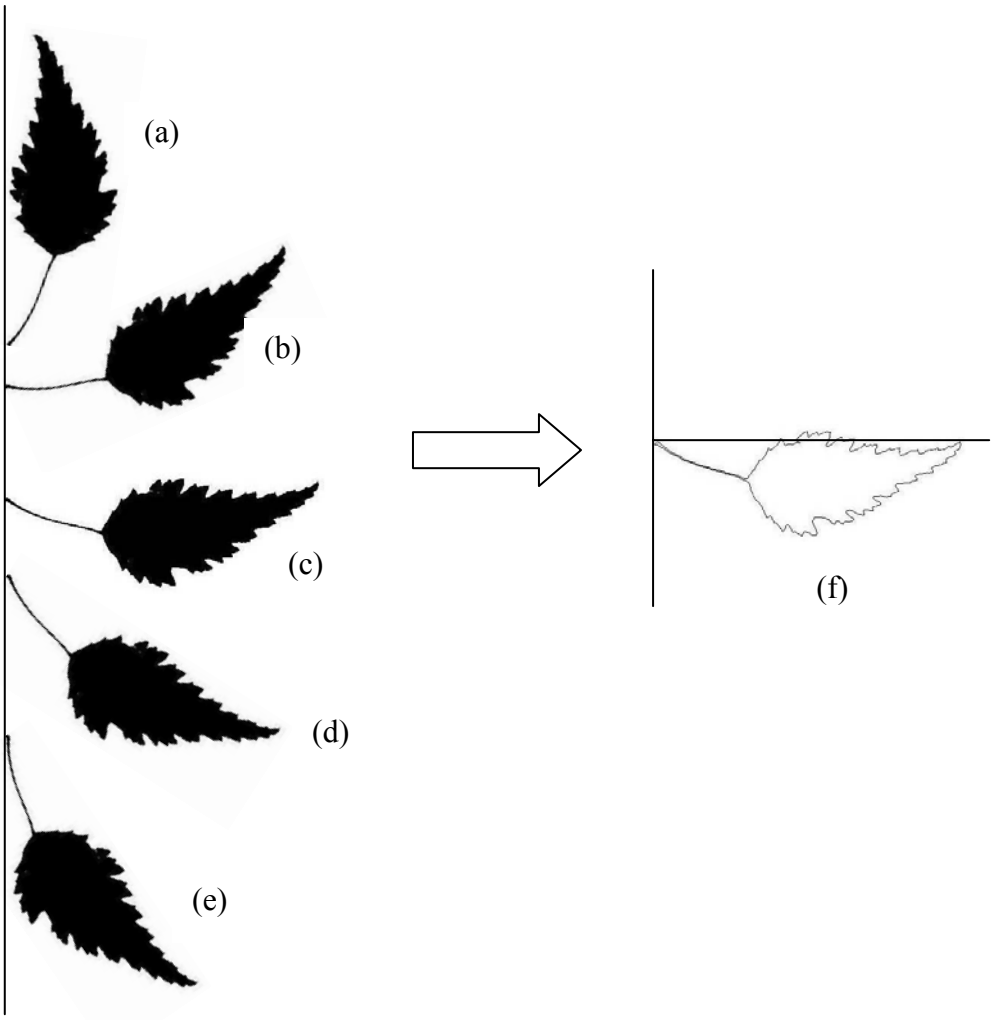

Figure 4.3. Illustration of the contour rotation technique. All these positions, (a), (b), (c), (d) and (e) of the sample leaf image gives the same contour image in (f) due to the contour rotation technique.

A new list of boundary points was computed for each image (after rotation). For example, the new list of boundary point for the image in figure 4.3(f) is in table 4.3.

Edgelist Index(i)	Boundary Coordinates	
	x	y
0	76	158
1	78	157
2	79	156
3	80	156
-	-	-
-	-	-
546	476	174
547	475	175
548	474	175
549	473	176
550	472	176
551	471	176
-	-	-
-	-	-
1109	80	160
1110	79	160
1111	78	160
1112	77	160
1113	76	160
1114	76	159

Table 4.3. Adjusted edgelist (after rotation) of the image in figure 4.3(f). Some parts of the list have been omitted.

4.6 Shape representation

4.6.1 Contour representation with shape signatures

Following four shape signatures were calculated to represent the leaf boundary. The first two are the most common shape signatures used in shape-based image retrieval systems found in the literature. The latter two proposed shape signatures were

specially designed for leaf image retrieval for the plant biometric presented in this thesis.

1. Centroid-distance (described in section 2.2.2.1)
2. Complex-coordinates (described in section 2.2.2.2)
3. Distribution of full-width to length ratio

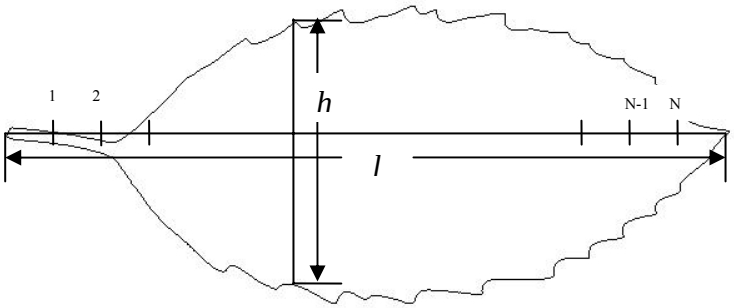

Figure 4.4. Full-width to length ratio.

If the line that represent the maximum length of the leaf is divided into N equal segments and *h(t)* is the width of the leaf at the point which divide the line at a ratio t : N-t, then full-width to length ratio function can be defined as

$$p(t) = \frac{h(t)}{l} \quad t = 1, 2, \ldots\ldots N\text{-}1$$

4. Distribution of half-width to length ratio

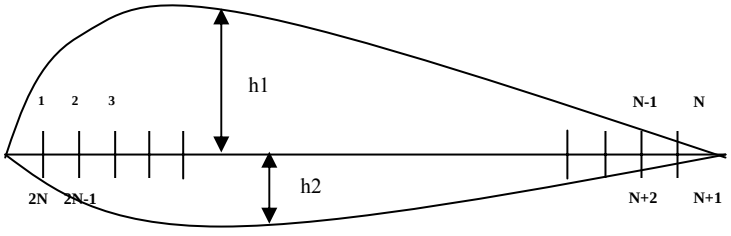

Figure 4.5. Half-width to length ratio.

The line that connects the base and the tip of the leaf (mid rib line) is used to divide the leaf into two parts, upper and lower. N number of points are marked on that line with equal distance. For the upper half, these points are numbered from 1 to N (from the base of the leaf) and for the lower half, these are numbered from N+1 to 2N (from the tip of the leaf). Then half-width to length ratio function $p(t)$ can be defined as

$$p(t) = h_1(t) \qquad t=1, 2, \ldots N$$
$$= h_2(t) \qquad t= N+1, N+2, \ldots, 2N$$

where $h_1(t)$ is the width of upper half of the leaf and $h_2(t)$ is the width of upper half of the leaf at point t. This signature is useful to measure the asymmetry of the leaf blade.

4.6.1.1 Shape normalization (number of sampling points = 2^n, $n \in N$)

For matching purposes, the shape boundary of the object and models must have same number of data points. In addition to that, to facilitate the use of fast Fourier transform, the number of sampled points should be a power-of-two integer. For the shape signatures, complex-coordinates and centroid-distance, equal arclength sampling was used to normalize the sizes of the shapes. The equal arclength sampling method selects candidate points spaced at equal arc length along the shape boundary. For the shape signatures full-width to length ratio and half-width to length ratio, sampling points are selected as described in figure 4 and figure 5.

For example, the biometric vectors obtained from above four shape signatures: centroid-distance, complex-coordinates, full-width to length ratio distribution and

half-width to length ratio distribution for the image in figure 4.3(f) are shown in table 4.4 to table 4.7 respectively.

Vector Index	Value	Vector Index	Value	Vector Index	Value	Vector Index	Value
0	0.536591	16	0.140392	32	0.426731	48	0.159333
1	0.492891	17	0.094609	33	0.397066	49	0.201354
2	0.44966	18	0.134089	34	0.370617	50	0.195849
3	0.404679	19	0.157798	35	0.32866	51	0.20543
4	0.362753	20	0.137801	36	0.3093	52	0.204976
5	0.318712	21	0.16995	37	0.268066	53	0.210299
6	0.277492	22	0.207351	38	0.258668	54	0.218399
7	0.237125	23	0.207119	39	0.224903	55	0.211012
8	0.203431	24	0.255338	40	0.2212	56	0.219346
9	0.18266	25	0.285263	41	0.221634	57	0.240209
10	0.166739	26	0.315796	42	0.201473	58	0.280099
11	0.159784	27	0.350156	43	0.176913	59	0.321312
12	0.121515	28	0.391743	44	0.17732	60	0.365196
13	0.128624	29	0.433955	45	0.186339	61	0.407047
14	0.131989	30	0.479804	46	0.178938	62	0.451786
15	0.127451	31	0.460497	47	0.150471	63	0.494843

Table 4.4. Biometric vector for centroid-distance signature of the image in figure 4.3(f).

vector index	x	y	vector index	x	y	vector index	x	y	vector index	x	y
0	-217	-29	16	16	-55	32	172	-27	48	-1	65
1	-200	-21	17	11	-37	33	161	-18	49	5	82
2	-183	-13	18	28	-47	34	151	-8	50	-12	79
3	-165	-6	19	44	-47	35	134	-5	51	-25	80
4	-148	-1	20	44	-35	36	126	7	52	-37	75
5	-130	3	21	58	-38	37	109	9	53	-51	69
6	-113	7	22	74	-41	38	103	23	54	-64	62
7	-96	12	23	79	-30	39	88	26	55	-74	44
8	-83	0	24	97	-38	40	84	33	56	-85	28
9	-73	-15	25	111	-35	41	79	44	57	-97	14
10	-62	-28	26	124	-35	42	66	49	58	-114	8
11	-49	-43	27	139	-33	43	53	49	59	-131	5
12	-33	-37	28	155	-39	44	47	55	60	-149	0
13	-27	-45	29	172	-42	45	44	62	61	-166	-5
14	-14	-52	30	189	-51	46	29	67	62	-184	-11
15	0	-52	31	184	-38	47	13	60	63	-201	-19

Table 4.5. Biometric vector for complex-coordinates shape signature of the image in figure 4.3(f). x and y are the real and imaginary parts of each vector element respectively.

Vector Index	Value	Vector Index	Value	Vector Index	Value	Vector Index	Value
0	0.012225	16	0.002445	32	0.315403	48	0.146699
1	0.007335	17	0.002445	33	0.332518	49	0.156479
2	0.007335	18	0.00489	34	0.271394	50	0.144254
3	0.00489	19	0.01467	35	0.281174	51	0.117359
4	0.00489	20	0.08313	36	0.286064	52	0.09291
5	0.002445	21	0.124694	37	0.266504	53	0.100244
6	0.002445	22	0.158924	38	0.268949	54	0.100244
7	0.002445	23	0.217604	39	0.276284	55	0.080685
8	0.002445	24	0.224939	40	0.266504	56	0.06846
9	0.002445	25	0.254279	41	0.266504	57	0.070905
10	0.002445	26	0.293399	42	0.207824	58	0.07335
11	0.002445	27	0.264059	43	0.220049	59	0.056235
12	0.002445	28	0.276284	44	0.207824	60	0.046455
13	0.002445	29	0.288509	45	0.215159	61	0.046455
14	0.002445	30	0.325183	46	0.200489	62	0.031785
15	0.00489	31	0.325183	47	0.168704	63	0.03423

Table 4.6. Biometric vector for full-width to length ratio distribution of the image in figure 4.3(f)

Vector Index	Value	Vector Index	Value	Vector Index	Value	Vector Index	Value
0	0.00978	16	0.02934	32	0.04401	48	0.298288
1	0.031785	17	0.031785	33	0.06846	49	0.290954
2	0.051345	18	0.036675	34	0.095355	50	0.283619
3	0.061125	19	0.017115	35	0.0978	51	0.259169
4	0.07335	20	0.012225	36	0.122249	52	0.232274
5	0.080685	21	0.017115	37	0.129584	53	0.185819
6	0.08802	22	0.007335	38	0.161369	54	0.124694
7	0.0978	23	0.00489	39	0.176039	55	0.110024
8	0.105134	24	0.02445	40	0.205379	56	0.102689
9	0.114914	25	0.017115	41	0.217604	57	0.09291
10	0.07335	26	0.036675	42	0.229829	58	0.08313
11	0.03912	27	0.02445	43	0.256724	59	0.075795
12	0.00978	28	0.031785	44	0.256724	60	0.06357
13	0	29	0.022005	45	0.254279	61	0.05379
14	0.002445	30	0.01956	46	0.242054	62	0.036675
15	0.031785	31	0.012225	47	0.300734	63	0.017115

Table 4.7. Biometric vector for half-width to length ratio distribution of the image in figure 4.3(f).

4.6.2 Polygonal approximation

All the contours were approximated with polygons using the hop-along algorithm (section 2.2.4.1). Indices of the edges of the edgelist that correspond to the vertices of the polygon were stored in an integer array. For example, figure 4.6 shows the different approximated polygons resulted from hop-along algorithm for the image in figure 4.1(b) with different parameter values. For each vertex, the corresponding index from the boundary list in table 4.3 is in table 4.8.

The source code for this hop-along algorithm is listed in Appendix II (b).

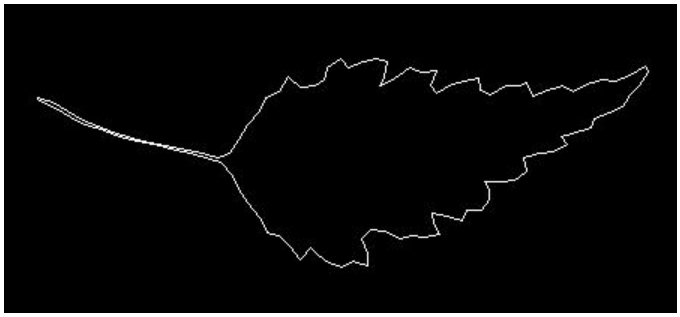

(a) Number of vertices = 105

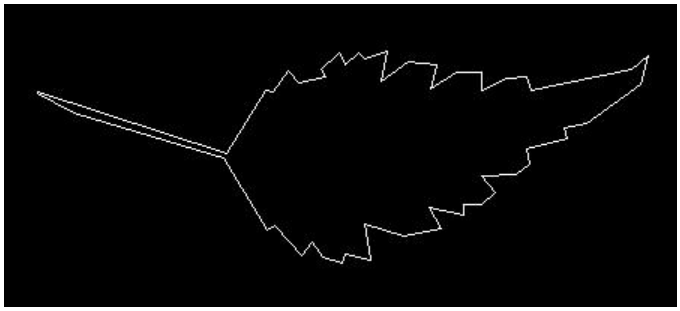

(b) Number of vertices = 52

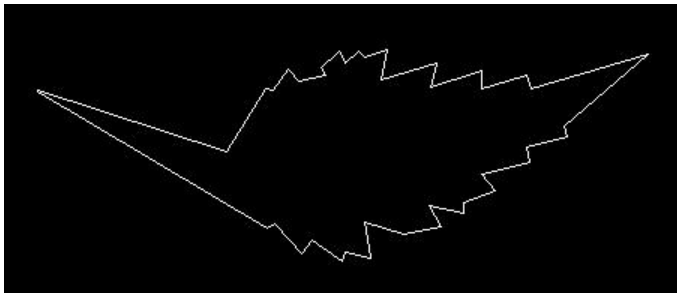

(c) Number of vertices = 42

Figure 4.6. Several polygonal approximations to the image in figure 4.1(b).

Vertex number	N	Vertex number	N	Vertex number	N	Vertex number	N
1	0	14	297	27	594	40	803
2	126	15	315	28	609	41	830
3	171	16	336	29	616	42	854
4	176	17	352	30	644	43	871
5	190	18	370	31	654	44	877
6	199	19	388	32	665	45	890
7	217	20	400	33	688	46	900
8	225	21	417	34	702	47	910
9	239	22	431	35	716	48	934
10	248	23	440	36	728	49	939
11	257	24	512	37	735	50	989
12	262	25	524	38	758	51	1089
13	277	26	544	39	775	52	1114

Table 4.8. Vertices of the approximated polygon of the image in figure 4.3(f). N is the corresponding index of the boundary list in table 4.3.

4.7 Stem Detection

It is clear that for all the leaf images, the uppermost left point of the image is the starting point of the stem. An algorithm (described below) was developed to find the end-point of the stem where figure illustrates the terms used in this algorithm.

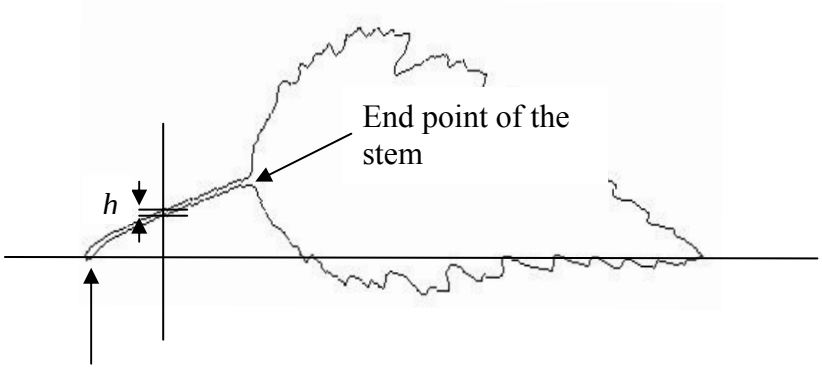

Figure 4.7. Stem detection process.

Stem detection algorithm

1. Starting from the starting point of the stem, a vertical line is moved along the horizontal line (the line that connects the most left and most right points of the image).
2. At each point of the horizontal line the two intersection points of the vertical line and the contour is obtained by traversing along the contour in both clockwise and anticlockwise directions.
3. The distance between the two intersection points (step 2) is calculated as the vertical height of the contour (*h*).
4. This process is continued until *h* becomes greater than a threshold value. At this position, the middle point of the line connecting the two intersectional points is calculated as the end-point of the stem.

In step 2 of the above algorithm, traversing is in both a clockwise and anticlockwise direction to search for the two intersectional points which is essential since otherwise it could lead to erroneous results for some leaves. For example, the following leaf contour (figure 4.8) has more than two intersectional points at the end of the stem.

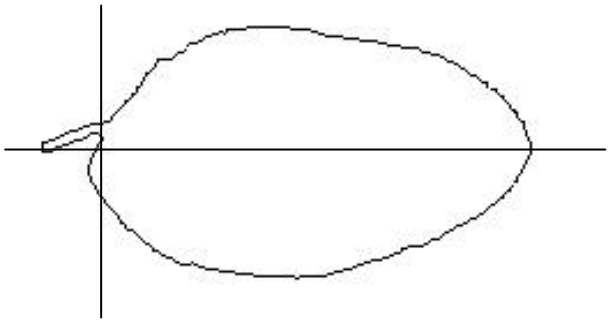

Figure 4.8. Leaf with oblique base .

The threshold value in step 4 was determined by analysing the leaf width to length ratio distributions of all the leaf images (figure 4.9) and 0.04 was taken as the threshold value since for stems, this distribution is always less than 0.04 (except the leaves without stems).

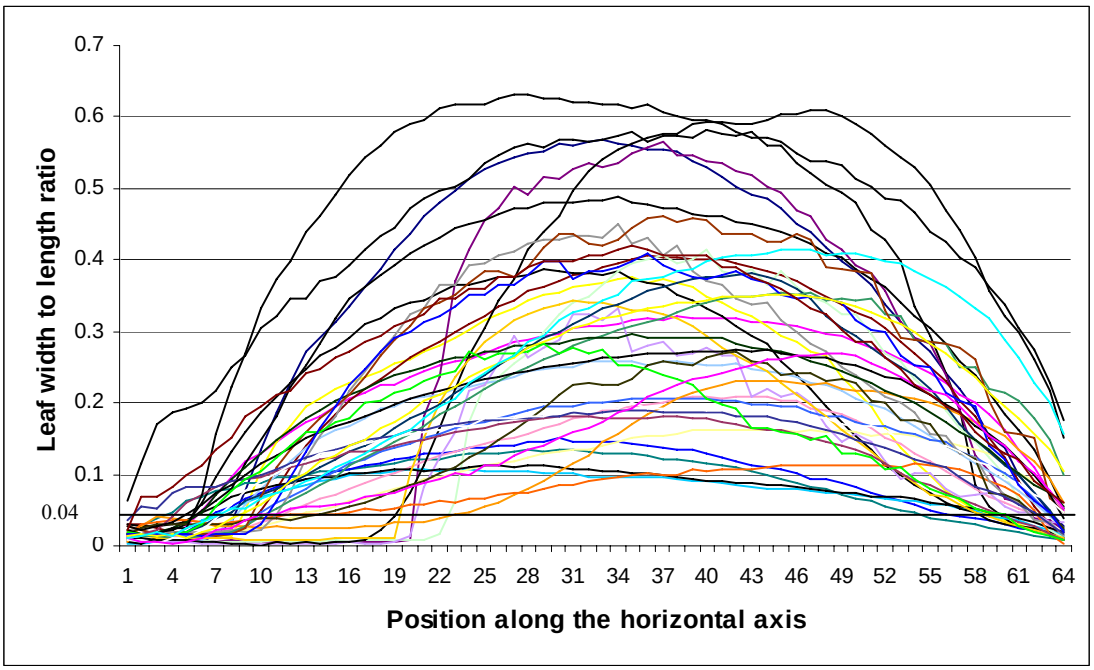

Figure 4.9. leaf width to length ratio distribution. For clarity, a line corresponds to one image of each species is shown here.

4.8 Global shape descriptors

Area, perimeter and compactness were calculated for each leaf. Compactness is measured by P^2/A, where P and A are perimeter and area respectively. In addition to these descriptors, the ratio, perimeter to maximum length is also calculated. These parameter values for four selected leaves are in figure 4.10.

(a)

Compactness = 20.72

Perimeter/length =

(b)

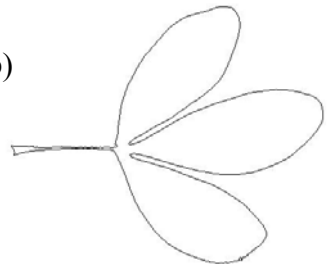

Compactness = 61.20

Perimeter/length = 4.2

(c)

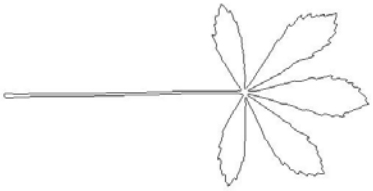

Compactness = 204

Perimeter/length =

(d)

Compactness = 23.68

Perimeter/length = 2

Figure 4.10. Compactness and the perimeter to maximum length ratio of four selected leaves. (a). Simple leaf with a coarse margin, (b). Tri-foliate leaf, (c). Five-foliate leaf and (d). Simple leaf with a smooth margin.

4.9 Extraction of local information

Other than the shape signatures and global shape descriptors, local information of leaf margins: margin coarseness, stem length to leaf blade length ratio and curvature of leaf tip were analysed and quantified.

4.9.1 Margin coarseness

After a polygonal approximation, type of the leaf margin (simple or serrate) and the number of teeth per predefined length was obtained by analyzing the polyline

segments of the leaf margin. The whole leaf contour was divided into four sections along the horizontal axis with equal lengths. Then convex vertices of the middle two upper parts of the contour were counted and taken as the number of teeth (figure 4.11).

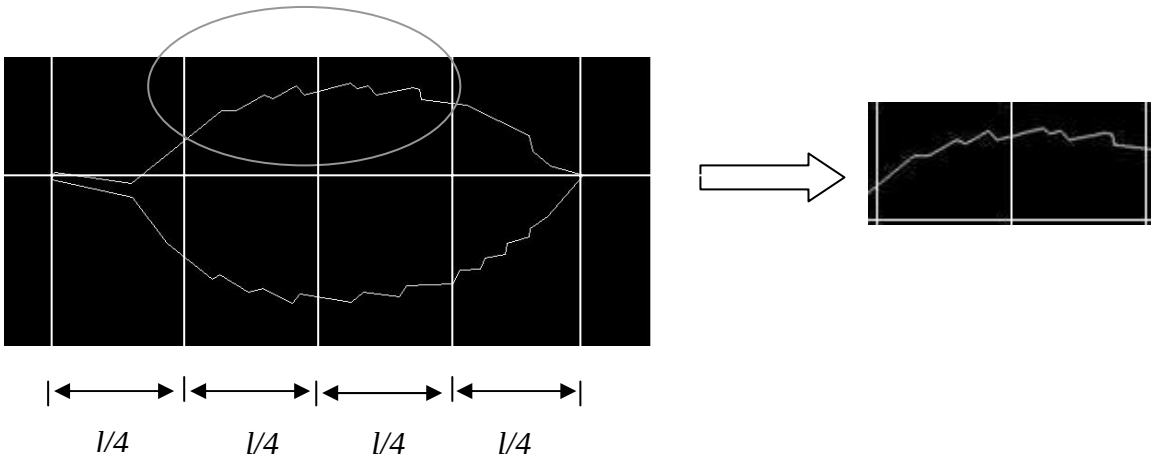

Figure 4.11. Coarseness calculation of leaf margin. *l* is the length of the leaf.

4.9.2 Stem length to blade length ratio

Stem length was detected using the stem detection process (section 4.7) and stem length to blade length ratio (figure 4.12) was calculated in all the 200 leaf images.

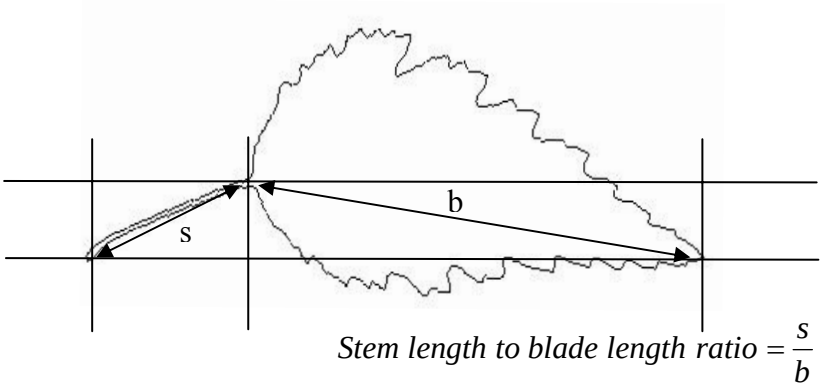

Figure 4.12. Stem length and blade length of a leaf.

4.9.3 Curvature of the leaf tip

The whole leaf length was divided into 16 parts (fig 4.13) and the difference between the gradients of two contour segments (between the lines *a* and *b,* and the lines *b* and *c*), tan ($\theta_{1)}$ and tan ($\theta_{2)}$ was calculated as the curvature.

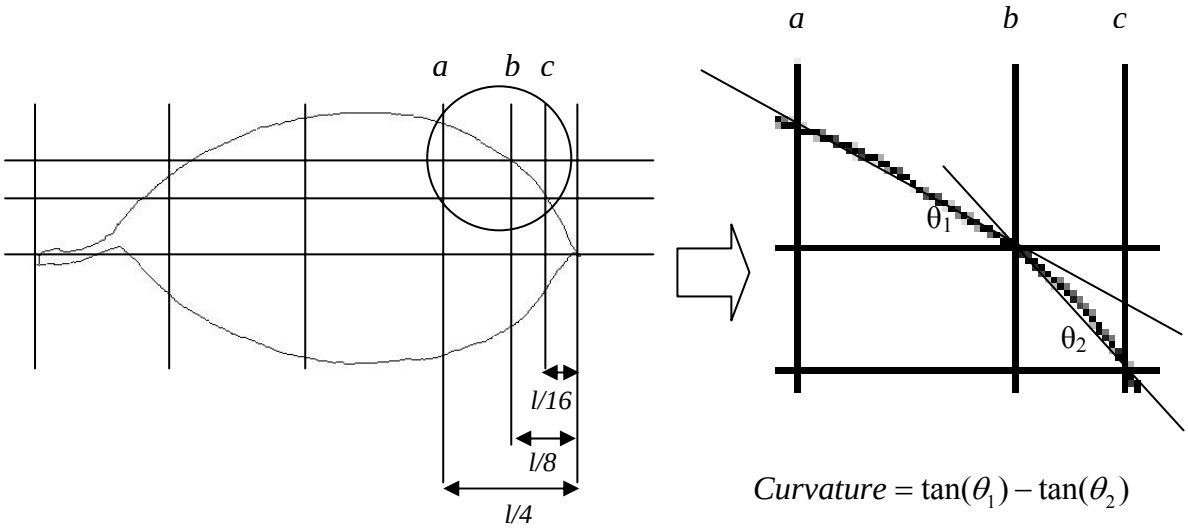

Figure 4.13. Calculation of leaf tip curvature (*l* is the total leaf length).

4.10 Shape retrieval with biometric vectors

Out of the four shape signatures described in section 4.6.1, centroid-distance, full-width to length ratio and the half-width to length ratio are invariant to scale, translation and rotation. The reference images were matched with the query image with these three shape signatures. Shapes cannot directly be matched with complex-coordinates since it is not invariant to scale and rotation.

4.10.1 Discrete Fourier transform on shape signatures

Fourier descriptors (FDs) are compact and easy to handle. Rotational invariance can easily be achieved with them. All leaf shapes were matched using the Fourier descriptors obtained from the above four signatures.

- **Invariant feature vectors for each shape signature (to index the shape**)

For complex-coordinates, all the N descriptors except the first one are needed to index the shape (1st descriptor depends only on the position of the shape and can be discarded). These descriptors are invariant to translation since their corresponding signatures are invariant to translation. By ignoring the phase information and taking only the magnitude values of FDs, rotational invariance can be achieved. Scale normalization is achieved by dividing the magnitude values of all other descriptors by the magnitude value of the second descriptor. The invariant feature vector used to index the shape is then given by

$$f = [\frac{|FD_2|}{|FD_1|}, \frac{|FD_3|}{|FD_1|}, ..., \frac{|FD_{N-1}|}{|FD_1|}]$$

Since all the other shape signatures (except complex-coordinates) are real valued, there are only N/2 different frequencies in the Fourier transform and therefore, only half of the Fourier descriptors are needed to index the shape. For centroid-distance signature, after dividing the first half of FDs by the first FD (to achieve the scale invariance) invariant feature vector obtained is

$$f = [\frac{|FD_1|}{|FD_0|}, \frac{|FD_2|}{|FD_0|}, ..., \frac{|FD_{N/2}|}{|FD_0|}]$$

Shape signatures, full-width to length ratio and half-width to length ratio are all invariant under translation, rotation and scale. Therefore, the invariant feature to index the shape is

$$f = [|FD_0|, |FD_1|, ..., |FD_{N/2}|]$$

- **Similarity measure**

The Euclidean distance *d* between two feature vectors can be used as the similarity measurement.

$$d = (\sum_{i=0}^{Nc} |f_m^i - f_d^i|^2)^{1/2}$$

where f_m is the feature vector for model shape and f_d is the feature vector for a data shape. *Nc* is the number of harmonics needed to index the shape.

The biometric vectors of complex-coordinates, centroid-distance, full-width to length ratio and half-width to length ratio for the image in figure 4.3(f) are shown in table 4.9 to table 4.12 respectively.

Vector Index	Value
0	0.256069
1	0.353167
2	0.162165
3	0.081317
4	0.036947
5	0.006287
6	0.023956
7	0.009047
8	0.020614
9	0.011936
10	0.040088
11	0.001585
12	0.004219
13	0.013321
14	0.016496
15	0.006813

Vector Index	Value
16	0.0044
17	0.013929
18	0.012731
19	0.009116
20	0.011241
21	0.023411
22	0.010002
23	0.013707
24	0.004702
25	0.005892
26	0.007641
27	0.012285
28	0.009784
29	0.015882
30	0.006148
31	0.007679

Vector Index	Value
32	0.008857
33	0.013159
34	0.007449
35	0.008732
36	0.01433
37	0.009003
38	0.0213
39	0.007676
40	0.012677
41	0.013031
42	0.009087
43	0.013196
44	0.02273
45	0.02285
46	0.006339
47	0.027058

Vector Index	Value
48	0.022159
49	0.027072
50	0.002832
51	0.011512
52	0.011902
53	0.024079
54	0.01241
55	0.084308
56	0.046318
57	0.103451
58	0.068931
59	0.148688
60	0.123149
61	1.985428

Table 4.9. Biometric vector: Fourier descriptors of complex-coordinates of the image in figure 4.3(f)

Vector Index	Value	Vector Index	Value	Vector Index	Value	Vector Index	Value
0	0.052462	8	0.02734	16	0.020172	24	0.006824
1	0.515858	9	0.019672	17	0.002893	25	0.003029
2	0.092421	10	0.023021	18	0.005733	26	0.004585
3	0.222892	11	0.011975	19	0.00479	27	0.00421
4	0.073342	12	0.028039	20	0.012156	28	0.005311
5	0.098169	13	0.011083	21	0.003691	29	0.009712
6	0.027524	14	0.01011	22	0.011771	30	0.002439
7	0.036405	15	0.004484	23	0.010175	31	0.01233

Table 4.10. Biometric vector: Fourier descriptors of centroid-distance of the image in figure 4.3(f)

Vector Index	Value	Vector Index	Value	Vector Index	Value	Vector Index	Value
0	0.130387	9	0.001881	18	0.001097	27	0.000671
1	0.076832	10	0.001	19	0.001872	28	0.000259
2	0.021299	11	0.001546	20	0.001303	29	0.000725
3	0.009975	12	0.000595	21	0.001436	30	0.00103
4	0.007821	13	0.00226	22	0.001089	31	0.001185
5	0.003268	14	0.002672	23	0.000421	32	0.001184
6	0.002464	15	0.001523	24	0.001563		
7	0.003867	16	0.001384	25	0.00244		
8	0.003714	17	0.000077	26	0.001955		

Table 4.11. Biometric vector: Fourier descriptors of full-width to length ratio distribution of the image in figure 4.3(f)

Vector Index	Value	Vector Index	Value	Vector Index	Value	Vector Index	Value
0	0.066741	9	0.002029	18	0.001217	27	0.000996
1	0.072324	10	0.001552	19	0.000468	28	0.001481
2	0.035344	11	0.001861	20	0.000291	29	0.001251
3	0.0102	12	0.001544	21	0.000892	30	0.001015
4	0.01094	13	0.001739	22	0.000975	31	0.000598
5	0.005411	14	0.002203	23	0.000461	32	0.000267
6	0.002732	15	0.000557	24	0.000842		
7	0.005169	16	0.001802	25	0.000887		
8	0.003031	17	0.001172	26	0.001787		

Table 4.12. Biometric vector: Fourier descriptors of half-width to length ratio distribution of the image in figure 4.3(f)

4.11 Summary

Two hundred images were prepared for the experiment. Contour of each image was extracted using an auto adaptive thresholding technique. To achieve the rotational invariance, all the contours were rotated until the line that connects the starting point of the stem and the furthermost point of the contour from the starting point of the stem becomes horizontal. Four shape signatures (complex-coordinates, centroid-distance, full-width to length ratio and half-width to length ratio), three local features (margin coarseness, stem length to blade length ratio, leaf tip curvature) and leaf compactness were calculated. Biometric vectors were constructed using both raw values and the Fourier descriptors of the four shape signatures for leaf image retrieval.

Chapter 5

Results, Analysis and Discussion

Out of the five images of each species, one image was used as the test image and the other four were used as the reference images. Each of the test images was tested against the reference images and an ordered list of retrievals was obtained so that the best matched image is at the top of the list. Since no prototype object exists for a leaf of a particular species, all the retrievals were done using both methods described in section 2.3 (distance to the nearest neighbour and to the nearest centroid of the cluster points of each species from the test image). For example, tables 5.1 and 5.2 show the retrieval lists for six different test images using Fourier descriptors the shape signature: full-width to length ratio distribution, with the nearest neighbourhood search and with the nearest centroid search respectively. Retrievals clearly show that the nearest centroid search recognizes the correct species more efficiently than the nearest neighbour search. Therefore, all the remaining results in this chapter are based on the retrievals of nearest centroid search only.

		Test Images											
		a1.jpg		*b1.jpg*		*c1.jpg*		*d1.jpg*		*e1.jpg*		*f1.jpg*	
		Im	*D*	*Im*	*D*	*Im*	*D*	*Im*	*D*	*Im*	*D*	*Im*	*D*
Order of Retrieval	1	a2	0.149	b2	0.058	ap4	0.231	d3	0.247	e2	0.406	f3	0.106
	2	a3	0.356	al3	0.147	ap2	0.242	d2	0.28	e4	0.427	ai5	0.151
	3	a5	0.357	al4	0.167	ad3	0.275	a4	0.644	e5	0.486	ap1	0.158
	4	an5	0.383	al2	0.197	ap3	0.284	a1	0.704	e3	0.543	s2	0.186
	5	s1	0.39	b3	0.215	ap5	0.3	a2	0.707	u5	0.717	f4	0.22
	6	s4	0.428	ag3	0.224	ad2	0.315	an2	0.719	p3	0.844	at4	0.285
	7	an4	0.487	ag1	0.23	m3	0.333	an4	0.721	f2	0.862	ai2	0.289
	8	a4	0.51	ag4	0.238	ag5	0.348	an3	0.777	ai1	0.867	at3	0.308
	9	an3	0.554	at4	0.273	ag4	0.364	s4	0.797	ai3	0.876	ai1	0.356
	10	s3	0.56	al1	0.274	ad5	0.371	an5	0.807	a5	0.877	b3	0.363
	11	an2	0.574	ag5	0.298	ag2	0.372	s1	0.817	a3	0.884	at2	0.382
	12	s5	0.582	al5	0.306	m4	0.379	a5	0.849	f5	0.898	ae1	0.389
	13	ai4	0.622	ae3	0.307	j1	0.386	d5	0.921	f4	0.899	ai3	0.395
	14	d1	0.704	at3	0.322	ag3	0.392	a3	0.938	f3	0.9	ap3	0.401
	15	ai1	0.723	m3	0.323	c3	0.401	d4	0.961	ai4	0.901	at5	0.402
	16	f2	0.733	aq1	0.337	k4	0.412	an1	0.975	s2	0.911	c5	0.403
	17	d2	0.742	ag2	0.346	j5	0.413	s3	0.979	s5	0.913	b2	0.421
	18	f4	0.769	aq5	0.353	ad1	0.418	s5	1.022	ai2	0.92	ag2	0.426
	19	ai3	0.776	ae1	0.353	c4	0.422	ai4	1.045	f1	0.924	ad2	0.426
	20	d3	0.816	ae4	0.376	j4	0.427	j2	1.113	ai5	0.926	ad1	0.426
	21	ad4	0.845	af3	0.376	c5	0.43	at1	1.132	u4	0.927	b1	0.434
	22	at1	0.854	ae2	0.377	ag1	0.433	f2	1.157	c5	0.934	ag4	0.439
	23	ai2	0.864	m4	0.382	ad4	0.445	ai1	1.17	s3	0.97	aq1	0.45
	24	j2	0.89	af2	0.405	c2	0.447	ai3	1.176	k1	0.975	b4	0.45
	25	f5	0.891	m5	0.405	m2	0.471	f4	1.212	c3	0.98	c3	0.45
	26	ap1	0.918	at5	0.406	k5	0.472	at2	1.232	ap1	0.981	ap4	0.451
	27	c2	0.923	af4	0.411	m5	0.481	ad4	1.254	c4	1.007	f2	0.46
	28	ad1	0.933	aq2	0.414	f3	0.508	b4	1.255	p1	1.017	at1	0.463
	29	s2	0.948	b4	0.419	al4	0.51	at5	1.263	ad1	1.026	ag5	0.464
	30	ai5	0.953	ap2	0.422	b2	0.511	f5	1.28	c2	1.032	c4	0.478
	31	b4	0.957	at2	0.423	at4	0.513	ai2	1.285	k5	1.034	ae2	0.49
	32	f1	0.966	b5	0.432	ap1	0.521	b5	1.292	u2	1.037	ap2	0.495
	33	f3	0.972	f1	0.434	aj4	0.527	at3	1.331	ae1	1.046	k5	0.496
	-	-	-	-	-	-	-	-	-	-	-	-	-
	-	-	-	-	-	-	-	-	-	-	-	-	-
	56	c1	1.204	k4	0.635	at2	0.619	k5	1.555	aq5	1.166	ag1	0.573
	57	ad2	1.231	j5	0.637	k2	0.633	j3	1.561	af1	1.178	af1	0.582
	58	b2	1.259	c5	0.64	ae2	0.642	p3	1.569	af4	1.182	f5	0.584
	59	e4	1.263	ad1	0.643	f4	0.642	c1	1.578	af2	1.197	al2	0.588
	-	-	-	-	-	-	-	-	-	-	-	-	-
	-	-	-	-	-	-	-	-	-	-	-	-	-
	199	ac2	2.555	d4	2.364	d4	2.251	ab1	2.856	d4	2.317	d4	2.171

Table 5.1. Nearest neighbourhood search: Order of retrievals for six different test images using the Fourier descriptors of full-width to length ratio shape signature. Under each test image, the gray area indicates all the retrieved images in the retrieval list until the test image matches all the relevant reference images. *D* is the Euclidian distance between the test image and the reference image (part of the table is omitted).

		Test Images											
		a1.jpg		*b1.jpg*		*c1.jpg*		*d1.jpg*		*e1.jpg*		*f1.jpg*	
		sp	*D*	*sp*	*D*	*sp*	*D*	*sp*	*D*	*sp*	*D*	*sp*	*D*
Order of Retrieval	1	*a*	0.0794	ag	0.0849	ap	0.0946	an	0.569	e	0.2042	at	0.134
	2	*an*	0.4129	aq	0.1251	j	0.1063	a	0.8808	p	0.397	c	0.1638
	3	*s*	0.811	ae	0.1948	ag	0.1795	d	0.9671	s	0.4599	j	0.1876
	4	*e*	0.8195	as	0.2037	c	0.2157	e	1.6164	a	0.714	ad	0.2126
	5	*p*	0.9247	b	0.2111	b	0.2187	s	1.6187	ai	0.769	b	0.2166
	6	*ai*	1.2069	af	0.2117	as	0.243	p	1.6757	f	0.9052	k	0.2205
	7	*f*	1.4084	al	0.2143	aq	0.2518	ai	2.0448	ad	0.9649	ap	0.2329
	8	*ad*	1.4744	ap	0.2226	at	0.2554	f	2.2301	an	1.0358	f	0.2354
	9	*k*	1.6054	j	0.2474	k	0.3226	ad	2.3133	k	1.0486	as	0.2668
	-	-	-	-	-	-	-	-	-	-	-	-	-
	-	-	-	-	-	-	-	-	-	-	-	-	-
	39	*i*	2.9747	an	2.3145	an	2.1856	i	3.8023	i	2.4332	an	1.9581
	40	*ab*	2.9848	d	3.7729	d	3.6386	ab	3.8098	ab	2.4425	d	3.4108

Table 5.2. Nearest centroid search: Order of retrievals for six different test images using the Fourier descriptors of full-width to length ratio shape signature. Under each test image, the gray area indicates all the retrieved images in the retrieval list until the test image matches the correct species. *D* is the Euclidian distance between the test image and the centroid (part of the table is omitted).

The rest of the chapter is organized as follows. Section 5.1 shows the retrievals based on shape signatures. List of retrievals were obtained using both row values of shape signatures and the Fourier descriptors of them. Retrievals based on local features and with global shape descriptors are described in section 5.2 and 5.3 respectively. The retrievals using combinations of the features in all the above sections are analysed in section 5.4. Finally, section 5.5 summarises the results.

5.1. Retrievals based on shape signatures

Images were retrieved using both Fourier descriptors and the direct values of four shape signatures (complex-coordinates, centroid-distance, full-width to length ratio and half-width to length ratio) as explained in section 4.6.1.

5.1.1. Retrievals with Fourier descriptors

Results:

For clarity, table 5.3 to table 5.6 show the retrievals for first eight test images using Fourier descriptors of all the four shape signatures described above (see the appendix I(a) for full list of retrievals). The retrieval list shows only up to the species, which recognizes the test image correctly (only the gray area). For example, the correct species for the test image a1 is in the first place of the retrieval list and that for the test image b1 is in the fifth place of the list.

Test Image	a1.jpg	b1.jpg	c1.jpg	d1.jpg	e1.jpg	f1.jpg	g1.jpg	h1.jpg
Retrievals	a	ag	ap	an	e	at	g	g
	an	aq	j	a	p	c	t	h
	s	ae	ag	d	s	j	h	t
	e	as	c	e	a	ad	i	i
	p	b	b	s	ai	b	ab	l
	ai	af	as	p	f	k	l	ab
	f	al	aq	ai	ad	ap	v	v
	ad	ap	at	f	an	f	ac	ac
	k	j	k	ad	k	as	ak	ak

Table 5.3. Retrieval lists of first eight test images using Fourier descriptors of complex-coordinates shape signature.

Test Image	a1.jpg	b1.jpg	c1.jpg	d1.jpg	e1.jpg	f1.jpg	g1.jpg	h1.jpg
Retrievals	a	ag	ad	d	e	at	g	g
	an	al	j	an	p	j	t	t
	s	m	ap	a	a	f	i	i
	d	b	c	p	c	ap	ab	ab
	ai	ae	at	s	ai	b	l	l
	f	ap	b	ai	s	ag	h	h

Table 5.4. Retrieval lists of first eight test images using Fourier descriptors of centroid-distance shape signature.

Test Image	a1.jpg	b1.jpg	c1.jpg	d1.jpg	e1.jpg	f1.jpg	g1.jpg	h1.jpg
Retrievals	a	ag	ad	an	e	as	g	h
	p	aq	ap	d	p	aq	h	g
	s	af	af	a	ai	j	ab	ab
	an	al	j	s	f	ad	t	t
	ai	ap	ae	p	as	f	i	i
	f	b	c	ai	c	ap	l	l
	d	j	aq	f	s	at	n	n

Table 5.5. Retrieval lists of first eight test images using Fourier descriptors of full-width to length ratio distribution.

Test Image	a1.jpg	b1.jpg	c1.jpg	d1.jpg	e1.jpg	f1.jpg	g1.jpg	h1.jpg
Retrievals	a	ag	ad	an	e	f	g	g
	s	al	k	d	ai	at	ab	ab
	an	ap	ae	a	f	ad	i	i
	ai	b	af	s	ad	j	t	l
	d	j	aq	ai	s	b	l	t
	f	af	c	f	c	ap	h	h

Table 5.6. Retrieval lists of first eight test images using Fourier descriptors of half-width to length ratio distribution.

Analysis:

The total number of correctly recognized images with the number of retrieved images is shown in table 5.7. N1, N2, N3 and N4 correspond to complex-coordinates, centroid-distance, full-width to length ratio and half-width to length ratio respectively. For example, with N1, 27 species can be correctly identified if only the first image of the retrieval list is considered while 31 species can be correctly identified if the first two images were considered.

The graphical representation of the data in table 5.7 is in figure 5.1.

n	N1	N2	N3	N4
1	27	27	30	32
2	31	33	35	35
3	33	37	35	35
4	35	39	36	37
5	36	39	37	38
6	38	40	39	40
7	38	40	40	40
8	39	40	40	40
9	40	40	40	40
Total	40	40	40	40

Table 5.7. The number of correctly identified species in each attempt of the retrieval list using Fourier descriptors. (n: number of retrieved images, N1: Complex-coordinates, N2: Centroid-distance, N3: Full-width to length Ratio, N4: Half-width to length Ratio).

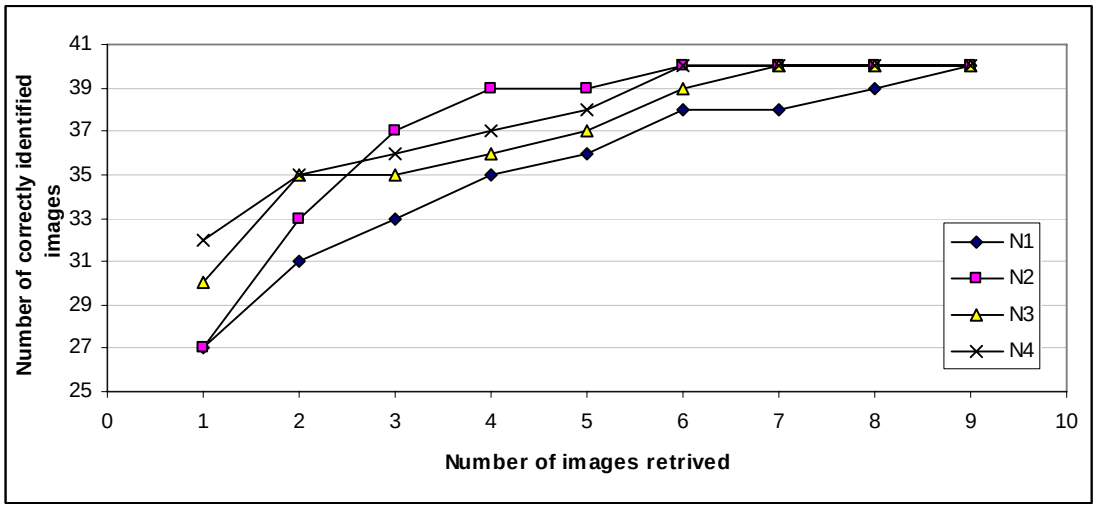

Figure 5.1. Comparison of the performance of the Fourier descriptors of four shape signatures; Complex-coordinates (N1), Centroid-distance (N2), Full-width to length Ratio (N3), Half-width to length Ratio (N4).

Discussion:

Out of the four lines graphed in figure 5.1, the curve associated with complex coordinates gives the lowest performance (if the first retrieved image is considered, out of 40 test images only 27 can be correctly identified and to identify all the 40 test images, 9 of the retrieved images should be taken into account). Half Width to Length Ratio is better than the Full-width to length Ratio signature since all the values of Full-width to length Ratio

is less than or equal to the values of Half Width to Length Ratio. If the first two retrieved images were considered then Half-width to Length Ratio and Full-width to length Ratio are better than the Centroid-distance.

Although the Fourier descriptors are compact, easy to handle (with well-developed theories behind them) and convenient to achieve shape invariance in shape representation, other important shape information is lost by ignoring the phase (to achieve the rotational invariance) when constructing the feature vectors only with magnitude values of Fourier descriptors. However, except for the complex-coordinates, all other three shape signatures (centroid-distance, full-width to length ratio, half-width to length ratio) are invariant to rotation (if the pictures were taken as described), to transformation and to scale. So, as the next step, instead of using Fourier descriptors, the feature vectors were constructed with direct (raw) values of these three shape signatures and the images were retrieved using those feature vectors.

5.1.2 Retrievals with direct values of shape signatures

Results:

For comparison with the retrievals with Fourier descriptors (table 5.3 to table 5.6), the retrieved image lists for the first eight test images using the direct values of half-width to length ratio, full-width to length ratio and centroid-distance are shown in table 5.8 to table 5.10 respectively (see appendix I(b) for full list of retrievals).

Test Image	a1.jpg	b1.jpg	c1.jpg	d1.jpg	e1.jpg	f1.jpg	g1.jpg	h1.jpg
Retrievals	a	al	c	d	e	f	h	h
	s	b	k	a	f	ai	g	g
	an	ag	m	an	ai	c	t	t
	ai	ae	j	s	k	ag	aj	ab
	f	m	ag	ai	c	ae	ab	aj
	d	af	ao	f	p	b	l	n
	at	at	ae	at	u	k	n	l

Table 5.8. Retrieval lists of first eight test images with the direct values of half-width to length ratio distribution.

Test Image	a1.jpg	b1.jpg	c1.jpg	d1.jpg	e1.jpg	f1.jpg	g1.jpg	h1.jpg
Retrievals	a	al	ad	d	e	f	g	h
	s	b	ap	a	f	at	h	g
	an	ag	c	an	ai	ai	t	t

Table 5.9. Retrieval lists of first eight test images with the direct values of full-width to length ratio distribution.

Test Image	a1.jpg	b1.jpg	c1.jpg	d1.jpg	e1.jpg	f1.jpg	g1.jpg	h1.jpg
Retrievals	a	ag	j	d	e	f	g	h
	an	al	c	a	s	at	t	g
	s	b	ap	an	ai	b	i	t
	ai	ae	ag	ai	a	ap	h	i

Table 5.10. Retrieval lists of first eight test images with the direct values of centroid-distance.

Analysis:

The total number of correctly recognized images with the number of retrieved images is shown in the table 5.11. N1, N2, N3 and N4 correspond to Complex-coordinates, Centroid-distance, Full-width to length ratio and Half-width to length ratio respectively. Figure 5.2 is the graphical representation of the data in table 5.11.

n	N2	N3	N4
1	33	32	24
2	36	39	31
3	38	40	35
4	40	40	36
5	40	40	37
6	40	40	39
--	--	--	--
--	--	--	--
17	40	40	39
18	40	40	40
Total	40	40	40

Table 5.11. The number of correctly identified species with the number of retrieved images using direct values of the shape signatures. (n: number of retrieved images, N2: Centroid-distance, N3: Full-width to Length Ratio, N4: Half-width to Length Ratio).

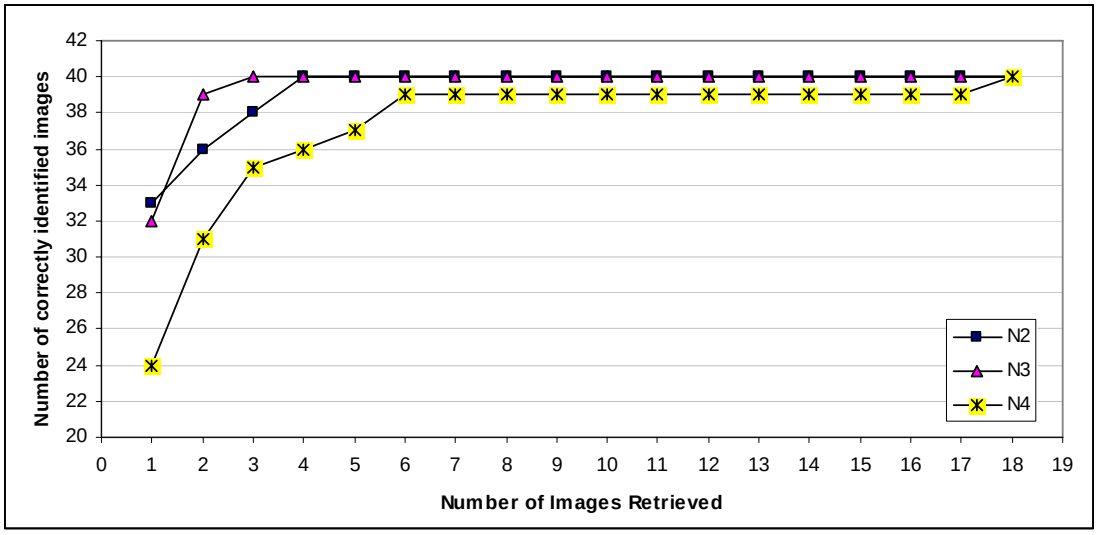

Figure 5.2. Comparison of the performance of the three shape signatures; Centroid - istance (N2), Full-width to length ratio (N3), Half-width to length ratio (N4) using direct values.

Discussion:

From figure 5.2, it is easy to observe that the shape signatures, Centroid-distance (N2) and Full-width to length ratio distribution (N3) perform better than the Half-width to length ratio distribution (N4) since the number of correctly identified species in each

number of retrieved images with N2 and N3 is always greater than or equal that with N4. They also perform better than their Fourier descriptors (Figure 5.1). If only the top image of the retrieval list is considered to recognise the species, then N2 is better than N3 since out of 40 species N2 recognises 33 correctly (compared to 32 species with N3). Otherwise, N3 is the best shape signature to recognise species.

All of the above feature vectors were constructed using the whole leaf including the leaf stem. Although the stem has important information for leaf recognition, in some instances it is undesirable to use the leaf stem for constructing feature vectors because

1) Of the same species, stems do not always show the same alignment with the mid rib of the leaves. Therefore, there is a considerable deviation between the Full-width to length ratio distributions of two leaves of the same species. For example, figure 5.3 shows different stem alignments of two leaves of same species.

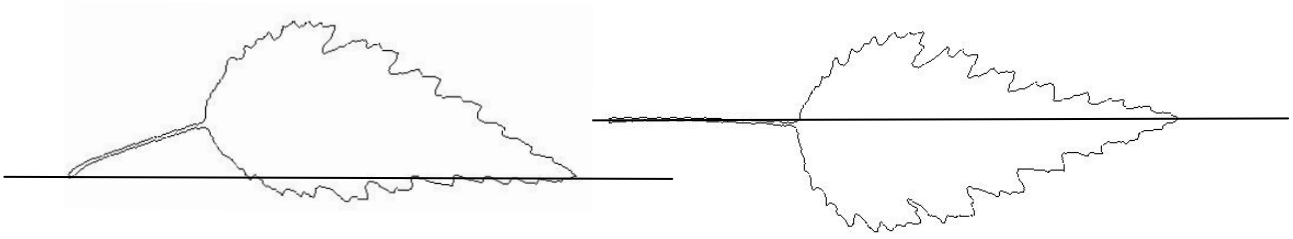

Figure 5.3. Different stem arrangement of two leaves of same species.

2) In the same species, it is possible to observe some deviations among the ratio, stem length to total leaf length. Therefore, again there can be a considerable deviation between the Full-width to length ratio distributions. For example, figure 5.4 shows two leaves of the same species with different stem lengths (relative to the total leaf length). Figure 5.5 is the Full-width to length ratio distributions of these two leaves.

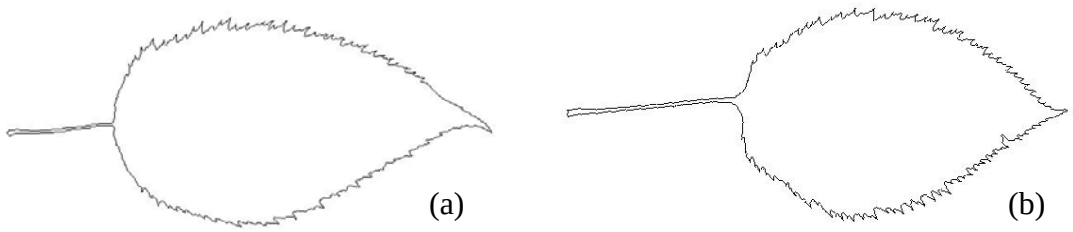

Figure 5.4. Different stem lengths of two leaves of same species.

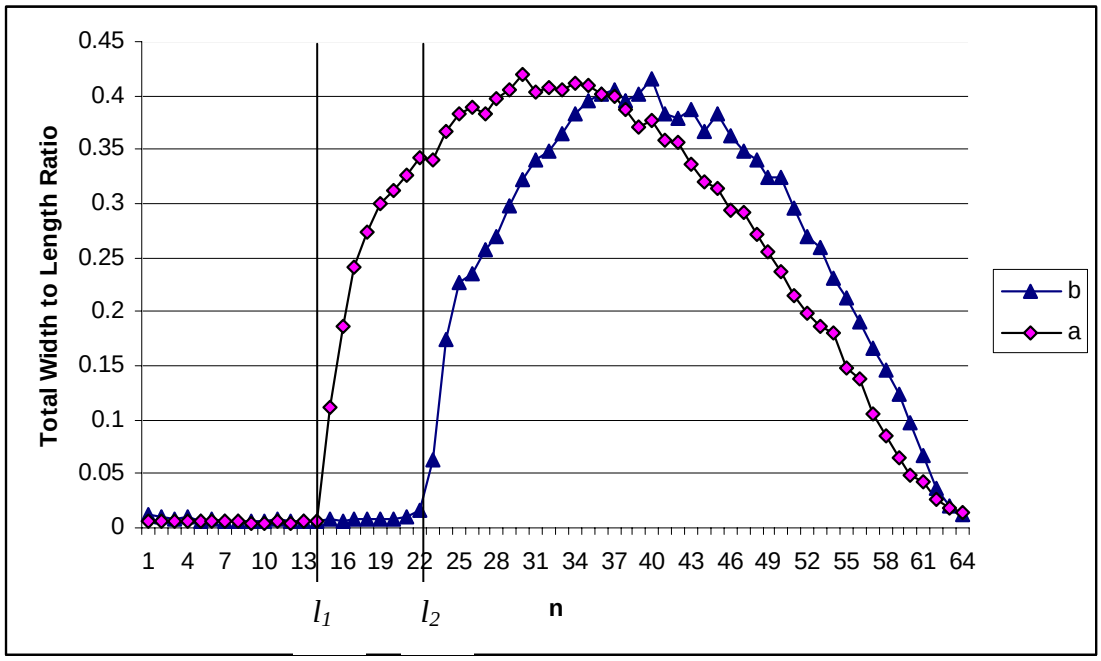

Figure 5.5. Full-width to length ratio distributions of the leaves in figure 5.4 (including the stem). The large amount of deviation between the lines l_1 and l_2 is due to the variation of the stem lengths.

From figure 5.5, it is clear that more similar distributions can be achieved if the distributions were calculated excluding the stem. Figure 5.6 shows the same distribution values for the leaves in figure 5.4 without the stem.

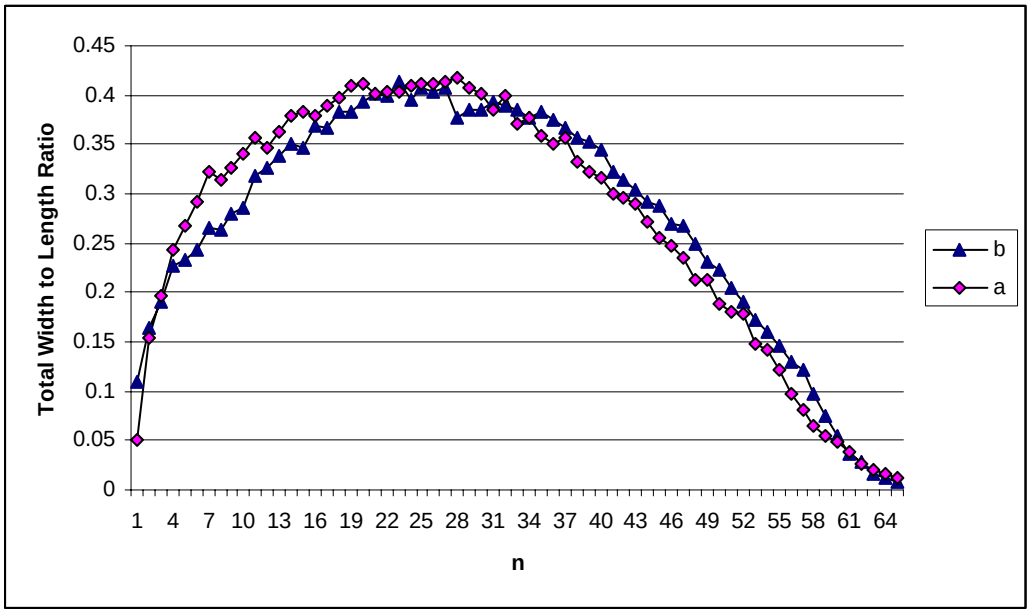

Figure 5.6. Full-width to length ratio distributions of the leaves in figure 5.4 (without stem).

5.1.3. Retrievals with direct values of shape signatures excluding stem

Results:

For all the leaf images, stems were excluded using the stem detection technique described in section 4.7 and all the shape signatures were recalculated. The list of retrievals in the best matching order was obtained from the full-width to length ratio distribution and it is shown in table 5.12.

Analysis:

The number of correctly identified species against the number of retrieved images in the retrieval list from the full-width to length ratio distribution, with and without stems is shown in figure 5.7 for comparison.

Test Image	a1.jpg	b1.jpg	c1.jpg	d1.jpg	e1.jpg	f1.jpg	g1.jpg	h1.jpg
Retrievals	a	b	j	d	e	f	g	h
	d	af	ap	a	a	at	h	g
	an	al	ad	p	d	b	i	t
	s	ag	c	an	an	ai	t	i

Test Image	i1.jpg	j1.jpg	k1.jpg	l1.jpg	m1.jpg	n1.jpg	o1.jpg	p1.jpg
Retrievals	i	j	c	l	m	n	o	p
	t	ad	ad	ak	al	ak	ao	an
	g	k	k	am	aj	aj	m	d
	h	c	ap	r	r	r	j	a

Test Image	r1.jpg	s1.jpg	t1.jpg	u1.jpg	v1.jpg	ab1.jpg	ac1.jpg	ad1.jpg
Retrievals	r	s	i	o	v	ab	ac	ad
	am	ai	t	u	ac	t	v	c
	aj	f	g	ao	l	i	ar	ap
	ak	a	h	j	ab	g	l	j

Test Image	ae1.jpg	af1.jpg	ag1.jpg	ah1.jpg	ai1.jpg	aj1.jpg	ak1.jpg	al1.jpg
Retrievals	ae	af	m	ah	ai	ak	ak	al
	at	aq	ag	n	f	aj	r	ae
	af	ae	al	aj	s	n	am	m
	al	at	ae	r	at	am	n	af

Test Image	am1.jpg	an1.jpg	ao1.jpg	ap1.jpg	aq1.jpg	ar1.jpg	as1.jpg	at1.jpg
Retrievals	am	an	ao	f	af	ar	as	at
	r	p	aj	ap	aq	ah	aq	f
	ak	d	m	b	at	v	af	b
	aj	a	n	at	b	l	at	ai

Table 5.12. Retrievals with full-width to length ratio distribution (excluding stem).

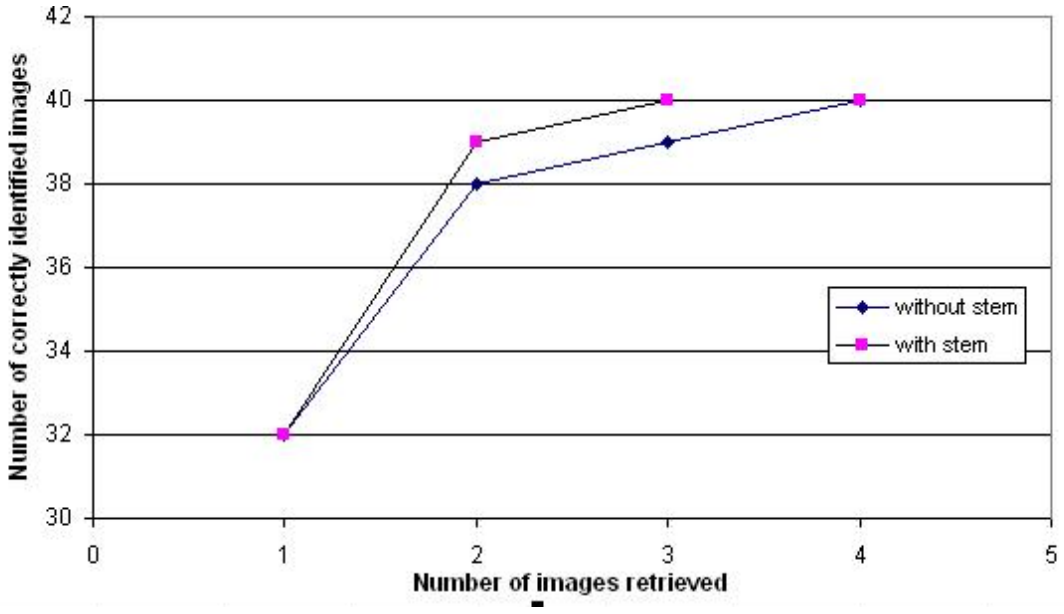

Figure 5.7. Performance comparison of Full-width to length ratio distribution with and without stem.

Discussion:

The results in figure 5.7 show that retrievals without stem are less efficient than retrievals with stem, since it always correctly identify lesser number of species than with -stem retrieval. When images that did not recognise the test image correctly (as the top image of the retrieval list) were analysed, it was clear that the three aspects of local information: stem length to leaf length ratio, leaf margin coarseness and curvature of the leaf tip, and the global shape descriptor, leaf compactness can be used efficiently to discriminate these images further. For example, sample leaves of incorrectly retrieved species in the first, second and third retrievals of the test image c1 and their global and local information are shown in figure 5.8 and in table 5.13 respectively.

c1 j1 ap1 ad1

Figure 5.8. Incorrectly identified species (j1, ap1 and ad1) for the test image c1 (Note: leaves are not shown in the actual scale and the images were matched without stems).

Species	c1	j	ap	ad	c
Number of teeth	1	0.2	3.8	9.6	0.6
Stem length to blade length ratio	0.170523	0.098	0.195	0.186	0.239
Tip curvature	0.354646	0.318265	-0.1416	0.037683	0.505585
Compactness	0.035061	0.049447	0.045741	0.030248	0.034679

Table 5.13. Comparison of local and global features between the test image c1 and its incorrectly and correctly recognised species.

From the values of number of teeth of table 5.13, clearly the species *ap* and *ad* can be eliminated from the retrieval list since they have toothed margins compared to *c1*. Furthermore, *c1* has much higher stem length to blade length ratio than the species *j* and much high leaf tip curvature than *ap* and *ad*. Therefore, the next matching species in the retrieval list, i.e. species *c*, can be identified as the correct species.

5.2 Extraction of local features

The average values for number of teeth (section 4.8.1), Stem length to blade length ratio (section 4.8.2) and leaf tip curvature (section 4.8.3) for each of the forty species are shown in the table 5.14. Same table for all two hundred (200) images is in appendix I(c).

Species	Number of teeth	Stem length to blade length ratio	Tip curvature
a	1	0.173	-0.18257
b	0.2	0.093	-0.30069
c	0.6	0.239	0.505585
d	6.8	0.015	-0.14924
e	4	0.483	0.221862
f	0	0.187	-0.40204
g	0.2	0.062	0.046916
h	0.4	0.110	-0.02455
i	0.2	0.106	-0.03506
j	0.2	0.098	0.318265
k	11.4	0.419	-0.11171
l	0.4	0.259	-0.19315
m	1.2	0.157	-0.11498
n	0	0.210	-0.06731
o	5.8	0.487	0.128657
p	1.4	0.452	-0.50866
r	0	0.190	-0.14117
s	0.2	0.105	-0.27235
t	0.2	0.093	-0.09012
u	0.2	0.476	0.127759

Species	Number of teeth	Stem length to blade length ratio	Tip curvature
v	0	0.122	-0.23393
ab	0.4	0.156	-0.22908
ac	0.6	0.029	-0.21074
ad	9.6	0.186	0.037683
ae	0.2	0.133	-0.35321
af	1	0.201	-0.22319
ag	0	0.097	-0.14902
ah	3.4	0.216	-0.28493
ai	2.6	0.145	-0.91458
aj	0.2	0.071	-0.03658
ak	0.4	0.064	-0.0928
al	0	0.073	-0.25047
am	0	0.157	-0.11348
an	0	0.104	-0.25211
ao	13.6	0.124	-0.21668
ap	3.8	0.195	-0.1416
aq	0	0.178	-0.31734
ar	0	0.185	-0.30682
as	0	0.126	-0.38365
at	0	0.030	-0.10892

Table 5.14. Average number of teeth in the middle segment of the leaf margin, stem length to blade length ratio and leaf tip curvature of all 40 species. Species that have non-simple leaf margins are shown in gray colour.

5.2.1 Leaf margin coarseness

According to the results in 5.14, some of the species with simple leaf margins also show a value in the “Number of teeth” column. This is due to the fact that margins of some leaves of these species show minor deviations from ideal simple leaf margins (this is explained in more detail in the next chapter). However, from table 5.14, it is clear that for all the species with simple margins, the value of the average number of teeth, which is normalised to be less than 1.00, can be used to discriminate the serrate-margined leaves from the simple-margined leaves.

5.2.2 Leaf tip curvature

Leaf tip curvature values of all the species (table 5.14) were sorted and figure 5.9 shows them in increasing order. The species that have higher negative curvature values have more convex-shaped leaf tips while the species that have higher positive values have shaper pointed tips. The species with a curvature around zero are lengthy (elongated) leaves since only those leaves can have same tangent values for both contour segments that are used to calculate the curvature.

5.2.3 Stem length to blade length ratio

Sorted values of stem length to blade length ratio of all species (table 5.14) are shown in the figure 5.10 in increasing order. For the selected set of forty species, this value ranges from 0.015 to 0.487.

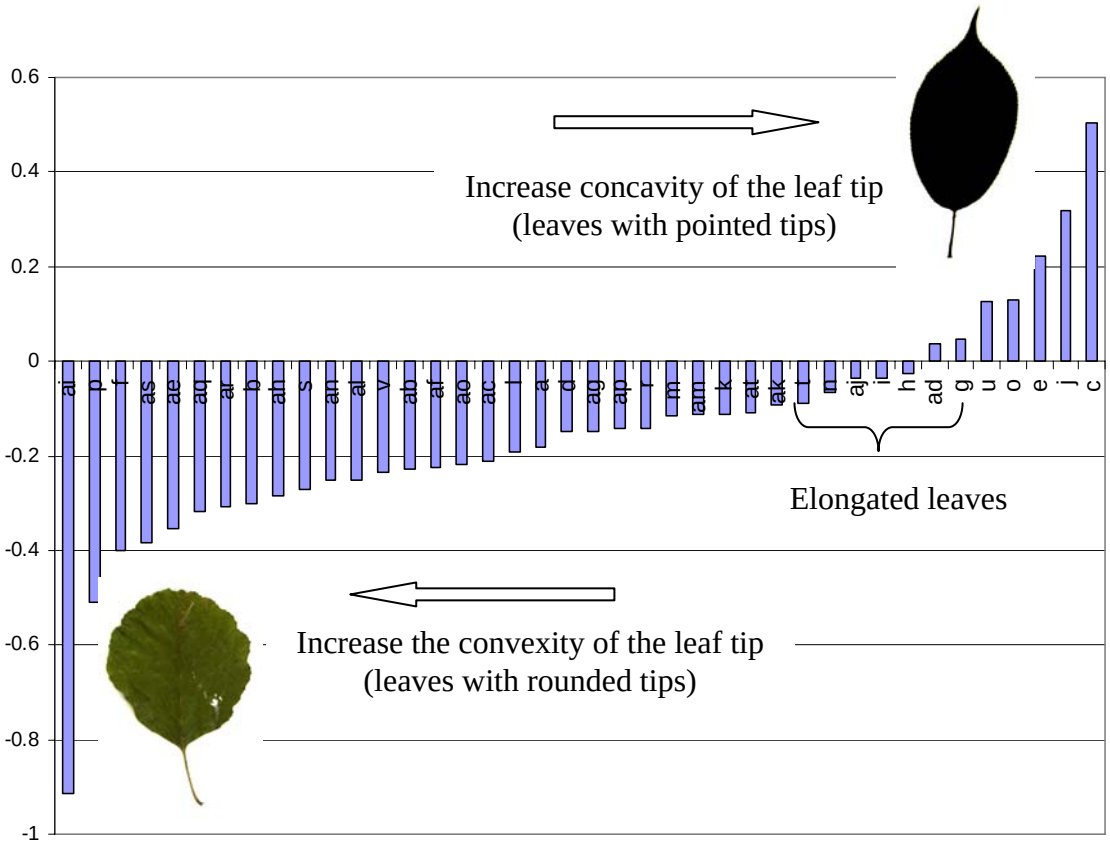

Figure 5.9. Variation of leaf tip curvature.

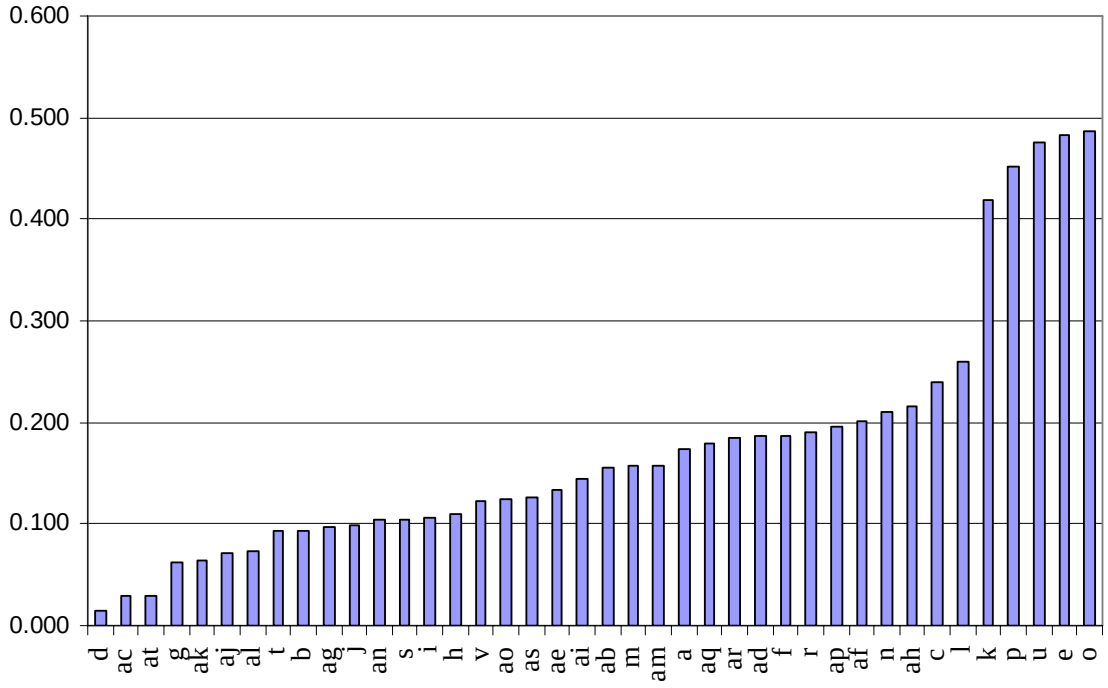

Figure 5.10. Variation of stem length to blade length ratio.

5.3 Global shape descriptors

Leaf compactness values (section 4.7) of all 200 leaf images were calculated and the average compactness value for each of the species is shown in the table 5.15. Sorted compactness values in increasing order are shown in figure 5.11 and it shows that there is a continuous variation of this global shape descriptor from 0.019 to 0.071.

Species	Compactness
a	0.0637122
b	0.0550936
c	0.0346786
d	0.0505302
e	0.0305992
f	0.0580338
g	0.0212096
h	0.0213754
i	0.0190796
j	0.049447
k	0.0199356
l	0.0263706
m	0.0426344
n	0.029717
o	0.0186586
p	0.050728
r	0.032172
s	0.0664058
t	0.0201982
u	0.035633

Species	Compactness
v	0.0275818
ab	0.0196366
ac	0.0254078
ad	0.0302484
ae	0.0456056
af	0.03782
ag	0.0513938
ah	0.0282084
ai	0.0483578
aj	0.0346734
ak	0.0293518
al	0.046575
am	0.0324258
an	0.0711802
ao	0.0223644
ap	0.045741
aq	0.0490716
ar	0.0362384
as	0.0513314
at	0.0580536

Table 5.15. Leaf compactness of all forty species.

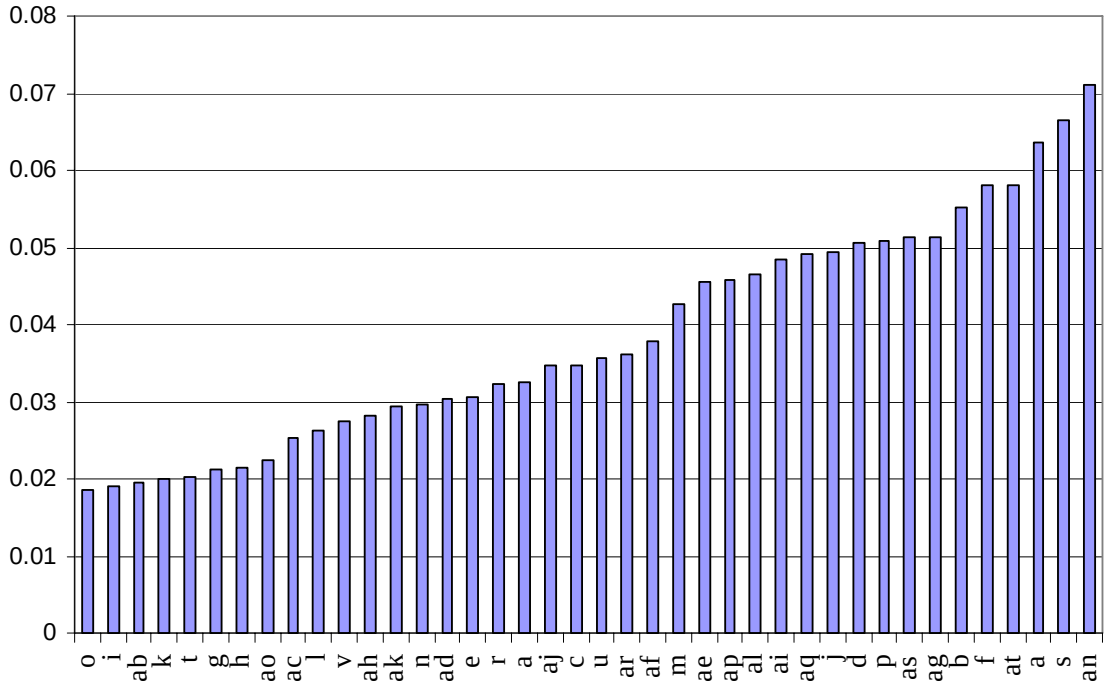

Figure 5.11. Variation of compactness.

5.4 Retrievals with combined features (shape signatures, local and global shape descriptors)

After obtaining the retrieval list using full-width to length shape signature, some threshold values based on global and local features were used to eliminate the incorrectly recognised species from the top of list until it finds the correct species. The elimination process is described below.

i) For each feature, calculate the threshold as the maximum deviation of that feature from each of the reference image to its centroid.

ii) For each test image, to test whether a particular retrieved species is acceptable or not, calculate the distance of each feature between the retrieved species and the test image. For every feature, if the distance is less than the corresponding threshold, the retrieved species is accepted. Otherwise, that species is

eliminated from the retrieved list. This testing process is applied to every species from the top of the list until it finds an acceptable species.

Results:

Threshold values for each global and local feature were calculated and shown below.

Threshold for number of teeth = 5.25

Threshold for stem length to blade length ratio = 0.362111

Threshold for leaf tip curvature = 1.094405

Threshold for compactness = 0.008865

The new retrieval lists for test images (after the elimination process) is shown in table 5.16.

Test Image	a1.jpg	b1.jpg	c1.jpg	d1.jpg	e1.jpg	f1.jpg	g1.jpg
Retrievals	a	b	c	d	e	f	g

Test Image	i1.jpg	j1.jpg	k1.jpg	l1.jpg	m1.jpg	n1.jpg	o1.jpg
Retrievals	i	j	k	l	m	n	o

Test Image	r1.jpg	s1.jpg	t1.jpg	u1.jpg	v1.jpg	ab1.jpg	ac1.jpg
Retrievals	r	s	i	u	v	ab	ac
	am	ai	t	ao	ac	t	v

Test Image	ae1.jpg	af1.jpg	ag1.jpg	ah1.jpg	ai1.jpg	aj1.jpg	ak1.jpg
Retrievals	ae	af	m	ah	ai	ak	ak
	at	aq	ag	n	f	aj	r

Test Image	am1.jpg	an1.jpg	ao1.jpg	ap1.jpg	aq1.jpg	ar1.jpg	as1.jpg
Retrievals	am	an	ao	ap	aq	ar	as

Table 5.16. Retrieval lists for forty (40) test images after elimination process.

Analysis:

A comparison between the retrievals with combined features (shape signature + global and local features) and two retrievals mentioned in sections 5.1.2 (shape signature with stem) and 5.1.3 (shape signature without stem) is shown in figure 5.12.

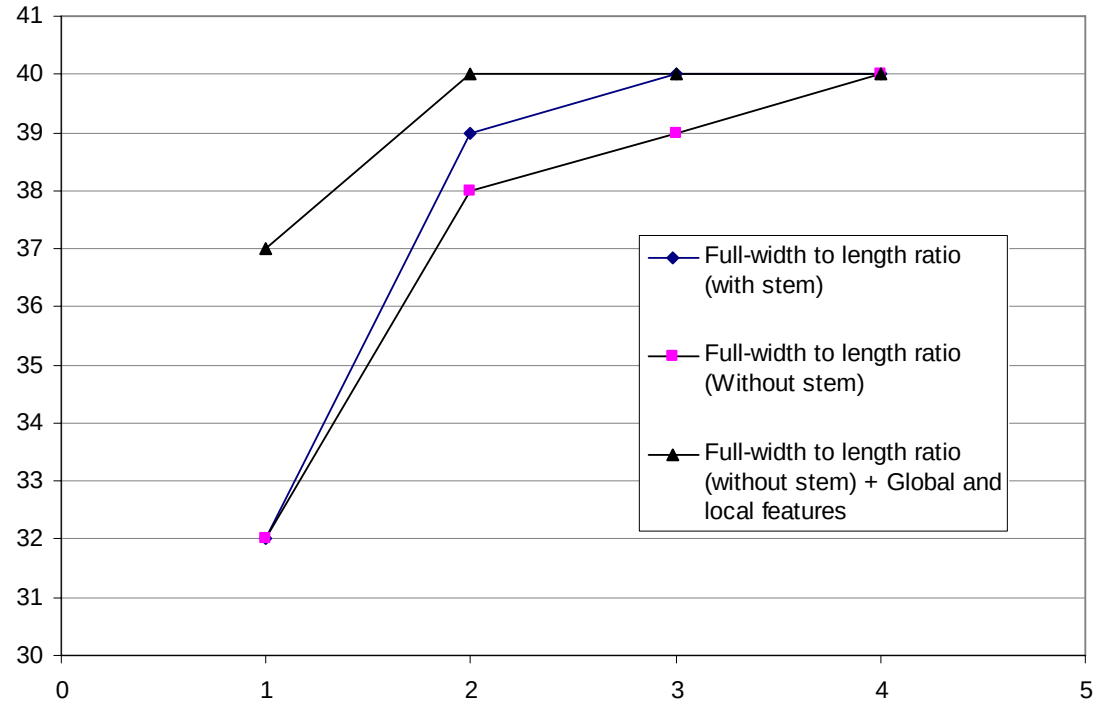

Figure 5.12. Comparison of species recognition.

Discussion:

As shown in figure 5.12, there can be seen a significant improvement in species recognition if both shape signatures and global and local features were used for species matching. Using this hierarchical method, 37 out of 40 species can be correctly identified if only the top image of the retrieval list is considered and all the correct species for the 40 test images can be identified if the top two images are considered.

5.5. Summary

Retrievals using Fourier descriptors of all the four shape signatures showed that the complex-coordinates shape signature has the lowest performance. If only the top image of the retrieval list was considered Fourier descriptors of half-width to length ratio distribution gave the best performance (can recognise 33 species out of 40 correctly).

Retrievals using raw values of shape signatures showed that the centroid-distance and the full-width to length ratio distribution perform better than the half-width to length ratio distribution. Centroid-distance shape signature gave the best performance by recognising 33 species out of 40 correctly in the first place of the retrieval list. Full-width to length ratio distribution performed much better than other two if top two (39 species out of 40) or top three (40 out of 40) images of the retrieval list was considered.

Retrievals using the shape signatures without stems of leaves showed the best performance with the full-width to length ratio distribution (32 species out of 40). Even though the correctly identified number of species of this shape signature is somewhat lesser than that of the previous with-stem shape signatures, without-stem shape signatures can be considered as more accurate shape signatures since of the same species, more similar leaf patterns can be observed without stems.

The retrieved image lists for each test image were refined by eliminating the unacceptable leaves using significantly different values of global and local shape descriptors. The proposed biometric system could recognise 37 species out of 40 if the top retrieved image was considered. If the top two retrieved images were considered system could recognise all the 40 test images correctly.

Chapter 6

Conclusion

A two-staged leaf identification biometric has been proposed in this thesis. In the first stage, matching species of the test image were listed using a biometric vector based on the shape signature: leaf width to length ratio distribution. In the second stage, the species were eliminated from the top of the list until an acceptable species based on global and local features of leaf images was found. The proposed biometric was able to successfully identify the correct species for 37 test images (out of 40).

The proposed biometric identified the correct species using features of the matching images unlike other leaf retrieval studies (Wang *et al*., 2003; Zhang & Lu, 2001; Nam *et al*., 2005a; Nam *et al*., 2005b; Nam & Hwang, 2005) which attempted to retrieve matching images from a database of images,demonstrating that it is not useful to calculate recall rate or precision since, for a given test image, there is only ever one correct species (output of the biometric). The proposed biometric approach was vindicated by identifying all the test images (100%) correctly if two species were returned compared to the low recall rates of Wang *et al*. (2003) (30%, if 10 images were returned) and Ye *et al*. (2004) (71.4%, if top 5 images were returned),.

Limitations and future work

Apart from the studies, which dealt with the two plant genera, Maple (Im *et al*., 1998) and Chrysanthemum (Mokhtarian & Abbasi, 2004 and Abbasi *et al*., 1997), all the other studies tried to retrieve leaf images without any prior categorization. Plant leaves have lot of similar shapes as well as completely different shapes between and within species. Therefore, to find out a common technique that can classify the wide range of leaf shapes without any prior categorization is quite a challenging task and the inappropriateness of the presented methods in the literature are reflected by their low recall rates.

The value of the leaf margin coarseness (number of convex vertices per contour segment) completely relied on the values of the parameters, which were used to find out the approximated polygon. For the same parameter values, the approximated polygon did not give the accurate value for the leaf margin coarseness for every species due to the large variation of leaf margins (figure 1.3) in different species. For example, even though the value of leaf margin coarseness of the species c, which has a serrated margin, should be greater than zero, the proposed algorithm calculated that of leaf c2 (figure 6.1) as zero (0). An adaptive algorithm, which determines the required parameter values by looking at the slope density function of the contour, would be a solution to this problem.

Figure 6.1. Sample leaf of the species c, which has a serrated margin.

For a given species, the proposed biometric constructed a template leaf using reference images and used this template as a prototype for the nearest neighbourhood matching. Therefore, the more the reference images, the better the prototype and the more accurate the biometric will be. In addition to this, to eliminate the unacceptable species from the list in the second stage, thresholds for each global and local feature were calculated as the maximum deviation of a particular feature that could vary from any of the centroids. This threshold calculation is more suitable when there are few reference images, since few images could not represent the shape features of all the leaves of a particular species. By having more reference images, for each feature, different thresholds can be calculated for each species as the maximum deviation of a particular feature that could vary from the centroid of that species, assuming the reference images could cover all the possible leaf shapes of that species. Then the corresponding thresholds can be used to more effectively eliminate each of the unacceptable species from the list to enhance the accuracy of the biometric.

There are two reasons for the biometric to eliminate all the species in the list of a particular test image in the second stage (i.e. no acceptable species is found).

a) Test image belongs to a new species (there are no reference images in the database) or
b) The reference images do not cover all the leaf shapes of the species that test image belongs to.

In both cases, without altering the techniques, the proposed biometric can be strengthened by adding reference images of new species to the database, or by adding more reference images of existing species when the reference images are not enough to cover the leaf shapes.

Bibliography

Abbasi, S., Mokhtarian, F., Kittler, J., 1997. *Reliable Classification of Chrysanthemum Leaves through Curvature Scale Space*, Proceedings of the First International Conference on Scale-Space Theory in Computer Vision, Utrecht, The Netherlands, July, pp. 284-295.

Ashton, M. S., Gunatilleke, S., de Zoysa, N., Dassanayake, M.D., Gunatilleke, N., Wijesundera, S., 1997. *A field guide to the common trees and shrubs of Sri Lanka*. WHT Publications, Sri Lanka, pp. 43-50.

Chang, J., Fan, K., 2002. *A new model for fingerprint classification by ridge distribution sequences*, Pattern Recognition, 35, pp. 1209-1223.

Chi, Z., Houqiang, L., Chao, W., 2003. *Plant Species Recognition based on Bark Patterns Using Novel Gabor Filter Banks*, IEEE International Conference on Neural Networks and Signal Processing, Nanjing, China, December, 14(17), pp. 1035-1038.

Cho-Huak, T., Roland, T. C., 1998. *On image analysis by the methods of moments,* IEEE Transactions on Pattern Analysis and Machine Intelligence 10(4) July, pp. 965-513.

Cottrell, G. W., 1990. *Extracting features from faces using compression networks: Face, identity, emotion and gender recognition using holons,* In D. Touretzky

(Ed.), Connection Models: Proceedings of the 1990 Summer School. San Mateo, CA: Morgan Kaufmann.

Cunha, J.B., 2003. *Application of image processing techniques in the characterization of plant leafs*, IEEE International Symposium on Industrial Electronics, 1(1), 9-11 June, pp. 612 – 616.

Fitz, A.P., Green, R.J., 1996. *Fingerprint classification using a hexagonal fast Fourier transform*, Pattern Recognition 29 (10), pp. 1587-1597.

Fu, A., Yan, H., Huang, K., 1997. *A curve bend function method to characterize contour shapes*, Pattern Recognition 30 (10), pp. 1661-1671.

Fu, H., Chi, Z., 2003. *A two-stage approach for leaf vein extraction*, IEEE International conference on neural networks & signal processing, pp. 208-210.

Gonzalez, R. C., Woods, R.E., Eddins, S. L., 2004. *Digital Image Processing Using MATLAB*, Pearson Prentice Hall, Pearson Education, Inc., New Jersey.

Heath, M.D., Sarkar, S., Sanocki, T., Bowyer, K., 1997. *A robust visual method for assessing the relative performance of edge-detection algorithms*, IEEE Transactions on Pattern Analysis and Machine Intelligence. 19 (12), pp. 1338-1359.

http://dallas.tamu.edu/weeds/anat.html (Texas Agricultural Experiment Station, Texas A&M University - Commerce). Retrieved 17 March 2008.

Im, C. Nishida, H. Kunii, T.L., 1998. *Recognizing plant species by laef shapes – A case study of the Acer family,* Proceedings of Fourteenth International Conference on Pattern Recognition, 2, pp. 1171-1173.

Jain, R., Kasturi, R., Schunck, B.G., 1995. *Machine Vision*, McGraw-Hill, Inc,USA.

Kauppinen, H., Seppänen, T., Pietikäinen, M., 1995. *An Experimental Comparision of Autoregressive and Fourier-Based Descriptors in 2D Shape Classification*,

IEEE transactions on Pattern analusis and Machine Intelligence, 17(2), pp. 201-207.

Kawagoe, M., Tojo, A., 1984, *Fingerprint pattern classification*, Pattern Recognition, 17 (3), pp. 295-303.

Li, Y.-F., Zhu, Q.-S., Cao, Y.-K.., Wang, C.-L., 2005. A Leaf Vein Extraction Method Based on Snake Technique, International Conference on Neural Networks and Brain, 2, 13-15 Oct, pp. 885-888.

Loncaric, S., 1998. *A survey of shape analysis techniques*, Pattern recognition, 31 (8), pp. 983-1001.

Maillet, M., S., Shariha, Y.M., 1997. *Skeleton location and evaluation based on local digital width in ribbon-like images*, Pattern Recognition, 30 (11), pp. 1855-1865.

Maltoni, D., Maio, D., Jain, A.K., Prabhakar, S., 2003. *Handbook of Fingerprint Recognition*, Springer-Verlag, NewYork, Inc.

Mokhtarian, F., Abbasi, S., 2004. *Matching Shapes With Self-Intersections: Application to Leaf Classification*, IEEE Transactions on Image Processing, 13(5), pp. 653-661.

Mukundan, R., 2005. *Radial Tchebichef Invariants for Pattern Recognition*, Proc. of IEEE Tencon Conference, Melbourne, pp. 2098-2103.

Mündermann, L., MacMurchy, P., Pivovarov, J., Prusinkiewicz, P., 2003. *Modeling lobed leaves*, Proceedings of the Computer Graphics International, July, pp. 60-65.

Nam, Y., Hwang, E., 2005. *A Shape-Based Retrieval Scheme for Leaf Images*, Lecture Notes in Computer Science 3767, Y.-S. Ho and H.J. Kim (Eds.), Springer-Verlag, pp. 876-887.

Nam, Y., Hwang, E., Byeon, K., 2005a. ELIS: *An Efficient Leaf Retrieval System*, Lecture Notes in Computer Science 3687, S. Singh *et al*. (Eds.), Springer-Verlag, pp. 589-597.

Nam, Y., Hwang, E, Kim, D., 2005b. CLOVER: *A mobile Content-Based Leaf Image Retrieval System*, Lecture Notes in Computer Science 3815, E.A. Fox *et al*. (Eds.), Springer-Verlag, pp. 139-148.

Park, J.-K., Hwang, E., Nam, Y., 2006. *A Venation-Based Leaf Classification Scheme*, Lecture Notes In Computer Science, 4182, pp. 416-428.

Parker, J.R., 1997. *Algorithms for Image Processing and Computer Vision*, John Wiley & Sons, Inc. pp 42-53.

Peng H.-L., Chen S.-Y., 1997. *Trademark shape recognition using closed contours*, Pattern Recognition Letters, 18, pp. 791-803.

Philips, R., 2002. *Flowering Plant Family Key*, http://www.colby.edu/info.tech/BI211/PlantFamilyID.html, (Retrieved 12 October 2006).

Rosin, P.L., 2003. *Assessing the behaviour of polygonal approximation algorithms*, Pattern Recognition 36, pp. 505-518.

Saitoh, T., Kaneko, T., 2000. *Automatic Recognition of Wild Flowers*, Pattern Recognition, 2000. Proceedings. 15th International Conference on, Volume 2, pp. 507 – 510.

Sajjanhar, A., Lu, G., Zhang, D., Zhou, W., 2007. *A Composite Descriptor for Shape Retrieval*, 6th IEEE/ACIS International Conference on Computer and Information Science, July, pp. 795 – 800.

Tieng, Q.M., Boles, W.W., 1997. *Recognition of 2D Object Contour Using the Wavelet Transform Zero-Crossing Representation*, IEEE Transactions on Pattern Analysis and Machine Intelligence, 19(8), pp. 910-916.

Veltkamp, R., 2001. *Shape Matching: similarity measures and algorithms*. International Conference on Shape Modeling and Applications, Genova, Italy. pp. 188-197.

Wang, Z., Chi, Z., Feng, D., 2003. *Shape based leaf image retrieval*, IEEE Proceedings, Visual Image Signal Process, 150 (1), pp. 34-43.

Wang, Z., Chi, Z., Feng, D., 2002. *Fuzzy integral for leaf image retrieval.*, Proceedings of the 2002 IEEE International Conference on Fuzzy Systems, Honolulu, USA, May, 1, pp. 372 – 377.

Wang, Z., Chi, Z., Feng D, Wang, Q., 2000. *Leaf Image Retrieval with Shape Features*, Lecture Notes in Computer Science: Advances in visual information systems, R.Laurini(Ed.), Springer-Verlag, pp. 477-488.

Wu, Q., Zhou, C., Wang, C., 2006. Feature Extraction and Representation of Plant Leaf for Image Retrieval, H.T.Shen et al.(eds): APWeb Workshops, Lecture Notes in Computer Science 3842, pp. 127-131.

Yang, H.S., Lee, S.U., Lee, K.M., 1998. *Recognition of 2D Object Contours Using Starting-Point-Independent Wavelet Coefficient Matching*, Journal of Visual Communication and Image Representation, 9 (2), pp. 171-181.

Ye, Y., Chen, C., Li, C.-T., Fu, H., Chi, Z., 2004. *A computerized Plant Species Recognition System*, Proceedings of 2004 International Symposium on Intelligent Multimedia, Video and Speech Processing, Hong Kong, pp. 723-726.

Zhang, D., Lu, G., 2002. *Generic Fourier Descriptors for Shape-based Image Retrieval*, IEEE International Conference on Multimedia and Expo, 2002. ICME '02. Proceedings 1, pp. 425-428.

Zhang, D., Lu, G. 2001. *A comparative study on shape retrieval using Fourier descriptors with different shape signatures*, International conference on intelligent multimedia and distance education in Fargo, ND, USA, June.

Zhang,G., Wang, X., Huang, D., 2004. *A Hypersphere Method For Plant leaves Classification*, Proceedings of 2004 International Symposium on Intelligent Multimedia, Video and Speech Processing, pp. 165-168.

Appendix I

(a) Retrieval lists for all 40 test images using Fourier descriptors of all the four shape signatures (lists shows only upto the species that recognizes the test image correctly (gray area).

Test Image	a1.jpg	b1.jpg	c1.jpg	d1.jpg	e1.jpg	f1.jpg	g1.jpg	h1.jpg
Retrievals	a	ag	ad	d	e	at	g	g
	an	al	j	an	p	j	t	t
	s	m	ap	a	a	f	i	i
	d	b	c	p	c	ap	ab	ab
	ai	ae	at	s	ai	b	l	l
	f	ap	b	ai	s	ag	h	h

Test Image	i1.jpg	j1.jpg	k1.jpg	l1.jpg	m1.jpg	n1.jpg	o1.jpg	p1.jpg
Retrievals	i	ap	k	l	m	n	o	p
	t	j	o	h	al	r	ao	d
	g	at	ad	ab	aj	am	k	an
	h	f	af	i	am	h	n	e

Test Image	r1.jpg	s1.jpg	t1.jpg	u1.jpg	v1.jpg	ab1.jpg	ac1.jpg	ad1.jpg
Retrievals	r	s	i	u	v	ab	ak	ad
	aj	f	t	ao	ac	t	ac	c
	am	ai	g	m	l	i	v	k
	h	c	h	ag	h	h	l	s

Test Image	ae1.jpg	af1.jpg	ag1.jpg	ah1.jpg	ai1.jpg	aj1.jpg	ak1.jpg	al1.jpg
Retrievals	ae	af	m	ah	ai	r	ak	al
	aq	as	al	ar	f	am	ar	m
	ag	aq	ag	ae	s	aj	ac	ar
	b	b	aj	ao	at	h	am	ak

Test Image	am1.jpg	an1.jpg	ao1.jpg	ap1.jpg	aq1.jpg	ar1.jpg	as1.jpg	at1.jpg
Retrievals	r	d	ao	j	aq	v	as	at
	am	an	ah	f	ae	ar	aq	f
	aj	a	n	ap	b	am	af	j
	h	ai	o	ai	at	n	f	s

Table A: Retrieval lists of 40 test images using Fourier descriptors of centroid-contour distance

Test Image	a1.jpg	b1.jpg	c1.jpg	d1.jpg	e1.jpg	f1.jpg	g1.jpg	h1.jpg
Retrievals	a	ag	ap	an	e	at	g	g
	an	aq	j	a	p	c	t	h
	s	ae	ag	d	s	j	h	t
	e	as	c	e	a	ad	i	i
	p	b	b	s	ai	b	ab	l
	ai	af	as	p	f	k	l	ab
	f	al	aq	ai	ad	ap	v	v
	ad	ap	at	f	an	f	ac	ac

Test Image	i1.jpg	j1.jpg	k1.jpg	l1.jpg	m1.jpg	n1.jpg	o1.jpg	p1.jpg
Retrievals	i	j	k	l	m	n	o	p

Test Image	r1.jpg	s1.jpg	t1.jpg	u1.jpg	v1.jpg	ab1.jpg	ac1.jpg	ad1.jpg
Retrievals	r	s	i	o	v	ab	ac	ai
	am	a	t	ah	ac	i	v	f
	aj	e	ab	ao	l	t	l	ad
	n	p	g	u	h	g	ak	k

Test Image	ae1.jpg	af1.jpg	ag1.jpg	ah1.jpg	ai1.jpg	aj1.jpg	ak1.jpg	al1.jpg
Retrievals	aq	af	al	ah	ai	n	ak	al
	ae	ae	af	aj	f	am	am	m
	ag	al	ae	r	ad	r	r	ao
	as	aq	m	n	k	ak	n	af
	af	m	ao	am	c	l	l	ae
	ap	ag	ag	ar	at	aj	v	ah

Test Image	am1.jpg	an1.jpg	ao1.jpg	ap1.jpg	aq1.jpg	ar1.jpg	as1.jpg	at1.jpg
Retrievals	am	d	ao	ad	aq	ar	as	at
	r	an	m	f	ae	r	b	ad
	aj	a	al	c	ag	am	at	f
	n	s	ae	at	af	ak	j	c
	ah	e	af	k	as	n	aq	b
	ak	p	o	ai	al	ah	ap	j
	ar	ai	ah	j	ao	aj	ag	k
	l	f	u	b	m	v	c	ap
	v	ad	ar	ap	ap	l	k	as

Table B: Retrieval lists of 40 test images using Fourier descriptors of complex-coordinates

Test Image	a1.jpg	b1.jpg	c1.jpg	d1.jpg	e1.jpg	f1.jpg	g1.jpg	h1.jpg
Retrievals	a	ag	ad	an	e	as	g	h
	p	aq	ap	d	p	aq	h	g
	s	af	af	a	ai	j	ab	ab
	an	al	j	s	f	ad	t	t
	ai	ap	ae	p	as	f	i	i
	f	b	c	ai	c	ap	l	l
	d	j	aq	f	s	at	n	n

Test Image	i1.jpg	j1.jpg	k1.jpg	l1.jpg	m1.jpg	n1.jpg	o1.jpg	p1.jpg
Retrievals	i	ad	k	l	m	n	o	p
	ab	j	u	h	ao	v	ac	a
	t	ap	c	g	ar	r	ah	s

Test Image	r1.jpg	s1.jpg	t1.jpg	u1.jpg	v1.jpg	ab1.jpg	ac1.jpg	ad1.jpg
Retrievals	r	s	i	o	v	i	o	ad
	am	a	ab	ar	n	ab	ac	c
	aj	ai	t	ao	ac	t	ah	j
	ak	f	g	u	r	g	v	as
	v	at	n	ac	am	n	r	f

Test Image	ae1.jpg	af1.jpg	ag1.jpg	ah1.jpg	ai1.jpg	aj1.jpg	ak1.jpg	al1.jpg
Retrievals	af	af	al	ah	ai	l	ak	al
	ap	ap	af	n	f	r	am	m
	j	j	ae	v	s	am	aj	ae
	ad	aq	ag	ar	as	ak	r	af
	ae	ag	m	r	at	n	n	ag
	aq	ad	ap	ao	b	aj	l	ao
	ag	ae	aq	aj	aq	v	ah	ar

Test Image	am1.jpg	an1.jpg	ao1.jpg	ap1.jpg	aq1.jpg	ar1.jpg	as1.jpg	at1.jpg
Retrievals	am	d	ao	as	aq	ah	as	at
	ak	an	ar	aq	ap	ar	f	f
	aj	a	ah	f	ag	aj	at	ai
	r	s	aj	j	j	r	aq	as
	n	p	r	ad	af	ao	b	b
	ah	ai	m	at	ad	n	ai	s
	v	f	am	ap	b	am	j	aq

Table C: Retrieval lists of 40 test images using Fourier descriptors of full-width to length ratio distribution

Test Image	a1.jpg	b1.jpg	c1.jpg	d1.jpg	e1.jpg	f1.jpg	g1.jpg	h1.jpg
Retrievals	a	ag	ad	an	e	f	g	g
	s	al	k	d	ai	at	ab	ab
	an	ap	ae	a	f	ad	i	i
	ai	b	af	s	ad	j	t	l
	d	j	aq	ai	s	b	l	t
	f	af	c	f	c	ap	h	h

Test Image	i1.jpg	j1.jpg	k1.jpg	l1.jpg	m1.jpg	n1.jpg	o1.jpg	p1.jpg
Retrievals	g	j	k	l	m	am	ak	p
	ab	ap	u	g	ao	ak	o	ai
	i	c	ae	h	aj	v	am	s
	t	ad	af	t	al	o	ar	as
	h	ag	ad	ab	r	n	ah	f
	l	b	ao	i	ah	ar	u	e

Test Image	r1.jpg	s1.jpg	t1.jpg	u1.jpg	v1.jpg	ab1.jpg	ac1.jpg	ad1.jpg
Retrievals	aj	s	ab	ao	v	ab	ac	c
	r	a	g	u	ac	i	v	j
	n	ai	i	m	l	g	ar	ad
	ao	at	l	ah	ah	l	l	f

Test Image	ae1.jpg	af1.jpg	ag1.jpg	ah1.jpg	ai1.jpg	aj1.jpg	ak1.jpg	al1.jpg
Retrievals	ae	af	al	ah	ai	aj	ak	al
	as	ad	ae	ar	ad	ah	v	ao

Test Image	am1.jpg	an1.jpg	ao1.jpg	ap1.jpg	aq1.jpg	ar1.jpg	as1.jpg	at1.jpg
Retrievals	am	d	ao	f	aq	ar	as	at
	r	an	ah	ad	af	ah	aq	f
	n	a	aj	at	b	am	b	ai
	ah	s	r	b	ae	v	at	b
	ar	ai	n	j	al	r	f	s
	aj	p	ar	ap	ag	n	ai	j

Table D: Retrieval lists of 40 test images using Fourier descriptors of half-width to length ratio distribution

(b) Retrieval lists for all 40 test images using raw values of all the four shape signatures (lists shows only upto the species that recognizes the test image correctly (gray area).

Test Image	a1.jpg	b1.jpg	c1.jpg	d1.jpg	e1.jpg	f1.jpg	g1.jpg	h1.jpg
Retrievals	a	ag	j	d	e	f	g	h
	an	al	c	a	s	at	t	g
	s	b	ap	an	ai	b	i	t
	ai	ae	ag	ai	a	ap	h	i

Test Image	i1.jpg	j1.jpg	k1.jpg	l1.jpg	m1.jpg	n1.jpg	o1.jpg	p1.jpg
Retrievals	i	j	k	l	m	r	o	p
	g	ap	ad	g	aj	n	ao	a
	t	ag	c	h	al	l	ah	s
	ab	c	u	ab	n	aj	k	ai

Test Image	r1.jpg	s1.jpg	t1.jpg	u1.jpg	v1.jpg	ab1.jpg	ac1.jpg	ad1.jpg
Retrievals	aj	s	i	u	v	ab	ac	c
	am	a	t	m	ar	i	l	k
	n	f	g	ae	l	g	r	j
	r	ai	ab	al	am	t	ab	ad

Test Image	ae1.jpg	af1.jpg	ag1.jpg	ah1.jpg	ai1.jpg	aj1.jpg	ak1.jpg	al1.jpg
Retrievals	ae	af	al	ah	ai	aj	ak	al
	aq	aq	m	n	s	n	v	ae
	ag	as	ag	ar	f	am	aj	m
	af	b	ae	ae	at	l	n	r

Test Image	am1.jpg	an1.jpg	ao1.jpg	ap1.jpg	aq1.jpg	ar1.jpg	as1.jpg	at1.jpg
Retrievals	am	an	ao	ap	aq	ar	as	at
	aj	d	aj	at	b	n	aq	f
	n	a	o	f	ae	l	af	b
	r	s	m	c	ag	r	b	s

Table E: Retrieval lists of 40 test images using raw values of centroid-contour distance

Test Image	a1.jpg	b1.jpg	c1.jpg	d1.jpg	e1.jpg	f1.jpg	g1.jpg	h1.jpg
Retrievals	a	al	ad	d	e	f	g	h
	s	b	ap	a	f	at	h	g
	an	ag	c	an	ai	ai	t	t

Test Image	i1.jpg	j1.jpg	k1.jpg	l1.jpg	m1.jpg	n1.jpg	o1.jpg	p1.jpg
Retrievals	i	j	u	l	m	n	o	p
	t	ad	k	ab	al	r	n	as
	g	ag	ae	r	aj	am	u	ai

Test Image	r1.jpg	s1.jpg	t1.jpg	u1.jpg	v1.jpg	ab1.jpg	ac1.jpg	ad1.jpg
Retrievals	r	s	i	o	v	ab	ac	ad
	am	a	t	u	ac	t	v	c
	n	ai	g	k	l	i	ar	ap

Test Image	ae1.jpg	af1.jpg	ag1.jpg	ah1.jpg	ai1.jpg	aj1.jpg	ak1.jpg	al1.jpg
Retrievals	ae	af	al	ah	ai	ak	ak	al
	af	aq	ag	n	f	aj	aj	m
	al	ae	m	r	s	am	am	ae

Test Image	am1.jpg	an1.jpg	ao1.jpg	ap1.jpg	aq1.jpg	ar1.jpg	as1.jpg	at1.jpg
Retrievals	am	an	ao	f	aq	ar	as	at
	ak	d	aj	ap	af	ah	aq	b
	r	a	m	at	ae	v	af	ag

Table F: Retrieval lists of 40 test images using raw values of full-width to length ratio distribution

Test Image	a1.jpg	b1.jpg	c1.jpg	d1.jpg	e1.jpg	f1.jpg	g1.jpg	h1.jpg
Retrievals	a	al	c	d	e	f	h	h
	s	b	k	a	f	ai	g	g
	at	at	ae	at	u	k	n	l

Test Image	i1.jpg	j1.jpg	k1.jpg	l1.jpg	m1.jpg	n1.jpg	o1.jpg	p1.jpg
Retrievals	i	j	u	l	m	n	am	p
	ab	ag	ae	r	al	r	ad	ai
	g	c	k	n	aj	t	ak	as
	h	m	af	ab	ak	l	o	f
	l	b	ah	t	ag	m	ah	aq

Test Image	r1.jpg	s1.jpg	t1.jpg	u1.jpg	v1.jpg	ab1.jpg	ac1.jpg	ad1.jpg
Retrievals	ak	s	i	o	v	ab	ac	ap
	ah	a	ab	u	ac	i	v	ad
	aj	an	g	ah	ar	g	ar	at
	am	at	h	ak	ah	ak	ah	c
	r	b	ak	m	ab	l	l	ag
	n	f	t	am	l	h	ab	b
	ar	ad	am	k	ak	v	n	j

Test Image	ae1.jpg	af1.jpg	ag1.jpg	ah1.jpg	ai1.jpg	aj1.jpg	ak1.jpg	al1.jpg
Retrievals	k	af	al	ah	s	ak	t	al
	ae	ae	ag	n	f	aj	r	m
	c	aq	ap	r	ai	g	n	ag
	m	al	b	ar	at	h	aj	ae
	f	ar	m	l	b	r	--------	af
	af	b	at	aj	ap	n	17 spp ak1	b

Test Image	am1.jpg	an1.jpg	ao1.jpg	ap1.jpg	aq1.jpg	ar1.jpg	as1.jpg	at1.jpg
Retrievals	am	an	am	ap	af	l	as	at
	ak	d	ak	ad	ae	n	aq	b
	i	a	ao	at	aq	r	af	ad
	ah	s	ad	b	al	ah	b	ap
	ar	ai	ap	s	f	v	at	s
	ab	f	aj	ag	b	ar	f	ag
	v	at	m	aq	ag	ac	ae	j

Table G: Retrieval lists of 40 test images using raw values of half-width to length ratio distribution

(c) Values of leaf margin coarseness (number of teeth), stem length to blade length ratio, leaf tip curvature and the leaf compactness of all 200 leaf images.

Test Image	Compactness	Curvature	No of teeth	Stem length to blade length ratio
a1.pgm	0.0660	-0.0405	1	0.1576
a2.pgm	0.0668	-0.1397	0	0.1684
a3.pgm	0.0603	-0.1944	2	0.1817
a4.pgm	0.0625	-0.2881	1	0.1752
a5.pgm	0.0629	-0.2500	1	0.1826
b1.pgm	0.0513	-0.2857	1	0.0986
b2.pgm	0.0496	-0.1833	0	0.1105
b3.pgm	0.0552	-0.3816	0	0.1012
b4.pgm	0.0595	-0.4242	0	0.0850
b5.pgm	0.0599	-0.2286	0	0.0717
c1.pgm	0.0351	0.3546	1	0.1705
c2.pgm	0.0360	0.5294	0	0.2388
c3.pgm	0.0366	0.5811	0	0.2486
c4.pgm	0.0304	0.7102	2	0.2776
c5.pgm	0.0352	0.3526	0	0.2615
d1.pgm	0.0474	-0.7667	4	0.0177
d2.pgm	0.0527	-1.0893	8	0.0113
d3.pgm	0.0482	-0.0376	11	0.0184
d4.pgm	0.0558	0.3438	3	0.0195
d5.pgm	0.0485	0.8036	8	0.0096
e1.pgm	0.0306	-0.1767	2	0.4847
e2.pgm	0.0287	0.3133	6	0.4458
e3.pgm	0.0263	0.1250	3	0.5045
e4.pgm	0.0349	0.4310	2	0.4715
e5.pgm	0.0325	0.4167	7	0.5097
f1.pgm	0.0546	-0.4034	0	0.1869
f2.pgm	0.0602	-0.4531	0	0.1864
f3.pgm	0.0544	-0.4262	0	0.1941
f4.pgm	0.0599	-0.3446	0	0.1951
f5.pgm	0.0610	-0.3828	0	0.1701
g1.pgm	0.0214	-0.0033	0	0.0572
g2.pgm	0.0224	0.1034	0	0.0818
g3.pgm	0.0204	-0.0122	0	0.0786
g4.pgm	0.0209	0.0038	0	0.0469
g5.pgm	0.0208	0.1429	1	0.0477
h1.pgm	0.0223	-0.0663	0	0.1092
h2.pgm	0.0186	0.0497	0	0.1040
h3.pgm	0.0211	-0.0132	2	0.1225
h4.pgm	0.0208	-0.0276	0	0.1022
h5.pgm	0.0241	-0.0653	0	0.1097
i1.pgm	0.0184	-0.0882	0	0.1122
i2.pgm	0.0196	-0.0606	0	0.0999
i3.pgm	0.0198	0.0012	1	0.1169
i4.pgm	0.0186	0.0303	0	0.1121
i5.pgm	0.0191	-0.0579	0	0.0883
j1.pgm	0.0503	0.3545	1	0.0990
j2.pgm	0.0581	0.2432	0	0.0873
j3.pgm	0.0495	0.3606	0	0.0892
j4.pgm	0.0475	0.3517	0	0.1001
j5.pgm	0.0419	0.2813	0	0.1157

Test Image	Compactness	Curvature	No of teeth	Stem length to blade length ratio
k1.pgm	0.0153	-0.2879	14	0.5453
k2.pgm	0.0199	0.0000	12	0.4121
k3.pgm	0.0184	-0.1930	7	0.5508
k4.pgm	0.0243	0.0500	8	0.2918
k5.pgm	0.0219	-0.1277	16	0.2941
l1.pgm	0.0257	-0.2778	1	0.2365
l2.pgm	0.0293	-0.1379	0	0.2342
l3.pgm	0.0315	-0.1964	0	0.2634
l4.pgm	0.0230	-0.1806	0	0.2663
l5.pgm	0.0224	-0.1731	1	0.2938
m1.pgm	0.0414	0.0517	2	0.1433
m2.pgm	0.0394	-0.2901	2	0.1458
m3.pgm	0.0460	-0.1333	1	0.1695
m4.pgm	0.0449	-0.1094	1	0.1577
m5.pgm	0.0416	-0.0938	0	0.1679
n1.pgm	0.0282	-0.1000	0	0.2155
n2.pgm	0.0308	-0.1167	0	0.1819
n3.pgm	0.0313	-0.0862	0	0.1951
n4.pgm	0.0290	0.0319	0	0.2203
n5.pgm	0.0293	-0.0656	0	0.2348
o1.pgm	0.0175	0.2511	5	0.4929
o2.pgm	0.0231	0.0926	5	0.4019
o3.pgm	0.0171	0.0926	5	0.4839
o4.pgm	0.0167	0.0781	8	0.5066
o5.pgm	0.0189	0.1288	6	0.5491
p1.pgm	0.0546	-0.7135	2	0.4248
p2.pgm	0.0538	-0.5192	1	0.4116
p3.pgm	0.0505	-0.2407	1	0.3904
p4.pgm	0.0469	-0.3426	2	0.5036
p5.pgm	0.0479	-0.7273	1	0.5274
r1.pgm	0.0334	-0.2110	0	0.1812
r2.pgm	0.0343	-0.2857	0	0.1994
r3.pgm	0.0271	-0.0222	0	0.2242
r4.pgm	0.0340	-0.0931	0	0.1726
r5.pgm	0.0321	-0.0938	0	0.1707
s1.pgm	0.0715	-0.2210	0	0.1002
s2.pgm	0.0576	-0.1758	0	0.1344
s3.pgm	0.0632	-0.4377	0	0.0996
s4.pgm	0.0725	-0.2778	0	0.0781
s5.pgm	0.0672	-0.2496	1	0.1111
t1.pgm	0.0189	-0.0147	0	0.1008
t2.pgm	0.0213	-0.0857	0	0.0689
t3.pgm	0.0211	-0.1692	0	0.1049
t4.pgm	0.0190	-0.0857	0	0.1020
t5.pgm	0.0207	-0.0952	1	0.0894
u1.pgm	0.0311	0.2432	0	0.4281
u2.pgm	0.0372	0.0489	0	0.3728
u3.pgm	0.0343	0.2500	0	0.5272
u4.pgm	0.0376	0.1071	0	0.5458
u5.pgm	0.0381	-0.0105	1	0.5064

Table continues..

Test Image	Compactness	Curvature	No of teeth	Stem length to blade length ratio
v1.pgm	0.0272	-0.2081	0	0.0397
v2.pgm	0.0294	-0.3246	0	0.0280
v3.pgm	0.0302	-0.2344	0	0.5048
v4.pgm	0.0262	-0.1607	0	0.0190
v5.pgm	0.0248	-0.2419	0	0.0190
ab1.pgm	0.0181	-0.2909	0	0.2073
ab2.pgm	0.0199	-0.1944	1	0.1840
ab3.pgm	0.0201	-0.2145	0	0.1448
ab4.pgm	0.0201	-0.2294	1	0.0885
ab5.pgm	0.0200	-0.2162	0	0.1572
ac1.pgm	0.0243	-0.1279	2	0.0141
ac2.pgm	0.0219	-0.1500	0	0.0409
ac3.pgm	0.0218	-0.2082	0	0.0312
ac4.pgm	0.0282	-0.2848	0	0.0371
ac5.pgm	0.0308	-0.2827	1	0.0226
ad1.pgm	0.0309	-0.0395	10	0.2096
ad2.pgm	0.0284	0.0712	11	0.2270
ad3.pgm	0.0306	0.1053	7	0.1544
ad4.pgm	0.0328	0.0057	10	0.1450
ad5.pgm	0.0286	0.0457	10	0.1964
ae1.pgm	0.0480	-0.0814	1	0.1367
ae2.pgm	0.0468	-0.4404	0	0.1345
ae3.pgm	0.0461	-0.3697	0	0.1224
ae4.pgm	0.0463	-0.4086	0	0.1354
ae5.pgm	0.0409	-0.4660	0	0.1349
af1.pgm	0.0395	-0.0854	1	0.1940
af2.pgm	0.0348	-0.2239	2	0.1702
af3.pgm	0.0360	-0.1206	0	0.1835
af4.pgm	0.0386	-0.3250	2	0.2083
af5.pgm	0.0402	-0.3611	0	0.2497
ag1.pgm	0.0475	-0.2241	0	0.1014
ag2.pgm	0.0541	-0.1518	0	0.0978
ag3.pgm	0.0501	-0.0645	0	0.0906
ag4.pgm	0.0524	-0.2511	0	0.0981
ag5.pgm	0.0529	-0.0536	0	0.0981
ah1.pgm	0.0269	0.1389	3	0.2626
ah2.pgm	0.0290	-0.3333	4	0.2500
ah3.pgm	0.0280	-0.4085	3	0.0378
ah4.pgm	0.0294	-0.3929	4	0.2359
ah5.pgm	0.0277	-0.4287	3	0.2958
ai1.pgm	0.0492	-0.5833	3	0.1681
ai2.pgm	0.0475	-0.6176	2	0.1700
ai3.pgm	0.0479	-1.8500	1	0.0181
ai4.pgm	0.0527	-1.0219	4	0.2002
ai5.pgm	0.0445	-0.5000	3	0.1695
aj1.pgm	0.0295	0.1380	1	0.0679
aj2.pgm	0.0337	-0.0774	0	0.0687
aj3.pgm	0.0338	0.0401	0	0.0660
aj4.pgm	0.0417	-0.0846	0	0.0889
aj5.pgm	0.0347	-0.1989	0	0.0634

Test Image	Compactness	Curvature	No of teeth	Stem length to blade length ratio
ak1.pgm	0.0284	-0.0625	0	0.0238
ak2.pgm	0.0313	-0.1304	0	0.1439
ak3.pgm	0.0307	-0.0968	0	0.0361
ak4.pgm	0.0314	-0.0303	2	0.0422
ak5.pgm	0.0250	-0.1440	0	0.0741
al1.pgm	0.0445	-0.2614	0	0.0945
al2.pgm	0.0470	-0.2106	0	0.0301
al3.pgm	0.0486	-0.2702	0	0.0732
al4.pgm	0.0490	-0.3042	0	0.0711
al5.pgm	0.0437	-0.2059	0	0.0962
am1.pgm	0.0337	-0.1894	0	0.1373
am2.pgm	0.0321	-0.1979	0	0.1572
am3.pgm	0.0319	-0.1176	0	0.1660
am4.pgm	0.0335	0.0000	0	0.1616
am5.pgm	0.0310	-0.0625	0	0.1651
an1.pgm	0.0770	-0.2083	0	0.0972
an2.pgm	0.0685	-0.1754	0	0.0982
an3.pgm	0.0706	-0.4545	0	0.1452
an4.pgm	0.0715	-0.2300	0	0.0424
an5.pgm	0.0684	-0.1923	0	0.1367
ao1.pgm	0.0248	-0.1571	10	0.1189
ao2.pgm	0.0232	-0.1622	15	0.1108
ao3.pgm	0.0209	-0.0381	14	0.1329
ao4.pgm	0.0221	-0.3611	15	0.1220
ao5.pgm	0.0208	-0.3649	14	0.1331
ap1.pgm	0.0495	-0.6250	2	0.1977
ap2.pgm	0.0444	0.1351	1	0.2052
ap3.pgm	0.0433	-0.0488	4	0.2053
ap4.pgm	0.0487	-0.1119	5	0.1597
ap5.pgm	0.0429	-0.0574	7	0.2078
aq1.pgm	0.0496	-0.2300	0	0.1453
aq2.pgm	0.0495	-0.2045	0	0.1568
aq3.pgm	0.0503	-0.4120	0	0.1828
aq4.pgm	0.0477	-0.3312	0	0.2478
aq5.pgm	0.0483	-0.4091	0	0.1595
ar1.pgm	0.0331	-0.2996	0	0.1818
ar2.pgm	0.0385	-0.4598	0	0.1830
ar3.pgm	0.0385	-0.1687	0	0.2112
ar4.pgm	0.0372	-0.3333	0	0.1685
ar5.pgm	0.0339	-0.2727	0	0.1815
as1.pgm	0.0523	-0.4412	0	0.1095
as2.pgm	0.0520	-0.3752	0	0.1015
as3.pgm	0.0534	-0.4652	0	0.1330
as4.pgm	0.0516	-0.3311	0	0.1537
as5.pgm	0.0473	-0.3056	0	0.1307
at1.pgm	0.0580	0.0956	0	0.0234
at2.pgm	0.0590	-0.1111	0	0.0221
at3.pgm	0.0581	-0.5322	0	0.0189
at4.pgm	0.0569	-0.0819	0	0.0606
at5.pgm	0.0582	0.0850	0	0.0232

Table H: Values of leaf margin coarseness (number of teeth), stem length to blade length ratio, leaf tip curvature and the leaf compactness of all 200 leaf images.

Appendix II

(a)Compleate C source code for the boundary following algorithm

```
#define arraySize 10000

struct cordi {
     int i;
     int j;
  };

struct cordi kk, edgelist[arraySize];
int i=0,j=0,bj=0,bi=0,elc;
IMAGE binaryIm;

// struct cordi mostLeft(IMAGE im) returns the cordinates of the
//mostleft pixel of the image im.

// This assigns the coordinates of the mostleft pixel of the binary
//image to the structure variable kk.

kk = mostLeft(binaryIm);


edgelist[0].i=kk.i;
edgelist[0].j=kk.j;
i=kk.i;
j=kk.j;
bi=i;
bj=j-1;

for ( elc=1; ; elc++)
{
  if (bi==i && bj==j-1)
  {
    if (binaryIm->data[i-1][j-1]==0)
    {
      bi=i;
      bj=j-1;
      i=i-1;
      j=j-1;
      edgelist[elc].i=i;
      edgelist[elc].j=j;
    }
    else
    {
      if (binaryIm->data[i-1][j]==0)
      {
        bi=i-1;
        bj=j-1;
        i=i-1;
        edgelist[elc].i=i;
        edgelist[elc].j=j;
```

```
}
else
{
  if (binaryIm->data[i-1][j+1]==0)
  {
    bi=i-1;
    bj=j;
    i=i-1;
    j=j+1;
    edgelist[elc].i=i;
    edgelist[elc].j=j;
  }
  else
  {
    if (binaryIm->data[i][j+1]==0)
    {
      bi=i-1;
      bj=j+1;
      j=j+1;
      edgelist[elc].i=i;
      edgelist[elc].j=j;
    }
    else
    {
      if (binaryIm->data[i+1][j+1]==0)
      {
        bi=i;
        bj=j+1;
        i=i+1;
        j=j+1;
        edgelist[elc].i=i;
        edgelist[elc].j=j;
      }
      else
      {
        if (binaryIm->data[i+1][j]==0)
        {
          bi=i+1;
          bj=j+1;
          i=i+1;
          edgelist[elc].i=i;
          edgelist[elc].j=j;
        }
        else
        {
          if (binaryIm->data[i+1][j-1]==0)
          {
            bi=i+1;
            bj=j;
            i=i+1;
            j=j-1;
            edgelist[elc].i=i;
            edgelist[elc].j=j;
          }
        }
      }
    }
```

```
      }
    }
  }
}

else
{
  if (bi==i-1 && bj==j)
  {
    if (binaryIm->data[i-1][j+1]==0)
    {
      bi=i-1;
      bj=j;
      i=i-1;
      j=j+1;
      edgelist[elc].i=i;
      edgelist[elc].j=j;
    }
    else
    {
      if (binaryIm->data[i][j+1]==0)
      {
        bi=i-1;
        bj=j+1;
        j=j+1;
        edgelist[elc].i=i;
        edgelist[elc].j=j;
      }
      else
      {
        if (binaryIm->data[i+1][j+1]==0)
        {
          bi=i;
          bj=j+1;
          i=i+1;
          j=j+1;
          edgelist[elc].i=i;
          edgelist[elc].j=j;
        }
        else
        {
          if (binaryIm->data[i+1][j]==0)
          {
            bi=i+1;
            bj=j+1;
            i=i+1;
            edgelist[elc].i=i;
            edgelist[elc].j=j;
          }
          else
          {
            if (binaryIm->data[i+1][j-1]==0)
            {
              bi=i+1;
              bj=j;
              i=i+1;
              j=j-1;
```

```
                edgelist[elc].i=i;
                edgelist[elc].j=j;
              }
              else
              {
                if (binaryIm->data[i][j-1]==0)
                {
                  bi=i+1;
                  bj=j-1;
                  i=i;
                  j=j-1;
                  edgelist[elc].i=i;
                  edgelist[elc].j=j;
                }
                else
                {
                  if (binaryIm->data[i-1][j-1]==0)
                  {
                    bi=i;
                    bj=j-1;
                    i=i-1;
                    j=j-1;
                    edgelist[elc].i=i;
                    edgelist[elc].j=j;
                  }
                }
              }
            }
          }
        }
      }
    }
  }
  else
  {
    if (bi==i && bj==j+1)
    {
      if (binaryIm->data[i+1][j+1]==0)
      {
        bi=i;
        bj=j+1;
        i=i+1;
        j=j+1;
        edgelist[elc].i=i;
        edgelist[elc].j=j;
      }
      else
      {
        if (binaryIm->data[i+1][j]==0)
        {
          bi=i+1;
          bj=j+1;
          i=i+1;
          edgelist[elc].i=i;
          edgelist[elc].j=j;
        }
        else
        {
```

```
if (binaryIm->data[i+1][j-1]==0)
{
   bi=i+1;
   bj=j;
   i=i+1;
   j=j-1;
   edgelist[elc].i=i;
   edgelist[elc].j=j;
}
else
{
   if (binaryIm->data[i][j-1]==0)
   {
      bi=i+1;
      bj=j-1;
      i=i;
      j=j-1;
      edgelist[elc].i=i;
      edgelist[elc].j=j;
   }
   else
   {
      if (binaryIm->data[i-1][j-1]==0)
      {
         bi=i;
         bj=j-1;
         i=i-1;
         j=j-1;
         edgelist[elc].i=i;
         edgelist[elc].j=j;
      }
      else
      {
         if (binaryIm->data[i-1][j]==0)
         {
            bi=i-1;
            bj=j-1;
            i=i-1;
            j=j;
            edgelist[elc].i=i;
            edgelist[elc].j=j;
         }
         else
         {
            if (binaryIm->data[i-1][j+1]==0)
            {
               bi=i-1;
               bj=j;
               i=i-1;
               j=j+1;
               edgelist[elc].i=i;
               edgelist[elc].j=j;
            }

         }
      }
   }
```

```
      }
    }
  }
}
else
{
  if (bi==i+1 && bj==j)
  {
    if (binaryIm->data[i+1][j-1]==0)
    {
      bi=i+1;
      bj=j;
      i=i+1;
      j=j-1;
      edgelist[elc].i=i;
      edgelist[elc].j=j;
    }
    else
    {
      if (binaryIm->data[i][j-1]==0)
      {
        bi=i+1;
        bj=j-1;
        i=i;
        j=j-1;
        edgelist[elc].i=i;
        edgelist[elc].j=j;
      }
      else
      {
        if (binaryIm->data[i-1][j-1]==0)
        {
          bi=i;
          bj=j-1;
          i=i-1;
          j=j-1;
          edgelist[elc].i=i;
          edgelist[elc].j=j;
        }
        else
        {
          if (binaryIm->data[i-1][j]==0)
          {
            bi=i-1;
            bj=j-1;
            i=i-1;
            j=j;
            edgelist[elc].i=i;
            edgelist[elc].j=j;
          }
          else
          {
            if (binaryIm->data[i-1][j+1]==0)
            {
              bi=i-1;
              bj=j;
              i=i-1;
```

```
                        j=j+1;
                        edgelist[elc].i=i;
                        edgelist[elc].j=j;
                      }
                      else
                      {
                        if (binaryIm->data[i][j+1]==0)
                        {
                          bi=i-1;
                          bj=j+1;
                          i=i;
                          j=j+1;
                          edgelist[elc].i=i;
                          edgelist[elc].j=j;
                        }
                        else
                        {
                          if (binaryIm->data[i+1][j+1]==0)
                          {
                            bi=i;
                            bj=j+1;
                            i=i+1;
                            j=j+1;
                            edgelist[elc].i=i;
                            edgelist[elc].j=j;
                          }

                        }
                      }
                    }
                  }
                }
              }
            }
          }
        }
      }
    }
  }
}
if   (edgelist[elc].i== kk.i && edgelist[elc].j== kk.j) break;
}
```

(b)Compleate C source code for the hop-along algorithm

```
#define thres 4.00

struct cordi {
     int i;
     int j;
  };

int maxpdsi(struct cordi a[], int start, int end)
{
  double pD,pd,max=0;
  int k,l;

  pD=sqrt((a[start].i - a[end].i)*(a[start].i - a[end].i)+ (a[start].j
          - a[end].j)*(a[start].j - a[end].j));
  for (k=start+1;k<end;k++)
  {
    pd=fabs(a[k].i*(a[start].j - a[end].j) + a[k].j *(a[end].i
         - a[start].i)+ a[end].j*a[start].i-a[start].j *a[end].i)/pD;
    if (pd>max)
    {
      max=pd;
      l=k;
    }
  }
  if (max<=thres)
  {
    return end;
  }
  else
  {
    return maxpdsi(a,start,l);
  }
}


#define arraySize 10000
#define thrAn 0.20

int hopalongvertices[arraySize];
int startvertex=0,endvertex=0,novertices=0, i=0;

hopalongvertices[0]=0;
startvertex=hopalongvertices[0];
endvertex=startvertex+pl;

for (i=1; ; i++)
{
  hopalongvertices[i]=maxpdsi(edgelist,startvertex,endvertex);
  startvertex=hopalongvertices[i];
  endvertex=startvertex+pl;
  if (endvertex>=elc-1)
    endvertex=elc-1;
  if (i!=1)
```

```
  {
    mp=atan2((edgelist[hopalongvertices[i-1]].i-
      edgelist[hopalongvertices[i-2]].i),(edgelist[hopalongvertices[i-
      1]].j-edgelist[hopalongvertices[i-2]].j));
    mc=atan2((edgelist[hopalongvertices[i]].i-
      edgelist[hopalongvertices[i-
      1]].i),(edgelist[hopalongvertices[i]].j-
      edgelist[hopalongvertices[i-1]].j));

    if (fabs(mc-mp)<thrAn)
    {
      hopalongvertices[i-1]=hopalongvertices[i];
      hopalongvertices[i]=0;
      i=i-1;
    }
  }
  if (startvertex==elc-1)
  {novertices=i;
    break;
  }
}
```